# Exploring the interaction between cortex and hippocampus to build spatial and visual grid cells : contributions to retrosplenial and entorhinal cortex modelling

Mingda Ju

# Explorer l'interaction entre le cortex et l'hippocampe pour construire des cellules de grille spatiales et visuelles : contributions à la modélisation du cortex rétrosplénial et du cortex entorhinal

# Exploring the interaction between cortex and hippocampus to build spatial and visual grid cells: contributions to retrosplenial and entorhinal cortex modelling

Thèse de doctorat pour l'obtention du titre de docteur délivré par CY Cergy Paris Université

Ecole doctorale n°405 Économie, Management, Mathématiques, Physique et Sciences Informatiques (EM2PSI)

Thèse présentée et soutenue à Cergy, le 09/02/2023, par

Mingda Ju

Devant le jury composé de :

| | | |
|---|---|---|
| Nicolas Rougier | Université de Bordeaux | Rapporteur |
| Denis Sheynikhovich | Sorbonne Université | Rapporteur |
| Emmanuel Daucé | Institut de Neurosciences de la Timone | Examinateur |
| Sylvia Wirth | Institute of Cognitive Sciences Marc Jeannerod | Examinatrice |
| Philippe Gaussier | CY Cergy Paris Université | Directeur de thèse |

# Acknowledgments

First of all, I would like to thank my Ph.D. supervisor, Prof. Philippe Gaussier. I remember the first day I came to the lab for an interview, his affability, and enthusiasm for research infected me and made me determined to follow in his footsteps. I was lucky to have a mentor who was professional but funny, rigorous but flexible. During these four years, he has taught me not only his vast knowledge but also his attitude toward research. During the epidemic, it was his encouragement and understanding that allowed me to persevere through the most challenging times and finish this thesis. I would also like to thank my master's supervisor, Prof. Gang Zheng, who recommended me to participate in this Ph.D. project. I learned a lot from him during the six months of my internship at Inria, and I am deeply aware of my shortcomings. His humility, selflessness, and professionalism have always made him a role model for me on my research path. I am also grateful to my friends, Mehdi Louis, and Yuechen, who have seen me through the ups and downs of my life and research work, and who have been by my side, giving me great encouragement and help. I would also like to thank the etis lab family. Many of my colleagues have helped me in various ways, and I am grateful to all of them for their kindness and goodwill so that I don't feel isolated and lonely in a foreign country. I owe my current platform to the support and encouragement of my family, especially my parents. Thank them for their selfless dedication. They are also the motivation for my efforts and the wellspring of my life.

致我的外公：

今天是一月十七日，我的外公吴士铸老先生于七年前的今天在和运动神经元疾病（渐冻症）抗争了八年之后与世长辞。他是我见过最坚强而又最温柔的人。当我在新冠疫情期间因为连续十天的咳嗽而身心疲惫之时，我想到他在生命最后三年的每一天都要承受因为肌肉萎缩而造成的剧烈咳嗽，而他所受的煎熬远不止此。可我却丝毫不记得他有过任何怨天尤人或是脆弱的表情。他的仁慈和悲悯则总在面对他人的苦难时出现。于他而言，被烈日暴晒的蚯蚓和路边晕倒的人类一样值得被帮助，他也确实付诸于行动。在二十年前，作为机械工程师的他用自己的机床手工打造了一辆四轮电动自行车，于是他便可以和我的外婆并肩骑行在扬州的大街小巷。

我问他明明就可以买到前后双人自行车，为什么要费力造一辆四轮的呢。他说两个人并肩坐着可以平等地欣赏风景，那年，他七十五岁。他让我明白了尊重的意义，他教会了我如何去爱别人，爱这个世界，爱一切生灵……他是我世界的光明。这篇论文对于人类科学来说，犹如沧海一粟微不足道，于我而言是人生中的一个节点。生命中的一切，我都期待能与你分享。

希望你平安，快乐。

# Contents

**List of Figures** **iv**

**List of Tables** **viii**

**Glossary of Symbols** **ix**

**Abstract** **1**

**Résumé français** **2**

**1 Biological background and State of the art** **8**
1.1 Spatial role and connectivity of retrosplenial cortex . . . . . 8
1.2 Path integration . . . . . 12
1.2.1 Neural field and Continuous attractor . . . . . 13
1.2.2 Head direction cell . . . . . 15
1.2.3 Integration of activity of head direction cell . . . . . 16
1.3 Self-organized maps to mimic cortical columns . . . . . 18
1.4 The place cell and hippocampal system . . . . . 20
1.5 Grid cells and the compressing role of entorhinal cortex . . . . . 24
1.6 Continuous attractor model . . . . . 25
1.6.1 1D continuous attractor models for head direction cells . . . 25
1.6.2 2D continuous attractor models for place cells . . . . . 26
1.6.3 2D continuous attractor models for grid cells . . . . . 26
1.7 Oscillatory interference model for place cells and grid cells . . . . . 27
1.8 Adaptive resonance theory and a model of grid cell . . . . . 29
1.9 Discussion . . . . . 30

**2 A model of path integration and representation of spatial context in the retrosplenial cortex** **34**
2.1 Abstract . . . . . 34
2.2 Introduction . . . . . 35
2.3 Computational Model . . . . . 37

2.4 Simulations . . . 42
2.4.1 Simulation in a spiral maze . . . 42
2.4.2 Simulation in W mazes . . . 45
2.4.3 Simulation on a treadmill . . . 50
2.5 Conclusion . . . 54

**3 Contribution of the retrosplenial cortex to path integration and spatial codes 60**
3.1 Abstract . . . 60
3.2 Introduction . . . 60
3.3 Computational model . . . 62
3.4 Parameters and moving pattern . . . 65
3.4.1 Recording of neurons learning MD activities in RSC . . . 66
3.4.2 Building place cells from PI information . . . 67
3.4.3 Robustness of the model . . . 68
3.5 Conclusion . . . 70

**4 Self organization of the entorhinal cortex grid cells: impact of the hippocampal feedback 73**
4.1 Introduction . . . 73
4.2 Ad hoc computational model of grid cells . . . 74
4.2.1 Septal signal generated from cortical signature . . . 84

**5 A computational model of visual grid cells applied to image recognition 94**
5.1 Abstract . . . 94
5.2 Introduction . . . 94
5.3 Computational model . . . 96
5.4 Model of the recognition mechanism relying on 'where' and 'what' information . . . 102
5.5 Results of simulations of the image recognition . . . 107
5.6 Conclusion . . . 120

**6 Discussion 121**

**Bibliography 126**

# List of Figures


1.1 Anatomy of RSC . . . . . 10
1.2 Anatomy of RSC across species . . . . . 12
1.3 An example of path integration . . . . . 13
1.4 Illustration of dynamic neural field . . . . . 14
1.5 Comparison between HD cells and Gaussian shapes . . . . . 16
1.6 Equivalence between the STM scheme (left) and a feed-forward scheme using synaptic learning from a constant input context (right). . . . . 18
1.7 Cerebral cortex . . . . . 19
1.8 Demonstration of the discretization of the activity of neurons on the PI field. . . . . 20
1.9 A schematic representation of the extended hippocampal system . . 21
1.10 Memory classification . . . . . 23
1.11 One-dimensional attractor map model for head direction encoding based on neural integration of head angular velocity signals. (McNaughton et al., 2006) . . . . . 26
1.12 Extension of the one-dimensional attractor map concept to two dimensions: a model for path integration. (McNaughton et al., 2006) . 27
1.13 Linear interference patterns in 2D . . . . . 28
1.14 Two linear interference patterns with preferred directions differing by 60° . . . . . 29
1.15 Anesthesia disrupts distance, but not direction, of path integration memory. (Pisokas et al., 2022) . . . . . 31
1.16 Comparison of continuous attractor model, oscillatory interference model and our model of the path integration and the grid cells. . . . 33

2.1 Comparison between the Gaussian shape and the firing range of HD cells found in biological experiments . . . . . 36
2.2 Model of the retrosplenial cortex with 1D field performing path integration and self-organizing blobs . . . . . 37
2.3 Schema of the contextual input $C_j$ . . . . . 39

2.4 Activity of one neuron in PI field when the animal moves in one direction at a constant speed . . . 41
2.5 Activity of neurons on PI field when the rat moves in a square spiral maze . . . 44
2.6 The rat moves in a square spiral maze . . . 45
2.7 Performance of PI mechanism under the perturbation of a white noise 45
2.8 Activity of neurons on PI field when the rat moves in a square spiral maze . . . 46
2.9 PI in the square spiral maze . . . 46
2.10 Activity of neurons on PI field when the rat moves in a triangle spiral maze . . . 47
2.11 The rat moves in a triangle spiral maze . . . 48
2.12 Representative neural activity from the W maze simulations using different decay constants . . . 49
2.13 Simulation where the mouse is head-fixed and running for 150cm on a treadmill . . . 51
2.14 Activity of three neurons on 3 different 1D Kohonen maps . . . 52
2.15 Place cell-like activity recorded from a global self-organizing map . . 53
2.16 Building MEC grid cells from the projection of RSC blob activity using a modulo operator . . . 55
2.17 Shape of the lateral interaction function . . . 59

3.1 Computation model of path integration (PI) in the retrosplenial cortex 62
3.2 Example of one activated neuron showing MD cell activity on the SOM when $\lambda$ equals to 0.1 . . . 66
3.3 Example of one activated neuron showing place cell activity on the SOM 67
3.4 The average directional and spatial information rates of the activity of neurons using different learning rates . . . 68
3.5 Activity of two neurons under the situation of High(top) and low(bottom) frequency recalibration . . . 69
3.6 Simple illustration of the modulo operation . . . 71

4.1 Architecture of a computational model to build grid cells from path integration fields . . . 74
4.2 Illustration of the modulo mechanism between neurons of the discretization layer and of the modulo layer . . . 75
4.3 Ad hoc selection of four grid cells each representing one quadrant of the environment. . . . 76
4.4 Two grid cells built from 2 pairs of neurons distant from 60 degrees on a path integration field . . . 77
4.5 A grid cell built by the architecture . . . 77

4.6 A model of grid cell using classical conditioning learning rule based on LMS to learn the grid pattern from a preexisting grid cell . . . . 79
4.7 Firing field of a preexisting grid cell built by our computational model as a teaching signal. . . . . 79
4.8 Grid cells learned by a classical conditioning learning rule . . . . . 80
4.9 Two PI neural fields used as the input to the discretization field . . . 81
4.10 Build GC using a blob-structured Kohonen map to learn the discretization in each direction . . . . . 82
4.11 Illustration of the Hebbian/anti-Hebbian learning mechanism. . . . . 83
4.12 Illustration of the update of activities and synaptic connections of neurons subject to the anti-Hebbian learning rule . . . . . 84
4.13 Build GC using a 2D anti-Hebb group to learn the modulo operation 85
4.14 Model of the grid cell based on the reciprocal connection between the hippocampus and the entorhinal cortex. . . . . 86
4.15 activities of the product of random pairs of neurons taken from 20000 neurons . . . . . 87
4.16 Grid cells learned from the hexagonal signal by one-shot learning . . 87
4.17 Septal signals built by one-dimensional Kohonen map with respectively a) 10, b) 20, and c) 50 neurons on the Kohonen map. . . . . 88
4.18 septal signals built by two-dimensional Kohonen map . . . . . 89
4.19 Activity of the septal signal learned by a self-organizing map when introducing a neighbour kernel in the second stage. . . . . 89
4.20 Activity of the septal signal learned by a self-organizing map when introducing a neighbour kernel in the second stage . . . . . 90
4.21 Illustration of the generation of grid cells . . . . . 92

5.1 Spatial representation in the primate entorhinal cortex. . . . . 95
5.2 Parallel processing streams into the hippocampus . . . . . 97
5.3 Visual place cell from the merging of 'what' and 'where' information 98
5.4 Biological model for the learning of one grid cell . . . . . 99
5.5 Hexagonal teaching signal and the activity of one grid cell learned from it . . . . . 101
5.6 Illustration of the log-polar mapping . . . . . 102
5.7 Images recognition using the combination of 'where' and 'what' information on the image . . . . . 104
5.8 Distribution of the firing field of the grid cell used for the recognition tasks . . . . . 107
5.9 One image used for the training session . . . . . 108
5.10 For the test session, 7 images are randomly selected from the data set of 200 images . . . . . 109

5.11 activity of 7 cells represents respectively 7 images presented sequentially 111
5.12 Example of Seven successive views from the data-set of 4000 images on the road . . . . . 112
5.13 The activities of 7 neurons in response to 70 successive views . . . . 113
5.14 The activities of 7 neurons in response to 70 successive views . . . . 114
5.15 The activities of 7 neurons in response to 70 successive views . . . . 115
5.16 Illustration of the generalization score (GS) and the robustness level of 3 sampled neurons during the process of the testing session . . . . 116
5.17 Scatter figure showing the GS and Robustness of the recognition of 7 neurons under different setups for visual localization . . . . . 117
5.18 The comparison of mean values of the GS and Robustness of the recognition of 7 neurons under different setups . . . . . 118

6.1 Illustration of pathways between cortices and the hippocampus accounting for the spatial representation and image recognition . . . . 124

# List of Tables

2.1 Comparison of the properties of the neurons in a VIF according to the learning rate or decay value and the recalibration method used . . . 50

5.1 Parameters of the model. $Nb_{nr}$ stands for the number of neurons. DoG: difference of Gaussian. GC: grid cells. AoI: area of interest. . . 119

# Glossary of Symbols

| Symbol | Meaning |
|---|---|
| **General notations** | |
| $\boldsymbol{ADN}$ | anterior dorsal nucleus of the thalamus |
| $\boldsymbol{DG}$ | dentate gyrus |
| $\boldsymbol{EC}$ | entorhinal cortex |
| $\boldsymbol{Hipp}$ | hippocampus |
| $\boldsymbol{HD}$ | head direction |
| $\boldsymbol{IT}$ | inferior temporal cortex |
| $\boldsymbol{LEC}$ | lateral entorhinal cortex |
| $\boldsymbol{MEC}$ | medial entorhinal cortex |
| $\boldsymbol{Ph}$ | parahippocampus |
| $\boldsymbol{PI}$ | Path integration |
| $\boldsymbol{PPC}$ | posterior parietal cortex |
| $\boldsymbol{Pr}$ | perirhinal cortex |
| $\boldsymbol{RSC}$ | retrosplenial cortex |
| $\boldsymbol{Sub}$ | subiculum |
| $\boldsymbol{VIF}$ | vector integration field |
| $\mathbf{1}\boldsymbol{D}$ | one-directional |
| $\mathbf{2}\boldsymbol{D}$ | two-directional |
| $\cdot$ | Dot product |

# Abstract

Since the discovery of place cells in the hippocampus, many structures including the entorhinal cortex and retrosplenial cortex, and their interactions with subcortical regions, such as the striatum and the septum, are proven to be involved in the spatial representation which contributes to the formation of the episodic memory along with the temporal representation. The main point of this thesis is to model the interaction of cortical areas and the hippocampus in the medial temporal lobe in order to understand the spatial representation and the recognition mechanism at the neuronal level of humans. Experiments conducted on monkeys, rodents and insects provided us with a global point of view in understanding the basic mechanism on which rely the spatial function, one of the most vital and primary functions to the survival of animals. Thereby, we assume that the spatial functions share some common properties across different species. Following this assumption, a generic model of the spatial function was perceived and has been tested, evolved, and improved for decades taking into account the contemporary biological recordings. Our current model aims to explain from the spatial function to more general functions such as visual recognition using a simple and comprehensive mechanism with respect to biological plausibility. We mainly address four questions: 1) What is the contribution of the retrosplenial cortex in conveying the information of path integration? 2) What is the role of the path integration neural field in the spatial function? 3) How to extend the retrosplenial cortex model to a more generic model explaining the process of perceptions other than the proprioception of self-motion? 4) What is the causal relationship between place cells and grid cells and how do they participate in the navigation and even in other perception processes such as the recognition of views? Our model explains the place cell-like activity found in the retrosplenial cortex and predicts local connectivity between the retrosplenial cortex and the path integration neural field. Grid cells can be generated from cortical inputs during navigation and visual exploration owing to a modulo mechanism implemented in our model. A reciprocal leaning mechanism is proposed to entangle the causal relationship between place cells and grid cells. We suppose that the spatial representation could be the epiphenomenon of a more general recognition mechanism.

# Résumé français

Depuis la découverte des cellules de lieu dans l'hippocampe, de nombreuses structures incluant le cortex entorhinal, le cortex rétrosplénial, et leurs interactions avec des régions sous-corticales, telles que le striatum et le septum, sont prouvées comme étant impliquées dans la représentation spatiale qui, avec la représentation temporelle, contribue à la formation de la mémoire épisodique. Le point principal de cette thèse est de modéliser l'interaction des zones corticales et de l'hippocampe dans le lobe temporal médian afin de comprendre la représentation spatiale et le mécanisme de reconnaissance au niveau neuronal chez l'homme. Les expériences menées sur des singes, des rongeurs et des insectes nous ont fourni un point de vue global sur la compréhension du mécanisme de base sur lequel repose la fonction spatiale, l'une des fonctions les plus vitales et primaires à la survie des animaux. Ainsi, nous supposons que les fonctions spatiales partagent certaines propriétés communes à différentes espèces. Suite à cette hypothèse, un modèle générique de la fonction spatiale a été perçu et a été testé, évolué et amélioré pendant des décennies en tenant compte des enregistrements biologiques contemporains. Notre modèle actuel vise à expliquer de la fonction spatiale à des fonctions plus générales telles que la reconnaissance visuelle en utilisant un mécanisme simple et complet en ce qui concerne la plausibilité biologique. Nous abordons principalement quatre questions : 1) Quelle est la contribution du cortex rétrosplénial dans la transmission de l'information de l'intégration du chemin ? 2) Quel est le rôle du champ neuronal de l'intégration du chemin dans la fonction spatiale ? 3) Comment étendre le modèle du cortex rétrosplénial à un modèle plus générique expliquant le processus des perceptions autres que la proprioception de l'auto-mouvement ? 4) Quelle est la relation causale entre les cellules de lieu et les cellules de grille et comment participent-elles à la navigation et même à d'autres processus de perception tels que la reconnaissance de vues ? Notre modèle explique l'activité des cellules de lieu trouvée dans le cortex rétrosplénial et prédit la connectivité locale entre le cortex rétrosplénial et le champ neuronal d'intégration du chemin. Les cellules de grille peuvent être générées à partir des entrées corticales pendant la navigation et l'exploration visuelle grâce à un mécanisme modulo mis en œuvre dans notre modèle. Un mécanisme d'appui réciproque est proposé pour enchevêtrer la relation causale entre les cellules de lieu et les cellules de grille.

Nous supposons que la représentation spatiale pourrait être l'épiphénomène d'un mécanisme de reconnaissance plus général.

# Introduction

Since the discovery of the place cells in the hippocampus (Hipp) and the grid cells in the entorhinal cortex (EC) we understand better how information related to internal information (vestibular and proprioceptive system, optical flow to compute path integration) or external information (visual landmark, sound, tactile or olfactory information) are exploited by the brain to create codes characterizing a specific place in the environment. Different models such as two-dimensional attractor models, oscillatory interference models and adaptive resonance theory models compete to understand how this information is constructed and how it is handled in behavioural tasks. One of the strong ideas in this thesis is to jointly consider the wide variety of behaviours involving ego and allocentric codes in order to develop and characterize a generic model explaining the observations made by biologists including the place cell-like activity in the retrosplenial cortex (RSC), grid cells in navigation and visual grid cells in EC. This thesis starts with the issue of the role of path integration computation in spatial processing. RSC is known to process path integration and visual information and to translate between egocentric (self-centred) and allocentric (world-centred) spatial information. The contribution of RSC in conveying information of path integration is further studied by complementary simulations using a novel network structure. Next, we propose a simple compression mechanism at the level of EC to address both the formation of grid cells (explaining the hexagonal paving) and the capability of Hipp in merging multimodel information necessary to explain the involvement of Hipp in the formation of episodic memories. Finally, our model proposes a new view of the hippocampal system where the hippocampus proper involves in the self-organization of EC.

## Contributions

Several papers are associated with the present thesis. One submitted paper entitled: *Temporal Integration Can Explain a Range of Spatial Representations in Cortex* proposes a temporal integration mechanism (or a low pass filter) can be used to explain the building of diverse spatial representations in cortices (e.g., RSC, posterior parietal cortex). We show the low pass filtering of movement direction cell activity is suffi-

cient to perform path integration and to explain the route-related activities recorded in RSC. We propose that various neural fields of path integration can be built to track different targets and to update information according to different references. We discuss the ability of RSC to maintain a perception of progress along a route and to switch between egocentric and allocentric frames of reference. Changing the neuron's time constant, its preferred direction, its initial activity level and the direction of the movement can produce a wide range of results that can be interpreted as cells having different functions or frames of reference in RSC. The model shows path integration can be approximated from low pass filters if their input is HD cells-like activities (1D ring of neurons). The simulation shows that the different recordings in RSC may correspond to the "signature" of path integration coded on a 1D ring of neurons. Simulations show that the cell activities are consistent with recordings from RSC (Alexander and Nitz, 2015) using our biologically inspired model.

In a published paper called: *A model of path integration and representation of spatial context in the retrosplenial cortex*, we studied in detail the impact of our vector integration field hypothesis. We explained different results obtained by Mao Mao et al., 2017 assuming Kohonen maps are clustering the local activities of our VIF. Inspired by recent biological experiments (Mao et al., 2017), we simulate animals moving in different environments (open space, spiral mazes and on a treadmill) to test the performances of our simple model of RSC conveying information of the path integration. The effect of different sizes of the bump of movement direction cells is studied to approximate path integration. The diverse activities obtained from self-organizing maps are also discussed to explain some results of the biological experiments. Taking inputs coming from a narrow neighbouring projection of our path integration field creates place cell-like activities in RSC when the mouse runs on the treadmill. This can be the result of local self-organizing maps representing blobs of neurons in RSC (e.g. cortical columns). Other simulations show that accessing the whole path integration field would induce place cells whatever the environment is. Since this property is not observed, we conclude that the categorization neurons in RSC should have access to only a small fraction of the path integration field. The connection between Hipp, RSC and EC is revealed through a novel perspective. We defend the idea that path integration can be performed outside Hipp by the information coming from RSC. We suppose some neurons in EC perform a code compression taking inputs from our path integration fields in RSC. The observation of visual grid cells is a good example of such a general compression mechanism in addition to classical grid cells. We suppose Hipp detects and codes transitions between multi-model states which is very important to detect new complex states for the learning of complex conditioning and/or the building of episodic memories. The mapping property can be an incidental effect of this general property when we study animals doing only navigation tasks.

An ongoing paper is now focusing on building grid cells in EC from the compression of afferent cortical activity using modulo operators that could result from a self-organization mechanism. Our model could explain why the visual exploration of an image (Killian et al., 2012) could induce grid cell activities in EC. We aim to design a coherent model accounting for different loops between the cortex and the hippocampal system (including EC) to explain the generation of grid cells in EC from the hippocampal place cells and the different cortical and subcortical inputs.

## Layout of the thesis

The biological background and state of the art of our model are introduced in chapter 2. Chapters 3, 4 and 6 in this thesis are written as individual papers. Each of them contains a complete abstract, introduction, simulation, and conclusion.

In chapter 3, we simulate animals moving in different environments (open space, spiral mazes and on a treadmill) to test the performances of a simple model of RSC acting as a path integration (PI) and as a categorization mechanism. The connection between Hipp, RSC and EC is revealed through a novel perspective. In our model, PI is performed by a 1D field of neurons acting as a simple low-pass filter of head direction (HD) cells modulated by the linear velocity of the animal. Recording of neurons on our 1D PI field shows these neurons would not be intuitively interpreted as performing PI. Using inputs coming from a narrow neighbouring projection of our PI field creates place cell-like activities in RSC when the mouse runs on the treadmill. Other simulations show that accessing the whole PI field would induce place cells whatever the environment is. Since this property is not observed, we conclude that the categorization neurons in RSC should have access to only a small fraction of the PI field.

In chapter 4, we emphasize the idea that RSC conveys path integration(PI) information to the hippocampal system. We further emphasize that the absence of place cells in RSC is due to the difficulty of neurons accessing the whole PI neural field. Our model shows the potential of the PI neural field in reproducing diverse neuronal activities such as place cells and movement direction cells involved in the spatial representation of animals. To address the cost and capability issue of Hipp due to the limited number of neurons and synaptic connections of each neuron and numerous afferent signals to Hipp including the proprioception of self-motion and the information of different types of perceptions. We propose the crucial role of EC as a hub to merge the different afferent cortical activities in order to build an efficient hash code for complex pattern recognition and novelty detection at the level of Hipp. We suppose the grid cells in navigation could be an epiphenomenon of this generic compression mechanism in EC.

In chapter 5, we introduce the hypothesis of the important role of the causal

relationship between the place cells and EC in the generation of grid cells and place cells during early development. Due to time constraints, the model accounting for the dynamic adaptation of the synaptic connectivity between Hipp and cortices and the interactive generation of place cells and grid cells has not been accomplished. Some of the preliminary simulation results are shown to support our hypothesis and encourage further research in the elaboration of this model.

In chapter 6, we propose a general model explaining the generation of the visual grid cell along with its involvement in the visual recognition tasks independent of the locomotion or speed information. We suggest EC plays the role of a compressor of not only the spatial information but also visual input in order to establish an efficient and stable representation of recognition in the hippocampal formation. The navigation feature could be the epiphenomenon of this general recognition mechanism.

# Chapter 1

# Biological background and State of the art

In this chapter, we will introduce neurobiological data related to the retrosplenial cortex (RSC), entorhinal cortex (EC) and hippocampus (Hipp) and modelling background, as well as an overview of the most discussed models. We will try to model in the next chapters for place recognition and navigation tasks. For decades, the aim of our group has been to build a general model accounting for basic mechanisms underpinning the navigation and recognition across species in order to contribute to a better understanding of the human brain. We therefore focused on the illustration and demonstration of the hippocampal formation and surrounding cortices of humans, which are widely considered to play an important role in spatial navigation and declarative memory. Nevertheless, biological studies in other species including insects, rodents and other mammals have also provided us insights to build a general model. It is well known that the human and rodent brain share common properties (Andersen et al., 2006) in their architecture and cell types not to mention the similarities in the neural layout and pathways within the hippocampal formation and surrounding cortices in all mammals. Experiments have shown that the primate Hipp has different spatial representations compared to the rodent Hipp due to the development of the primate fovea (Rolls and Wirth, 2018). The representations of spatial scenes rely on the spatial view cells in the primate Hipp while the place cell found in the rodent Hipp provides a representation of where the rodent is located. Nevertheless, the spatial representation of primates and rodents could still originate from homologous mechanisms.

## 1.1 Spatial role and connectivity of retrosplenial cortex

The retrosplenial cortex has long been associated with navigation, owing to its connectivity to other navigation-related regions. It is centrally situated between the

limbic areas including the hippocampus formation, the anterior thalamic nuclei, and the parahippocampal region and the cortical areas such as the prefrontal cortex, the parietal cortex and the visual cortex (Wyass and Van Groen, 1992; Reep et al., 1994; Vann et al., 2009; Czajkowski et al., 2013). In figure 1.1, we have a schematic overview of the organization of retrosplenial circuitry in rodents.

Its significance in navigation has been proven in the last twenty years. Technically, studies in humans can be problematic due to the position of RSC deep in the callosal sulcus and the difficulty in distinguishing RSC participation from that of surrounding areas (Fig. 1.2). Rodent models, on the other hand, are comparatively easier in assessing RSC contributions because of their relative size and accessibility, as well as similarities in structure and connectivity across species. The conception of our model of the PI process in RSC is directly inspired by the biological recordings of various species in order to preserve the generality of our model. Different recordings in RSC point to the possibility that RSC could play a crucial role in the PI. The spatial firing of hippocampal place cells has been found in blind rats by Save Etienne (Save et al., 1998). Cooper's team found that RSC inactivation selectively impairs navigation in darkness (Cooper and Mizumori, 1999) and they also found that RSC contributes to spatial memory and navigation without visual cues (Cooper et al., 2001). Other recordings indicate the involvement of RSC in the encoding and storage of spatial information (Czajkowski et al., 2014). The place cell activity found in RSC could also be a trace of this PI. In 2017, Mao and Mcnaughton's team (Mao et al., 2017) found a Sparse orthogonal population representation of spatial context in RSC. They have mice head-fixed moving on a 150-cm linear treadmill. A drop of sucrose water was delivered at a fixed location for every complete lap performing as a reset of one treadmill loop. When the mice run on the treadmill, the activity of neurons in RSC of mice is recorded. The authors found place cell-like activities with distinct neurons firing as the animal travels a specific distance in the treadmill.

Spatial navigation requires a continuous perception of progress along a route such as path integration and the ability to seamlessly switch between different frames of reference. The spatial information in an allocentric frame of reference often represents the position of objects relative to the environment extrinsic to the perceiver (e.g. place cells). An egocentric frame of reference includes spatial information about the location or action of the perceiver related to which the position of objects is represented (e.g. a desk to my left). A route-centric frame may be related to how much progress one has made on a navigation plan (e.g. ramped activity with the animal's progression) or may specify a route-specific action (e.g. stronger responses to one turn in a series of turns). In both cases, these responses are informative of the animal's position along route space, differing from place-specific or proprioceptive information.

All three of these reference frames have been observed in rodent brain record-

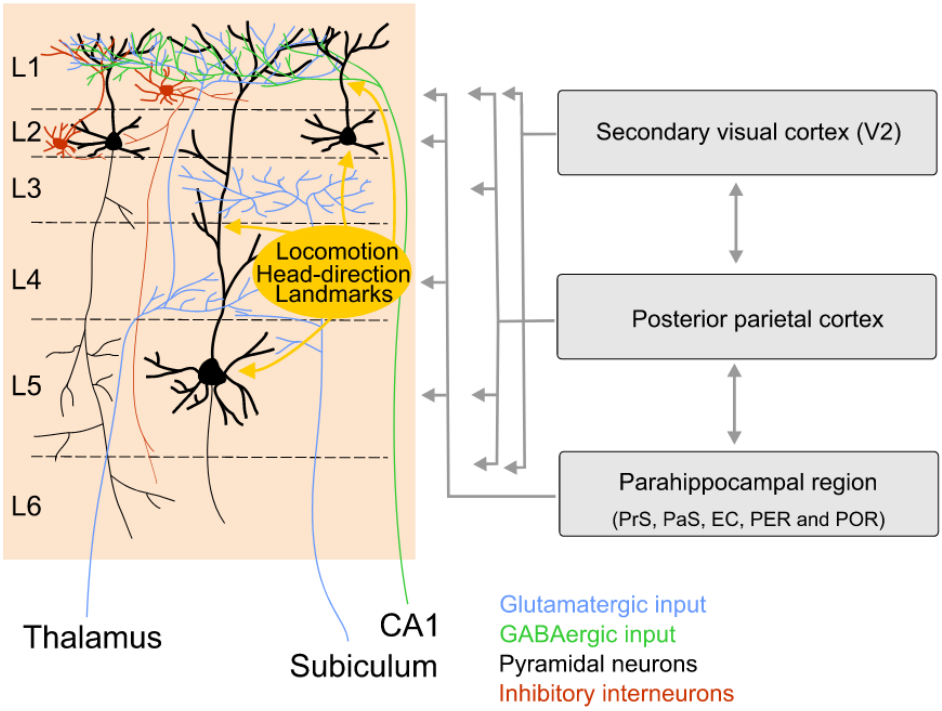


Figure 1.1: Schematic overview of the organization of retrosplenial circuitry in rodents. Retrosplenial cortex (RC) layer 1 integrates glutamatergic thalamic and GABAergic hippocampal inputs. Neurons from layers 2/3 and 5 extend their dendrites to this layer. Although the subicular input densely innervates layer 3, in mice, it evokes mainly perisomatic responses in layer 5 neurons, indicating functional collaterals in deeper layers. Inhibitory neurons of layer 1 possibly contact pyramidal neurons of layer 2, as in rats, those are inhibited by stimulation of layer 1. The inhibitory neurons of layer 1 innervate layer 1, but some axons also reach deep layers 5–6. Late spiking layer 2 neurons project to the contralateral hemisphere but also show extensive axonal arborizations in layer 5 and 6 in rats. Parvalbumin expressing GABAergic neurons in layer 2 may provide further feedforward inhibition to layer 2 pyramidal neurons. These interneurons extend their dendrites to layer 1, possibly receiving the same thalamic input. Together with layer 2 pyramidal neurons, their apical dendrites form dendritic bundles typical for the rat RC. Input from parahippocampal, parietal, and visual regions based on anatomical tracing in rats are shown in grey. Note that the RC is reciprocally connected with these regions, but for clarity, only the inputs are shown and the exact laminar termination may differ depending on specific subregions. The head direction, locomotion, and landmark information (yellow) that is provided by the different regions is integrated by both somatic and dendritic parts of the neurons. Abbreviations: EC, entorhinal cortex; PaS, parasubiculum; PER, perirhinal cortex; POR, postrhinal cortex; PrS, presubiculum. (Stacho and Manahan-Vaughan, 2022)

ings. Neurons in Hipp and several regions demonstrate that allocentric place fields respond to head direction, a form of allocentric coding (Cullen and Taube, 2017).

route modulated turn cells and cells that encode route progress in the posterior parietal cortex (PPC) have been found to encode route specificity (Nitz, 2006; Nitz, 2012). Recordings of neurons in RSC suggest an important role of RSC in translating between egocentric (perceiver-centered) and allocentric (environment-centered) frameworks (Vann et al., 2009; Mitchell et al., 2018). Studies indicate the role of RSC in processing "where and when" information (Ritchey et al., 2015; Todd and Bucci, 2015). Some neural models of spatial memory and imagery (Byrne et al., 2007; Bicanski and Burgess, 2018) emphasize the role of RSC in transforming an egocentric frame of reference to an allocentric frame of reference.

Experiments (Alexander and Nitz, 2015) showed the capability of RSC in mediating different forms of spatial representation due to its dense interconnections with multiple cortical and subcortical brain regions involved in the registration of animal's position. These regions having reciprocal connections with RSC includes the parietal cortex, hippocampus, MEC, subiculum, anterior cingulate and anterior thalamic nuclei (Wyass and Van Groen, 1992; Reep et al., 1994; Czajkowski et al., 2013). In the experiments, neurons in RSC fire selectively to the position in two distinct, external spatial frames of reference while simultaneously distinguishing the animal's left- versus right-turning behaviour which is characterized as an egocentric perception.

Works in (Bicanski and Burgess, 2016) focus on modelling head direction cells in RSC using a conjunctive representation of place and head directions to correct parallax issues related to visual landmarks.

The path integration mechanism and the transformation between allocentric and egocentric reference which are probably processed in RSC could underpin the navigation tasks in the Morris water maze (Morris, 1981), a task where the animal learns a platform location in the water and must then navigate to that location from four different starting locations using both proximal and distal cues or only the distal ones. The experiment showed that the rats managed to learn the platform location even without the proximal cues sustaining slightly longer escaping time than those who got access to the proximal cues. Impairments of goal finding in the Morris water maze are also observed after lesions of EC (Steffenach et al., 2005) or lesions of the medial septum (Marston et al., 1993). Lesions of RSC (Czajkowski et al., 2014) and parietal lesions (Hoh et al., 2003) both disrupt the performance in this task.

All these recordings suggest that navigation tasks require a system consisting of RSC and hippocampus formation which is consistent with the predictions of our model.

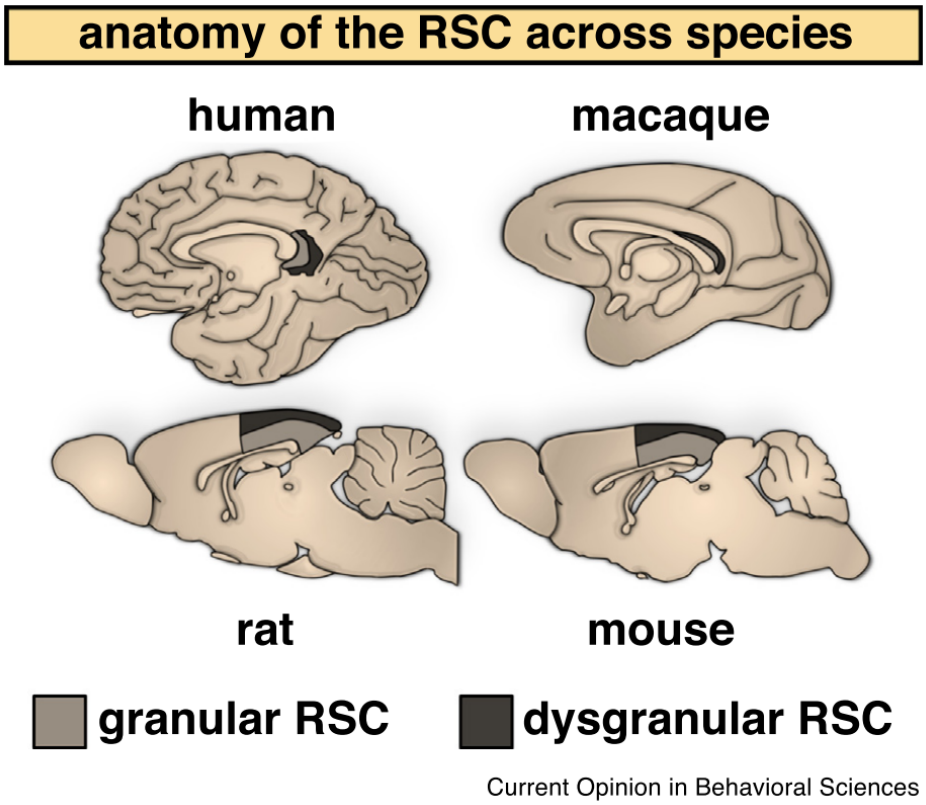


Figure 1.2: Anatomy of RSC across species. The gross anatomy of the retrosplenial cortex (RSC) across species is preserved. Human and macaque RSC wraps around the caudal aspect of the splenium of the corpus callosum while in rodents, it is located dorsally and spans nearly half the length of the cerebrum. RSC is subdivided into granular and dysgranular regions, corresponding to Brodmann areas 29 and 30, respectively. Despite differences in relative location and size, primate and rodent RSC displays similar cytoarchitectonic properties and shares homologous connectivity with other regions (Milczarek and Vann, 2020).

## 1.2 Path integration

Path integration calculates the current position and path back to a starting place by summing the vectors of distance and direction travelled. In the following sections, a primary model of path integration in RSC is introduced. In addition, some of the biologically inspired learning rules wildly used in our model are also explained preliminarily.

Our original model takes a theoretical one-dimensional ring of neurons to perform PI. The process of the path integration is based on the integration of movement direction information over a virtual vector integration field as illustrated in (fig. 1.3). Let's imagine an animal travels from origin to points A, B, and stopped at C.

The global homing vector from point C to the origin will be C0, the inverse of the sum of vectors 0A, AB and BC. The activity of neural fields with a cosine shape centered on each movement direction is shown in (fig. 1.3, right). The sum of the 3 curves has a maximum activity (bold curve) for the direction of the global movement. Details of the calculation of the path integration in our model will be further discussed in the next chapter.

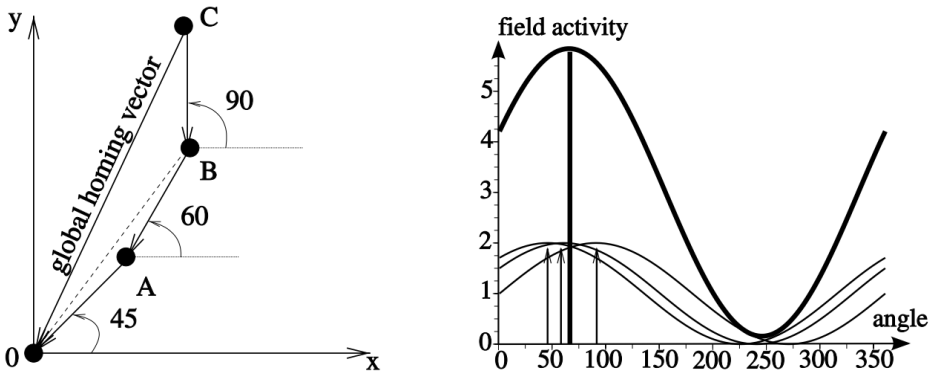


Figure 1.3: An example of path integration. Left figure shows a simulated trajectory composed of 3 movements of the same length in the direction 45°, 60°and 90°from an absolute direction. Right figure shows the sum of the associated 3 inputs (neural fields with a cosine shape centered on each movement direction). The sum of the 3 curves has a maximum activity for the direction of the global movement (Gaussier et al., 2007).

The conceptual path integration neural field is derived from the firing distribution of the head direction cells. The peak of each bump resides in the preferred direction of the corresponding HD cell. The ring of neurons is an attractor network as described in (McNaughton et al., 1991) as shown in (fig. 1.11).

### 1.2.1 Neural field and Continuous attractor

Population coding based on a population of neurons on a neural field is a way of coding information in a distributed manner opposite to single neuron coding. A popular concept of single neuron coding is the grandmother cell which would be activated only when we think of our grandmother. Similarly, other neurons could combine with different objects and be activated by the corresponding stimuli. The information contained in a single neuron is more intuitive and accessible compared to the information conveyed by a neural field. However, the population coding based on the neural field is redundant and stable which is crucial for the survival of animals and to avoid hard-wiring complex mathematical functions. The perturbation or damage in several neurons in a neural field would not dramatically disturb the overall information processed for each neuron in the neural field conveying a small portion of

the information. Bubbles of activity in brain tissue were found in 1956 (Beurle, 1956) leading to the study of continuous attractor in the neural field in which neighbouring neurons share similar characteristics and therefore creates a continuity in the neural space with the help of lateral connectivity. In the model of Amari (Amari, 1977b) the dynamic neural field was proposed in which neurons are subject to a center-on surrounding-off lateral connectivity (local excitation and distal inhibition). The lateral interaction kernel is often simulated by a difference of Gaussian functions (DoG) with the shape reminiscent of a Mexican Hat (fig. 1.4 top). The dynamic neural field model maintains a balance between competition and cooperation while the winner takes all mechanism is exclusively competitive. Let's imagine a neural field with a population of neurons linked closely together, forming a one-dimensional map. Each neuron is connected to its neighbors according to a rule defined by the lateral interaction kernel. This kernel is calculated by a difference of Gaussian functions (DoG), which gives it the shape of a Mexican hat. The center-on surrounding-off lateral connectivity is demonstrated in (fig. 1.4 bottom).

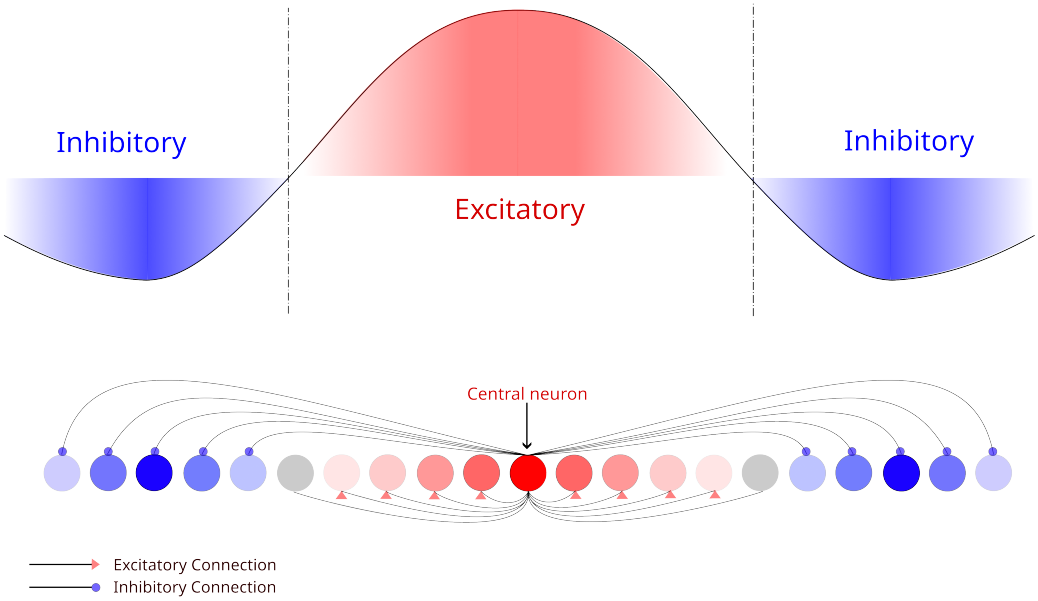


Figure 1.4: Top, an example of a lateral interaction kernel. Bottom, strength and type of lateral connections between the central neuron and its neighboring neurons as a function of distance.

This structure gives the population of neurons the attractor property that converges to the local maxima of the activity field. Let's imagine a circumstance where two bumps of activity appear in the local neural field. The competition feature of the network will dominate if two bumps are far away enough. The dynamics of the field will tend to select a more active one between them. On the other hand, if the two inputs are sufficiently close, the two fields will converge towards a single bump.

This bump results from the average of the two inputs which means the cooperation feature of the network acts.

The structure of the self-organizing map (Kohonen, 1982) which is "a generalization of the formation of direct topographic projections between two laminar structures known as retinotectal mapping" (Amari, 1980) is based on the dynamic neural field (Amari, 1977b). A neural field model was proposed to computationally investigate the formation and reorganization of topographic maps in the somatosensory cortex (Detorakis and Rougier, 2012). The concept of continuous attractor and neural field dynamics has been implemented into the application of an autonomous robot architecture. The robot system was endowed with a form of obstacle memory and thereby realized target acquisition and obstacle avoidance (Schöner et al., 1995b). The shape of the interaction kernel is important and must be parameterised according to the desired task. The width of the excitation bubble (positive part of the kernel) can be modulated for example. Note that a "Winner Takes All" type network is a special case of the neural field for which the excitation bubble of the kernel is reduced to the minimum (only 1 neuron). The network also includes recurrent links, which are not shown in the figures. This recurrence allows for temporal smoothing and thus effective filtering against noise or oscillations in the input. For example, if an input appears episodically following the malfunction of a sensor, the temporal dynamics of the network will not allow it to impose itself. It is necessary for input to remain stable and immobile for a certain period of time in order to be considered trustworthy and thus for a bubble of activity to emerge at the output. In contrast to the dynamic neural field, neurons on the path integration field do not require lateral interaction which frees itself from the topological constraint.

### 1.2.2 Head direction cell

The recorded HD cell activity can cover an area which seems to vary from 60° to 180° (Taube, 1995; Taube, 1998; Taube et al., 1990b). The Gaussian function shown in (fig. 1.5 b) with a positive value covering 120° looks like the HD cells found in the lateral mammillary nuclei. The cosine-shape bump of the firing rate is needed to perform a perfect computational integration while the use of the Gaussian-shape bump of the firing rate is more biologically plausible. The results differ according to the exact shape of the kernel used. It induces over or underestimations of the PI that could explain some of the systematic bias in PI observed in different species (Wehner et al., 1996; Wittmann and Schwegler, 1995).

In our model, the primary inputs are the head rotational speed and the linear speed. According to the head rotational speed, a bubble of activity is moved clockwise or counterclockwise on a ring of neurons corresponding to the HD cells.

The bump of the activity of HD cells is simply simulated by a cosine shape or

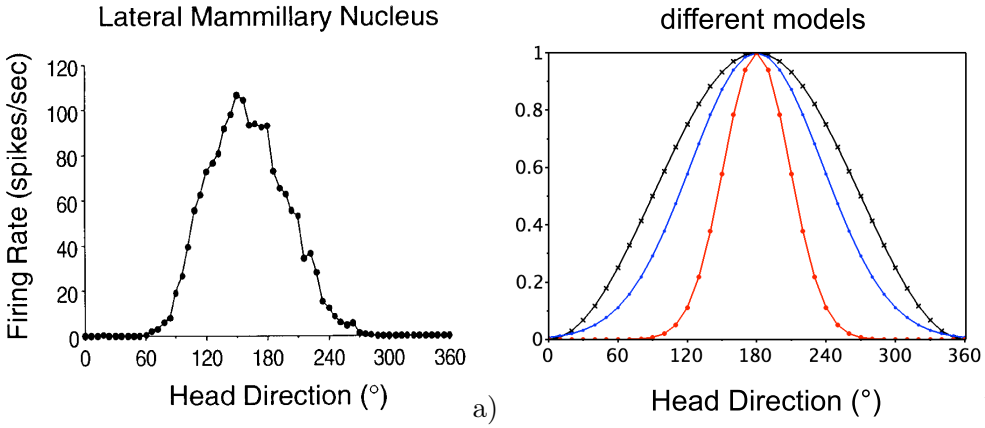


Figure 1.5: Comparison between HD cells and Gaussian shapes. a, Recording from Taube (Taube, 1998) of the mean frequency activity of one head direction cell. b, Comparison with a shifted cosine shape (in black) and two Gaussian shapes: in blue $\sigma = 1$ and in red $\sigma = 0.5$ with x-axis the $\theta$ angle converted in degrees x=$\theta/\pi \cdot 180$ and $\theta_0 = \pi/2$

a gaussian shape. To simplify, we will assume in the following sections that head direction corresponds to the direction of movement and that the recognition of some cues $D_j$ can be used to recalibrate the head direction.

### 1.2.3 Integration of activity of head direction cell

To calculate the path integration, short-term memory (STM) (fig. 1.6. left) and classical conditioning mechanism with least mean square rule (fig. 1.6. right) are two plausible candidates (Widrow and Hoff, 1960; Rescorla, Wagner, et al., 1972). Equations of the classical conditioning mechanism with LMS:

$$V_i(t) = f(\sum W_{ij} \cdot C_j) \text{ with } f(x) = \begin{cases} 0 & \text{if } x < 0 \\ x & \text{if } 0 \leq x < 1 \\ 1 & \text{if } x > 1 \end{cases} \tag{1.1}$$

The weight modification of the conditioning mechanism implemented with the LMS in our model is defined as:

$$dW_{ij} = \lambda C_j (H_i - V_i) \tag{1.2}$$

with $C_j$ (context) the conditional input, $V_i$ the output and $H_i$ (speed modulation HD activity) the desired output or the unconditional input. The conditional input is activated (activity = 1) when the animal moves ($C_j = 0$ otherwise). The weight $W_{ij}$ converges to the average of the $H_i$ values. $\lambda$ controls the learning rate of the

neuron's potential ($0 < \lambda < 1$). In the LMS rule, the learning rate is identical to the decay rate of the neuron's potential.

The simple feed-forward classical learning mechanism using LMS rule in our model is equal to using some recurrent connection (Grossberg, 1969; Grossberg, 1978; Elman, 1993; Dominey et al., 1995) representing a linear first-order recurrent filtering or an STM (see fig. 1.6).

Equations of the STM:

$$V_i(t) = (1 - \lambda)V_i(t - dt) + \lambda H_i(t) \tag{1.3}$$

On the other side, if we consider a conditioning mechanism implemented with the LMS (Least Mean square rule (Widrow and Hoff, 1960; Rescorla, Wagner, et al., 1972)) then the weight modification is defined as:

$$dW_{ij} = \lambda I_j(O_i^d - O_i) \tag{1.4}$$

with $I_j$ the conditional input, $O_i$ the output, and $O_i^d$ the desired output or the unconditional input. If we consider the unconditional stimulus is $H_i$ and the conditional link is related to one context always activated for the past (its activity is 1) and the conditional output is our vector field $V_i$ then the equation (1.4) is equivalent to:

$$dW_{ij} = \lambda(H_i - V_i) \tag{1.5}$$

Since the conditional input (i.e context) is set to 1 in a given experiment then the neuron output $V_i = W_i \cdot 1$. If we replace $W_i(t)$ by $W_i(t-dt)+dW_i(t-dt)$, we obtain:

$$V_i = W_i(t - dt) + \lambda(H_i(t - dt) - V_i(t - dt)) \tag{1.6}$$

Since we have also $V_i(t - dt) = W_i(t - dt) \cdot 1$, equation (1.6) can be rewritten as :

$$\begin{aligned} V_i &= V_i(t - dt) + \lambda(H_i(t - dt) - V_i(t - dt)) \\ &= (1 - \lambda)V_i(t - dt) + \lambda H_i(t - dt) \end{aligned} \tag{1.7}$$

We can see that equation (1.7) is the same as equation (1.3) except for the time step of $H_i$. The main difference is of course that in the first case, the memory relies on the recurrent reactivation of neurons while in the second case the memory is stored in the synaptic weights which makes the model simple and more feasible. The feedforward solution is also an easy way to modulate the time constant at the synaptic level and to maintain the field memory over a longer period if the animal is not moving. Thus, avoiding the risk of STM deterioration related to the need to always reenter the past activity. Moreover, since the constant input can be a context, a better control of when the field has to be modified can be achieved.

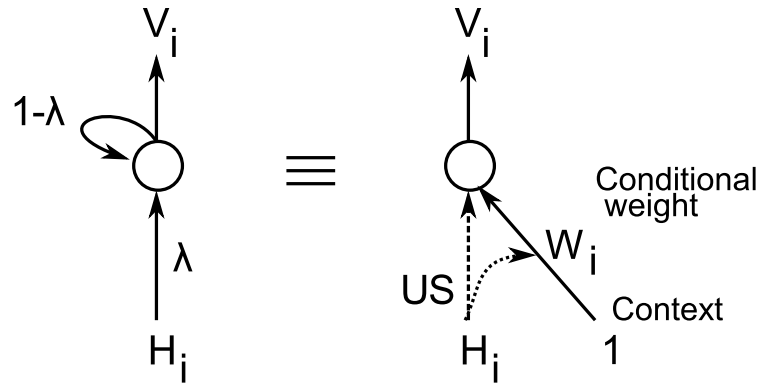


Figure 1.6: Equivalence between the STM scheme (left) and a feed-forward scheme using synaptic learning from a constant input context (right).

## 1.3 Self-organized maps to mimic cortical columns

The cerebral cortex mostly consists of the six-layered neocortex. It is usually subdivided into cortical columns that self-organize and perform categorization of their inputs (Burnod et al., 1999). There are 50–100 cortical minicolumns (1.7) in a hypercolumn, each comprising around 80 neurons. Connections "up" and "down" between neurons within the thickness of the cortex are much denser than connections that spread from side to side. Within an orientation column, neurons throughout the vertical thickness of the cortex respond to stimuli oriented at the same angle (Hubel and Wiesel, 1968; Hubel et al., 1977). A neighboring column will then have neurons responding to a slightly different orientation from the one next to it. In our model, we implement a self-organization map (SOM) in order to simulate the hypercolumns. Neurons on the cortical minicolumns are simulated by neurons on the one-dimensional SOM. The activity of neurons on the PI field is projected to a set of 1D SOM. Each neuron on the PI field projects to every neuron on a 1D SOM (Fig. 1.8). The problem with training the Kohonen map is that using subtraction to calculate the difference between the input vector and the weight vector is hard to find in the biological neurons. Cosine similarity is an alternative metric to avoid the subtraction operation.

The activity of neuron k on the SOM is the following:

$$E_j = \left( \frac{\sum P_i(t) \cdot W_{ij}(t)}{\sqrt{\sum P_i(t)^2 \cdot \sum W_{ij}(t)^2}} \right), j \in [1, M], i \in [1, N] \tag{1.8}$$

The index of the winner neuron $j^w$ is defined as:

$$j^w(t) = arg\ max\left(E_j\right), j \in [1, M] \tag{1.9}$$

N is the number of neurons on the PI field. M is the number of neurons on each 1D SOM. The synaptic weights between neurons on the input field $P_i$ and neurons on the SOM is updated by:

$$W_{ij}(t+dt) = \lambda_{som} \cdot (P_i(t) - W_{ij}(t)) \cdot S_j(t) \tag{1.10}$$

$\lambda_{som}$ is the learning rate of self-organization. The lateral connectivity of neurons on the 1D SOM is subject to a simple Gaussian function $h(d)$ such as:

$$\begin{aligned} S_j(t) &= h(d_j) \cdot S_{j^w}(t), \text{ with} \\ h(d_j) &= (\frac{1}{\sigma \cdot \sqrt{2 \cdot \pi}} \cdot exp^{-\frac{d_k^2}{2 \cdot \sigma}} \end{aligned} \tag{1.11}$$

$S_j(t)$ is the potential of the j-th neuron. $d_k$ represents the distance between the winner neuron $j^w$ and other neurons $j$ on the SOM.

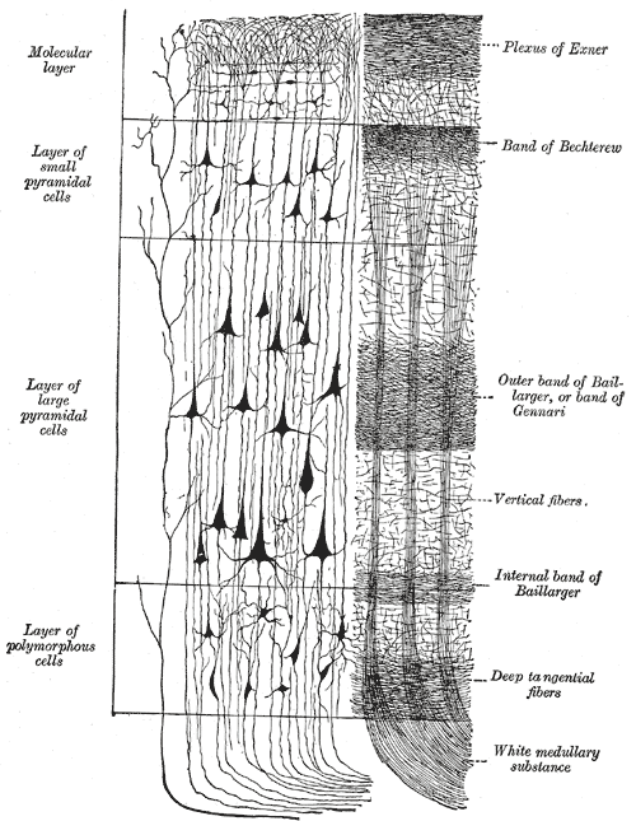


Figure 1.7: Cerebral cortex. To the left, the groups of cells; to the right, the systems of fibers. Quite to the left of the figure, a sensory nerve fiber is shown. Cell body layers are labelled on the left, and fiber layers are labelled on the right. (Gray, 1878)

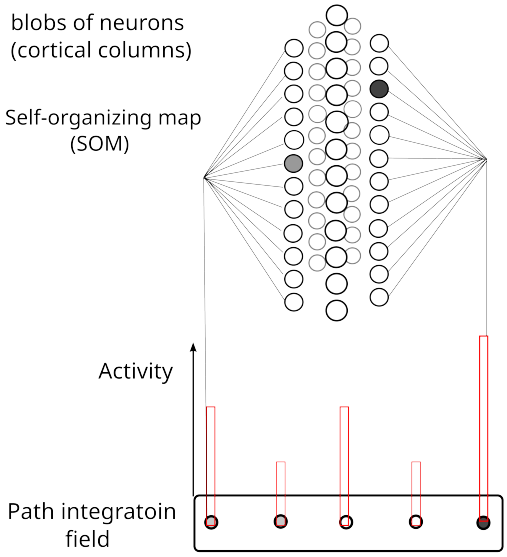


Figure 1.8: Demonstration of the discretization of the activity of neurons on the PI field.

The cortical hypercolumn is thereby simulated by the combination of multiple 1D SOMs with each neuron in the hypercolumn selectively sensitive to a certain travelling vector of the path integration.

## 1.4 The place cell and hippocampal system

The place cell responding specifically to the current location of the animal was first found by O'Keefe and Dostrovsky (O'Keefe and Dostrovsky, 1971) in Hipp. Different place cells have different firing locations (place field) (O'Keefe, 1976). No topological correlation was found among neighboring place cells (Wilson and McNaughton, 1993) while the size of the firing fields of place cells increases from dorsal to ventral hippocampus (Jung et al., 1994; Kjelstrup et al., 2008).

The hippocampus is important for spatial navigation, short-term memory, recognition, novelty detection, and long-term memory consolidation. It is composed of three substructures: the subiculum, CA1, CA2, CA3 regions and the dentate gyrus.

The entorhinal cortex communicates spatial and objects information to Hipp from the parahippocampal and perirhinal cortices, respectively. The fornix then transmits object-in-context information to the mammillary bodies, which in turn transport it to the anterior thalamic nuclei through the mammillothalamic tract. Despite the diffusion of the system, much of the information is conveyed through the cingulum to RSC, frontal and posterior neocortical regions, and back to Hipp.

The feed-forward link from the grid cell to the place cell has been widely accepted

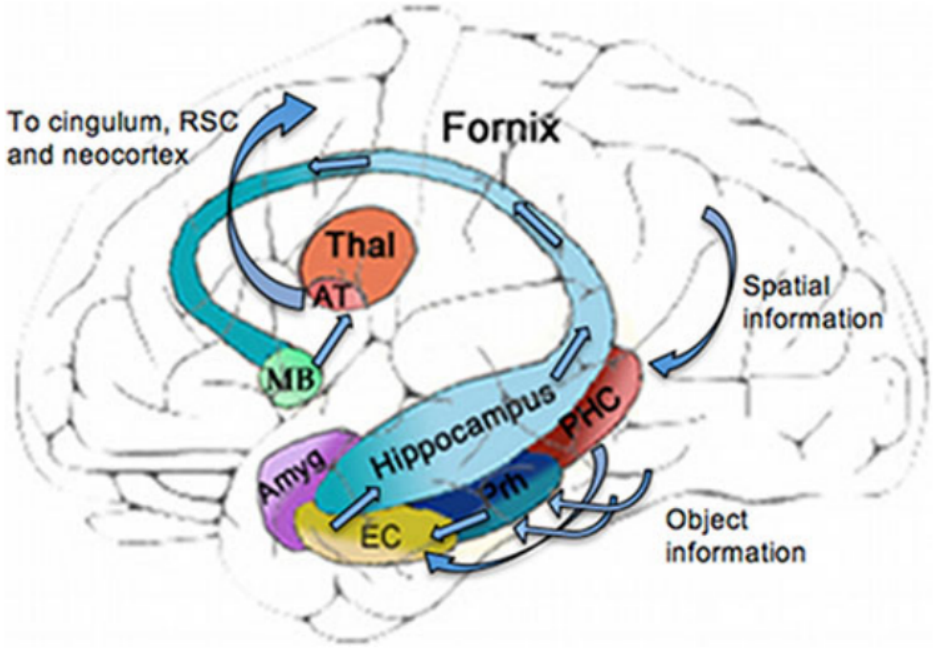


Figure 1.9: A schematic representation of the extended hippocampal system. Spatial and object information converge into the parahippocampal and perirhinal cortices, respectively, and are relayed to the hippocampus through the entorhinal cortex. Object in context information is then transmitted through the fornix to the mammillary bodies, and through the mammillothalamic tract to the anterior thalamic nuclei. From that point, the system becomes more diffuse, but much of the information is relayed through the cingulum to the retrosplenial cortex and to frontal and posterior neocortical structures, as well as back to the hippocampus. Amyg, amygdala; AT, anterior thalamus; EC, entorhinal cortex; MB, mammillary bodies; PHC, parahippocampal cortex; Prh, perirhinal cortex; RSC, retrosplenial cortex; Thal, thalamus. (Rosenbaum et al., 2014)

and thus become one of the essential pathways that account for the emergence of the place selectivity in Hipp (O'keefe and Burgess, 2005; Fuhs and Touretzky, 2006; McNaughton et al., 2006; Sheynikhovich et al., 2009; Pilly and Grossberg, 2012).

Nevertheless, biologists also found PC emerges before the maturation of the GC (Langston et al., 2010; Wills et al., 2010; Muessig et al., 2015), and new place codes can be generated under the septal disruption which disrupts theta oscillations and grid cell firing (Brandon et al., 2014). These recordings indicate that clear place selectivity in Hipp can emerge even without well-stabilized grid cells.

Besides the spatial information carried by grid cells, heterogeneous input including olfactory information, auditory information, and tactile information can contribute to the place selectivity in Hipp (Zhang and Manahan-Vaughan, 2015; O'keefe and Nadel, 1979; Save et al., 1998). It seems the motion-related information in con-

junction with stimulus recognition is sufficient for the location-specialized firing of place cells. In addition, the Visual information alone was sufficient for localized firing by 25 percent of place cells examined in experiments on head-fixed mice navigating in a virtual environment (Chen et al., 2013).

Redish and Touretzky (Redish and Touretzky, 1997) presented a conceptual framework accounting for the function of Hipp and its connected structures in navigation. The spatial code of place cells is supposed to be created from visual information of local views and idiomatic information conveyed by path integration via the subiculum. Hippocampal place cell models taking inputs from visual sensory and idiothetic path integration have been successfully implemented in real robots to accomplish navigation tasks (Arleo and Gerstner, 2000; Gaussier et al., 2002; Milford et al., 2004).

Since the discovery of the place cells, studies on the role of Hipp started from its involvement in spatial navigation and extend to a crucial contribution to the storage and retrieval of explicit (declarative) memories (Moser et al., 2015), including the recognition memory and the memory of the location underlying the episodic memory.

In 1957, WB Scoville and B Milner have shown dramatic evidence that bilateral removal of large portions of the hippocampal system and other temporal lobe structures produce a profound deficit in recent memory while leaving other cognitive functions and memory performance based on experience acquired before the lesion intact (Scoville and Milner, 1957). One hypothesis has been made that memories are first stored via synaptic changes in the hippocampal system, and that remote memory is based on accumulated neocortical changes (McClelland et al., 1995).

A memory category tree chart is illustrated in (fig.1.10), the bolded topics will be further discussed in this thesis.

Inspired by a neurobiological model of temporal sequences learning in Hipp (Banquet et al., 1997; Gaussier et al., 1998), the transition cell was introduced in (Gaussier et al., 2002; Cuperlier et al., 2006) to address the limitation of sequence learning based on the gradient-descend mechanism. The transition-prediction cell is crucial for the action selection when more than one movement is associated with one single place recognition. Each movement should link to one specific internal representation which is derived not from only the scene recognition but also the transition state. The transition cells take inputs from the derivative of the current place and the memory of the previous input. The activity of the transition cells is determined by the summation of the activity of all the inputs with a threshold mechanism. The synaptic linkage between the preceding input and the transition states on the cognitive map can be updated subject to the Hebbian learning rule, and thus enable the prediction of transitions. The transition memory used for the generation of the cognitive map in navigation tasks could be the epiphenomenon of the general contribution of Hipp in declarative memory.

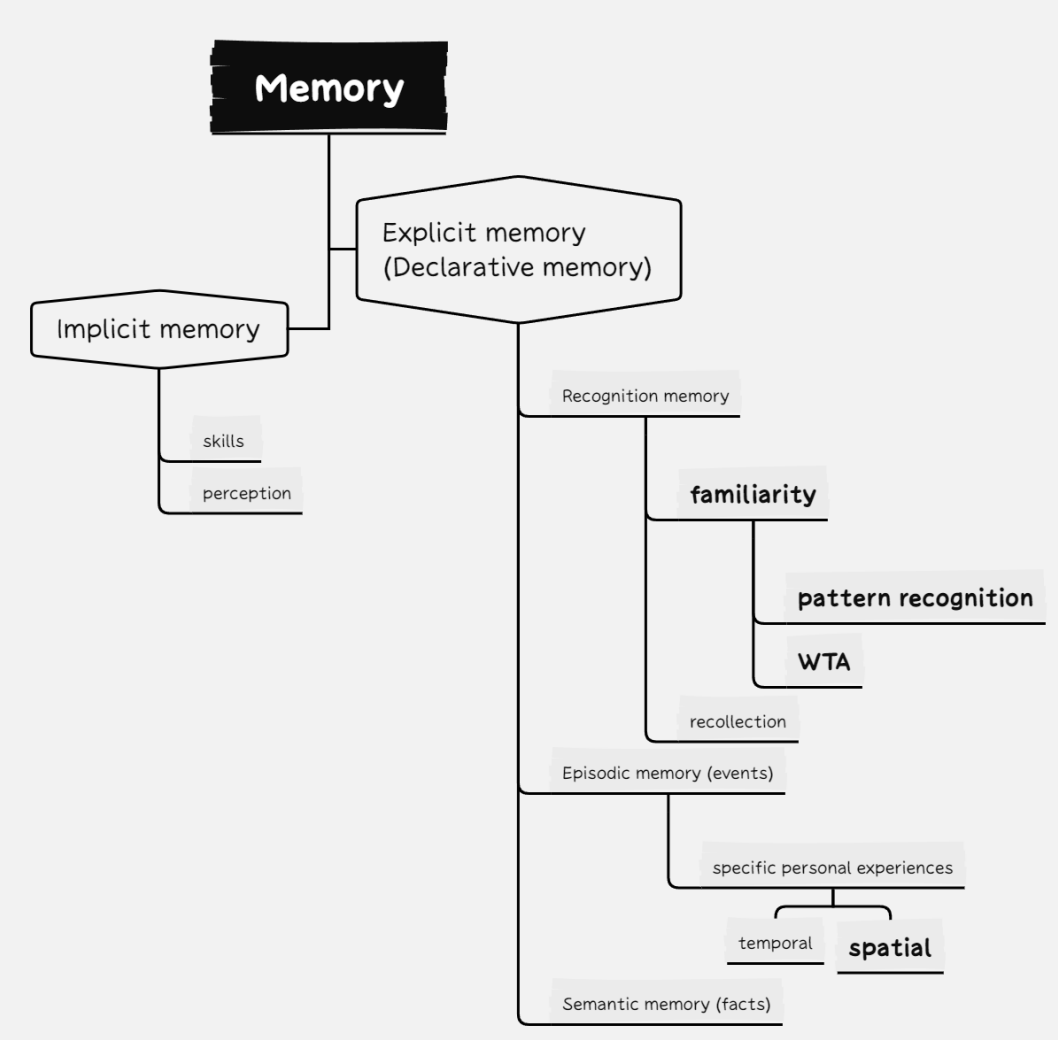


Figure 1.10: Memory category. Bolded parts are topics discussed in this thesis.

The self-organizing entorhinal–hippocampal loop underpinned the spatial representation and general recognition memory is mainly discussed in the last two chapters of this thesis. The connectivity between Hipp, medial septum (MS), and MEC is crucial for the self-organization of the grid cell modulated by the hippocampal signal. Various recordings have revealed that these three regions cooperate to establish spatial learning and memory. At the anatomical level, the MS has dense projections to Hipp and a reciprocal connection with EC (Alonso and Köhler, 1984). Both inhibitory and excitatory MS inputs are afferent to the MEC, from long-range Gamma-Aminobutyric acid GABAergic, cholinergic and glutamatergic neurons (Manns et al., 2001). Bonnevie's study (Bonnevie et al., 2013) discovered disruption of grid cell spatial firing after hippocampal inactivation, pointing to a putative excitatory drive from Hipp to the MEC. In our model, the hexagonal firing pattern of grid cells could be

self-organized taking afferent signals via the hippocampal-septal-entorhinal pathway. In addition, the spatial and visual input could be compressed in EC and afferent to Hipp in order to establish an efficient and stable representation of recognition. This recognition mechanism could be approximated by a pattern recognition algorithm using one-shot learning.

## 1.5 Grid cells and the compressing role of entorhinal cortex

The grid cell was first found in the dorsocaudal medial entorhinal cortex (Hafting et al., 2005). Grid cells are activated whenever *"the animal's position coincides with any vertex of a regular grid of equilateral triangles spanning the surface of the environment"*. Their orientation and spacing maintain persistent among neighbouring neurons with the spacing and size of individual fields increasing along dorsal-ventral axis of the dorsocaudal medial entorhinal cortex. Their vertex locations (phases) differ and tend to pave the whole exploring environment. External landmarks are required to anchor the grid map but are not necessary for the maintenance of the map. These findings suggest the relevance between grid cells and the path integration mechanism. The important contribution of grid cells in navigation has been progressively accepted during the last two decades. The grid pattern activity in EC has been widely reported among various species including rodents (Hafting et al., 2005), bats (Yartsev et al., 2011), primates (Killian et al., 2012), and humans (Jacobs et al., 2013; Nau et al., 2018). Two years after the first recording of grid cells in the mEC, Philippe Gaussier conceived a computational model of the grid cell resulting from a long-distance path integration system located outside the hippocampal formation, presumably in RSC.

We suggest in our model EC receives compressed information from different cortical regions to establish an efficient and stable representation of recognition in the hippocampal formation. The grid cells found in navigation and vision could be the epiphenomenon of this general compression mechanism.

The entorhinal cortex consists of medial and lateral parts. The medial entorhinal cortex is important for spatial processing and path integration while the lateral entorhinal cortex has some influence on both spatial and nonspatial processes in the object exploration task. (Van Cauter et al., 2013; Wilson et al., 2013)

Head direction cells are also recorded in the medial entorhinal cortex (Sargolini, 2005) following the findings of the grid cells. The same team proved that path integration is instrumental for grid cell spatial firing of rats in a circular 1D environment (Jacob et al., 2019). Increased size or scale of the grid firing field between the arena and the track was observed, while it was unmodified in arenas of different sizes. One

hypothesis has been proposed that the lack of visual cues during navigation could be responsible for the metrical properties of the grid cell map.

Our model is compatible with these biological findings and can be used to reproduce various results without modifying the model structure.

## 1.6 Continuous attractor model

George E. P. Box, who has been called "one of the great statistical minds of the 20th century", famously wrote, in various books and papers, that "all models are wrong, but some are useful". Except for our model, two other widely studied computational models are discussed in order to provide a general and objective point of view. One of them is the two-dimensional continuous attractor model (Fuhs and Touretzky, 2006; McNaughton et al., 2006; Burak and Fiete, 2009; Bonnevie et al., 2013) which is homogeneous to the broadly accepted model of the head direction cells based on the one-dimensional attractor ring model (Skaggs et al., 1994; Samsonovich and McNaughton, 1997). The oscillatory interference model (Burgess et al., 2007; Hasselmo, 2008) which was initially proposed to explain theta-phase precession in place cell firing (O'Keefe and Recce, 1993) evolved to explain the path integration and the generation of the grid cells. Indeed, each model has its own constraints and disadvantages which are hardly explained by biological recordings. Nevertheless, the development of these heterogeneous models trying to explain the spatial representation in the hippocampal system broadens our minds and is truly helpful to a better understanding of the nature of the brain.

### 1.6.1 1D continuous attractor models for head direction cells

In the one-dimensional attractor map model (Skaggs et al., 1994; Samsonovich and McNaughton, 1997) for head direction encoding (fig. 1.11), neurons are arranged in order of their preferential head direction. Each of them has connections with neighboring neurons with which the synaptic strength declines as a function of distance. A bump of activity is likely to be finally formed centered on the most active neuron with neighboring neurons having successively decreasing activity. The shape of the activity bump depends on the distribution of the neighboring synaptic connections. The distribution contains two factors: 1. The furthest neighboring neuron one neuron could innervate. 2. The decline rate of the synaptic strength. The decline rate determines the sharpness of the bump while the extension of the innervation controls the width. This one-dimensional continuous attractor model is widely accepted in explaining the property and the update of HD cells when the animal rotates.

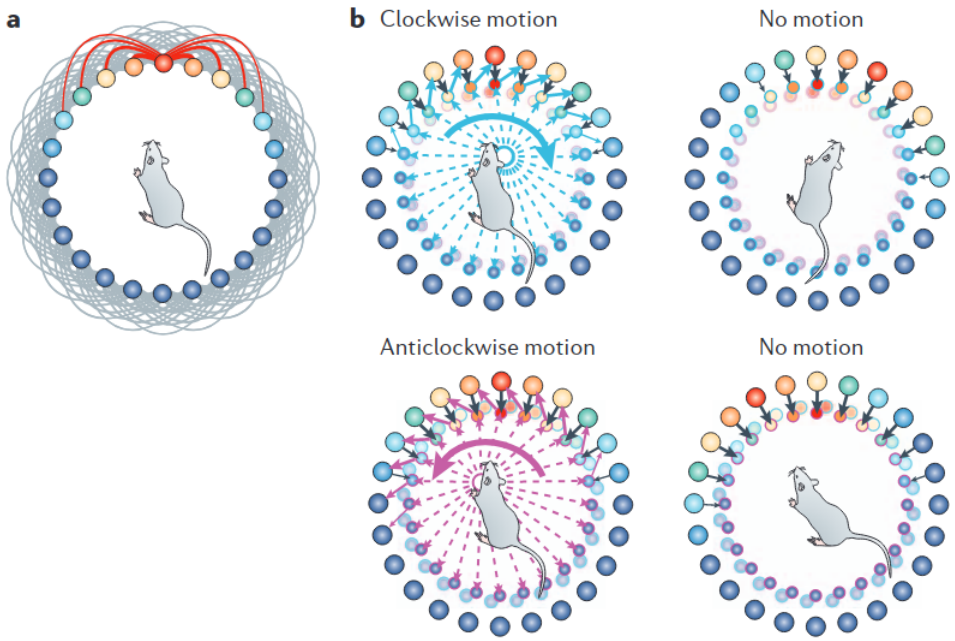


Figure 1.11: One-dimensional attractor map model for head direction encoding based on neural integration of head angular velocity signals. (McNaughton et al., 2006)

### 1.6.2 2D continuous attractor models for place cells

The 2D continuous attractor model (fig. 1.12) suggests that the path integration is performed in EC (Fuhs and Touretzky, 2006; McNaughton et al., 2006; Burak and Fiete, 2009; Bonnevie et al., 2013). A pre-existing regular map is required for the continuous update of the path integration. One pre-existing neuronal sheet corresponds to one movement direction of the animal. A large number of neurons on these sheets are required in order to maintain the accuracy of the path integration. The memory of the path integration in the continuous attractor model is stored in the reverberating neuronal activity. The torus is proposed to solve the boundary issue of the continuous attractor model. The place cells built from the torus map are essentially periodic depending on the size of the torus.

### 1.6.3 2D continuous attractor models for grid cells

The grid cell activity can be generated with the teaching signal from a self-organizing Turing network with short-range excitatory and long-range inhibitory connections. The activity of neurons in the sheet can converge to a steady state, which is characterized by a group of scattered peaks of activity ranging in a hexagonal form. The velocity input to the activity makes the pattern move in concert with the animal. When a peak passes over a neuron in the sheet, it spikes and behaves as a grid cell. In this model, grid cells must stabilize before Place cells to finally build the latter.

In the work of (Burak and Fiete, 2009), the accurate path integration and the periodic hexagonal spatial tuning pattern can be reproduced by the CANN with inputs to the model network conveying information about the rat's velocity and heading. The toroidal topology of the network avoids the border issues and thus enables accurate grid-cell-like responses over trajectories lasting around 10 minutes, with an integrated path of hundreds of meters. An aperiodic network is also discussed to accurately integrate rat velocity with an appropriate choice of parameters and inputs and without any perturbations. However, even subtle distortions of the pattern near the edges can globally destroy the grid-like responses for any neuron, including those far away from the edge of the network where the pattern is locally undistorted. A recent study (Gardner et al., 2022) conducted by the same researcher showed that the joint activity of grid cells from an individual module resides on a toroidal manifold by simultaneously recording hundreds of grid cells and investigating subsequent topological data analysis. The toroidal topology persists during awake states and sleep. This finding promotes the hypothesis that the grid cells firing derived from the CANN is based on the network of the periodic toroidal manifold.

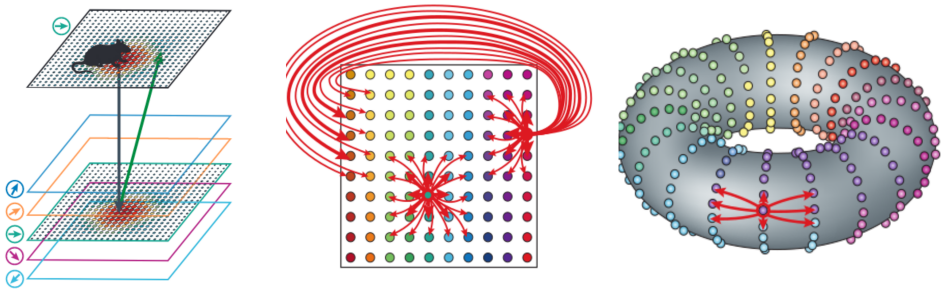

Figure 1.12: Extension of the one-dimensional attractor map concept to two dimensions: a model for path integration. (McNaughton et al., 2006)

## 1.7 Oscillatory interference model for place cells and grid cells

The oscillatory interference model (Burgess et al., 2007; Hasselmo, 2008) was initially proposed to explain theta-phase precession in place cell firing (O'Keefe and Recce, 1993) where place cells preferentially activate in bursts with a slightly shorter period than that of the extracellular theta rhythm. Typically, spikes of place cells appear at the theta rhythm's trough when the animal enters a place field and progressively advance in phase as the animal moves through the firing field. According to the oscillatory interference theory, interference patterns between neural oscillators give rise to spatial patterns of activity. These oscillators in rats have a frequency that is quite similar to the theta frequency. A pair of cosinoidal oscillators having

slightly different frequencies are composed of a velocity-controlled oscillator and a baseline theta oscillation. The beating interference pattern could emerge owing to the difference in frequency and thereby generates simultaneously the place fields and phase precession. A neural oscillator is a population of neurons that cycles through a periodic state while velocity-controlled oscillators modify their frequency in response to the animal's motion. The periodic stripe activity in (fig. 1.13 a) is formed by the product of the two cosinoidal oscillators in (fig. 1.13 c and d). This model predicts the periodic firing field of place cells due to the periodicity of the stripe activity which has not been observed in biology.

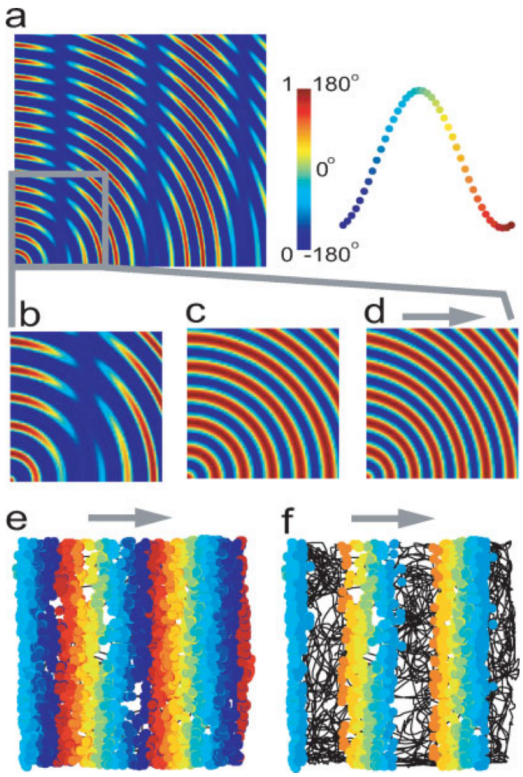


Figure 1.13: Linear interference patterns in 2D. (a) Interference between a velocity-controlled oscillator (VCO) and a baseline oscillation during constant velocity runs from the origin (bottom left). Expanded view (b–d) shows the baseline oscillation (c) and the VCO (d, gray arrow shows preferred direction). Both component oscillations are sinusoidal and the combined oscillation is the thresholded sum (a,b). (e) The firing of a neuronal VCO as the rat follows a 10 min foraging path (black line) in a square box. The VCO fires spikes at the peaks of its membrane potential oscillation (MPO). The locations of spike firing are shown colored by the phase of firing relative to the baseline oscillation. (f) The firing of the neuronal VCO in (e) when its MPO is modulated by the baseline oscillation and a firing threshold of 0.5 is applied. Color bar (top right) shows amplitude (0–1) and phase. (Burgess, 2008)

One hypothesis posits that constructive interference only occurs in the limited

spatial place field, whereas destructive interference which is generated by oscillators with equal frequencies but opposite phases occurs in the environment other than the place fields.

This issue was finally circumvented, following the discovery of periodic grid cell firing patterns in EC, by reapplying the model to the explanation of the path integration and the grid cell activity. The grid cell activity is supposed to be generated by the combination of two or more linear interference patterns of oscillators with preferred directions differing by 60°(fig. 1.14).

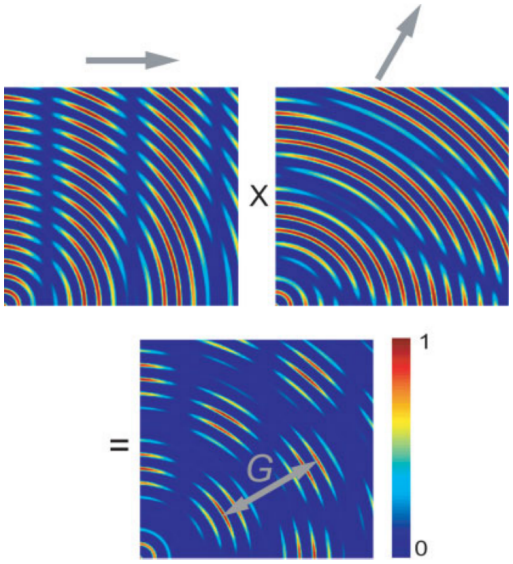


Figure 1.14: Two linear interference patterns with preferred directions differing by 60°(gray arrows, left and right, above) combine to produce a triangular grid (below grid scale = G). The linear interference patterns are the thresholded sum of a velocity-controlled oscillator and a baseline oscillation during constant velocity runs from the origin (bottom left). These patterns are multiplied to produce the grid pattern (below). The colorbar shows amplitude. (Burgess, 2008)

## 1.8 Adaptive resonance theory and a model of grid cell

The adaptive resonance theory is "a cognitive and neural theory of how advanced brains autonomously learn to attend, recognize, and predict objects and events in a changing world" with the prediction that "all conscious states are resonant states" (Grossberg, 2017). This theory was first introduced (Grossberg, 1982) in order to solve the stability–plasticity dilemma about how the brain combines fast learning and stable memory. The basic learning process based on the adaptive resonance theory consists of three parts: the feature pattern as the input, the outcome category, and the expectation. The linkage between the input feature pattern and the outcome

category is learned by adaptive weights so does the linkage between the outcome category and the expectation. The linkage is reinforced if the input feature pattern matches the category and is inhibited if the extent of the mismatch exceeds a certain vigilance level. The vigilance level determines how badly a match will be tolerated or how often a new match between an input pattern and a category is learned. The work in (Grossberg and Pilly, 2012) demonstrated the generation of entorhinal grid cells with spatial scales that increase along the dorsoventral axis using the self-organizing map. The hexagonal structure formation is generated by the coactivation of three stripe cells with preferred directions apart from 60°. The difference of 60°is assumed to be realised by a self-organizing mechanism (Mhatre et al., 2012). However, the number of stripe cells is originally selected which is not self-organized. Place cells representing much larger spaces than grid cells are supposed to be generated from the combination of grid cells of multiple scales. With the help of the adaptive resonance theory, the memory of the learned self-organizing map could be dynamically stabilized and therefore stabilize both the learned grid and place cell receptive fields. In addition, signals from the hippocampal place cells may also help to improve the spatial stability of learned grid fields. Our original model (Gaussier et al., 2002) focusing on the transition and prediction in the sequence learning and navigation tasks shares some common aspects with the adaptive resonance theory.

## 1.9 Discussion

Recent biological results (Pisokas et al., 2022) raised an objection to the continuous attractor models because of their dependence on the reverberating electrical activity of neurons maintaining the memory of the path integration. Ants were anesthetized (frozen) after their foraging journey and put into a new environment without any familiar sensory cues (fig. 1.15). During the freeze, no electrical activity is found in ants' brains. This freezing process therefore disrupts any kind of dynamics memories related to reverberating electrical activity in some neural circuits. Ants maintain the direction memory of PI activity after the complete cease of the activity. Only the distance memory is degraded due to the anesthesia. This finding suggests a fast-updating persistent process for the storage of the memory instead of the recurrent neural circuit. The memory of the path integration in the continuous attractor model is stored on the reverberating activity which is not robust to perturbations. The memory could be stored at the synaptic level to maintain robustness. We showed previously the mathematical equivalence between a classical conditioning mechanism with LMS and a STM mechanism (fig. 1.6). The advantage of a classical conditioning mechanism is that the memory is stored at the synaptic level which is robust to perturbation. The feedforward structure avoids the risk of STM deterioration related to the need to always retrieve the past activity.

In our model, the leaky integrator is implemented in order to integrate the activity and store at the synaptic level.

It is well known that insects and rodents have different brain structures and the mechanism that the path integration relies on could be different. Nevertheless, both of the species have similar HD cells property which is supposed to be one of the major inputs for the path interaction. Since the storage of the path integration of insects resides in the synaptic connectivity, we could ask if the path integration of rodents or mammalians is also maintained on the synaptic level as the classical conditioning rule we implemented in our model. Since path integration is an ancient ability of creatures, we have reasons to believe that different species share some common properties of path integration such as the storage of the path integration memory.

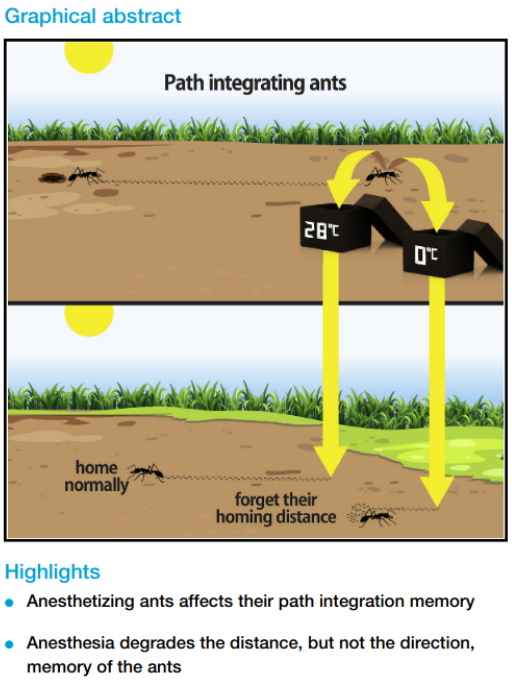


Figure 1.15: Anesthesia disrupts distance, but not direction, of path integration memory. (Pisokas et al., 2022)

Studies have shown that bats do not exhibit continuous theta rhythm when they crawl but still have grid cell activity. This finding has led to a dispute about the oscillatory interference model based on the theta oscillation despite some work proposing that the oscillatory interference models can perform velocity integration independently of any baseline oscillation including theta oscillations.

In addition, the hexagonal pattern of grid cells in the oscillatory interference models is generated by the product of three linear interference patterns with preferred directions differing by 60°. This selection of 60°is assumed to be realized by a self-

organizing mechanism which was not demonstrated in (Burgess et al., 2007).

Place cells built from the oscillatory interference model can not avoid the periodic firing field. The periodicity is induced by the periodic stripe activity. However, the periodicity of place cells is seldom observed in biological experiments. There is no such constraint on the periodicity of place cells in our model.

Both of the 2-D continuous attractor model and the oscillatory interference model adapted to the findings of grid cells and head direction cells in EC by claiming that the PI takes place inside EC. In 2-D continuous attractor models, path integration happens at the level of grid cells while in the oscillatory interference models, path integration occurs at the level of stripe cells, input to grid cells. These models take the movement direction calculated from sequential positions in the experimental data comprising the velocity input, rather than the HD at each position while citing HD recordings as the justification for velocity input. Recordings in EC (Raudies et al., 2015) indicate that coding of movement direction is not prominent in the medial EC, and HD can not directly replace movement direction in the mentioned types of models using PI to build the grid cells. Cortices such as RSC and the parietal cortex could be candidates for the seeking of the moving directional tuning and as the potential origin of the PI. Our model of the PI in RSC doesn't rely on the HD cell activity from EC.

In chapter 3, we simulate animals moving in different environments (open space, spiral mazes, and on a treadmill) to test the performances of a simple model of RSC acting as a path integration (PI) and as a categorization mechanism. The connection between Hipp, RSC, and EC is revealed through a novel perspective. In chapter 4, we emphasize the idea that RSC conveys PI information to the hippocampal system. We further emphasize that the absence of place cells in RSC is due to the difficulty of neurons accessing the whole PI neural field. In chapter 5, we introduce the hypothesis of the important role of the causal relationship between the place cells and EC in the generation of grid cells and place cells during early development. In chapter 6, we propose a general model explaining the generation of the visual grid cell along with its involvement in the visual recognition tasks independent of the locomotion or speed information. We suggest EC could compress not only the spatial information but also visual input in order to establish an efficient and stable representation of recognition in the hippocampal formation. The navigation feature could be the epiphenomenon of this general recognition mechanism.

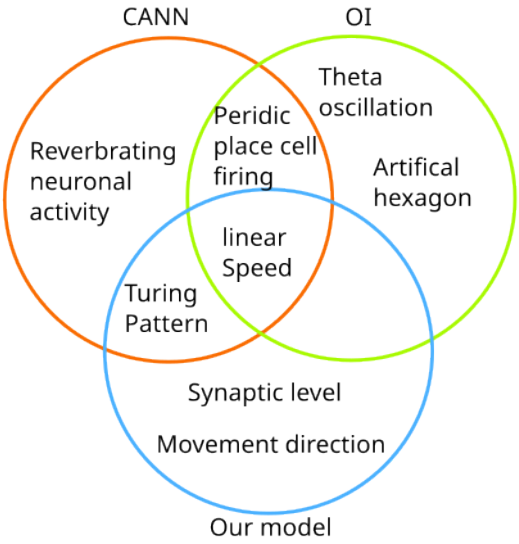


Figure 1.16: Comparison of continuous attractor model, oscillatory interference model and our model of the path integration and the grid cells.

# Chapter 2

# A model of path integration and representation of spatial context in the retrosplenial cortex [1]

## 2.1 Abstract

Inspired by recent biological experiments, we simulate animals moving in different environments (open space, spiral mazes and on a treadmill) to test the performances of a simple model of the retrosplenial cortex (RSC) acting as a path integration (PI) and as a categorization mechanism. The connection between the hippocampus, RSC and the entorhinal cortex (EC) is revealed through a novel perspective. We suppose that the path integration is performed by the information coming from RSC. Grid cells in the entorhinal cortex then can be built as the result of a modulo projection of RSC activity. In our model, PI is performed by a 1D field of neurons acting as a simple low-pass filter of head direction (HD) cells modulated by the linear velocity of the animal. Our paper focuses on the constraints on the HD cell shape for a good approximation of PI. Recording of neurons on our 1D PI field shows these neurons would not be intuitively interpreted as performing PI. Using inputs coming from a narrow neighbouring projection of our PI field creates place cell-like activities in the RSC when the mouse runs on the treadmill. This can be the result of local self-organizing maps representing blobs of neurons in the RSC (e.g. cortical columns). Other simulations show that accessing the whole PI field would induce place cells whatever the environment is. Since this property is not observed, we conclude that the categorization neurons in the RSC should have access to only a small fraction of the PI field.

[1] Ju, M., Gaussier, P. (2020). A model of path integration and representation of spatial context in the retrosplenial cortex. Biological Cybernetics, 114(2), 303-313.

**Keywords:** path integration, retrosplenial cortex, self-organization, allocentric navigation, egocentric navigation, entorhinal cortex

## 2.2 Introduction

The path integration mechanism has been found in many different species, from insects (Collett et al., 1996; Stone et al., 2017) to mammals (Etienne and Jeffery, 2004). The head direction (Sharp et al., 2001; Zhang, 1996) and the linear velocity of animals are vital to constructing PI which is considered as the integration of linear and angular self-motion (McNaughton et al., 2006). However, how and where this information is coded to build PI is still an open issue. Different recordings in the retrosplenial cortex (RSC) (Cooper and Mizumori, 1999; Save et al., 2001; Czajkowski et al., 2014) point to the possibility that RSC could play a crucial role in PI (Cooper et al., 2001). The 'place cells' activity found in RSC (Mao et al., 2017) could also be a trace of this PI. Thereby, we simulate in our model, the connection between head direction (HD) cells, which are found in many parts of the brain (Taube et al., 1990b; Taube, 1995) and 'place cells' in RSC. We suppose that PI could be integrated in this loop despite many other models (McNaughton et al., 1996; Redish and Touretzky, 1997; Fuhs and Touretzky, 2006) proposing that PI is built inside the hippocampus. In our model, the representation of the spatial location in RSC is supposed to be the discretization of PI. The correlation between the diverse activity in RSC and the local and global connectivity from PI field to RSC is revealed by the simulations.

By extracting the information from PI field generated by our model, we can mathematically rebuild the approximate animal trajectory using the activity of at least two distant neurons from one PI field (Gaussier et al., 2007). Essentially, the bump of the activity of neurons on a PI field represents nothing more than a homing vector. The way we interpret the activity of PI field to reveal the diverse activities of RSC is one of the critical contributions of this paper.

The recalibration strategy used when the animals perform a navigation task (Poucet et al., 2015) is discussed in a companion paper. An allocentric reference frame can be built from distant visual landmarks while an egocentric reference frame can be built from the local cues (Byrne et al., 2007). For instance, when the animal moves in the W mazes located at two different places in the environment (Alexander and Nitz, 2015), one local cue (orientation of the entrance of the w maze) can be used to create an egocentric reference frame.

It has been 30 years since the general properties of head direction cells were first described in (Taube et al., 1990a). Head direction tuning curves of HD cells recorded from different brain areas are illustrated in (fig. 2.1a). The directional firing range of the HD cells in rodents' brains is from around 90 to 240 degrees. Fig. 2.1b shows the

similarity between head direction tuning curves and a Gaussian shape with different $\sigma$. In this paper, we focus on a model where PI is integrated from one-dimensional bumps of HD cells in contrast to the usual two-dimensional attractor models (McNaughton et al., 2006). In our model, HD cells activity modulated by the linear speed of the animal is the input to generate an approximation of PI. RSC neurons activity is achieved through a low pass filter approximating the integration process. We also study the impact of the size of the HD bump on the performance of PI. Moreover, we will show that a simple discretization performed by self-organizing maps (Kohonen, 1990) can explain the results in (Mao et al., 2017) showing different place cell-like activities when a mouse runs on a treadmill (without spatial displacement). Our results also explain the absence of real place cell activity in RSC in many biological experiments where animals move freely in a 2D environment. Moreover, our model has no specific mechanism for navigation, which gives itself the possibility to be a global model for simulating the activity of neurons in different cortical areas.

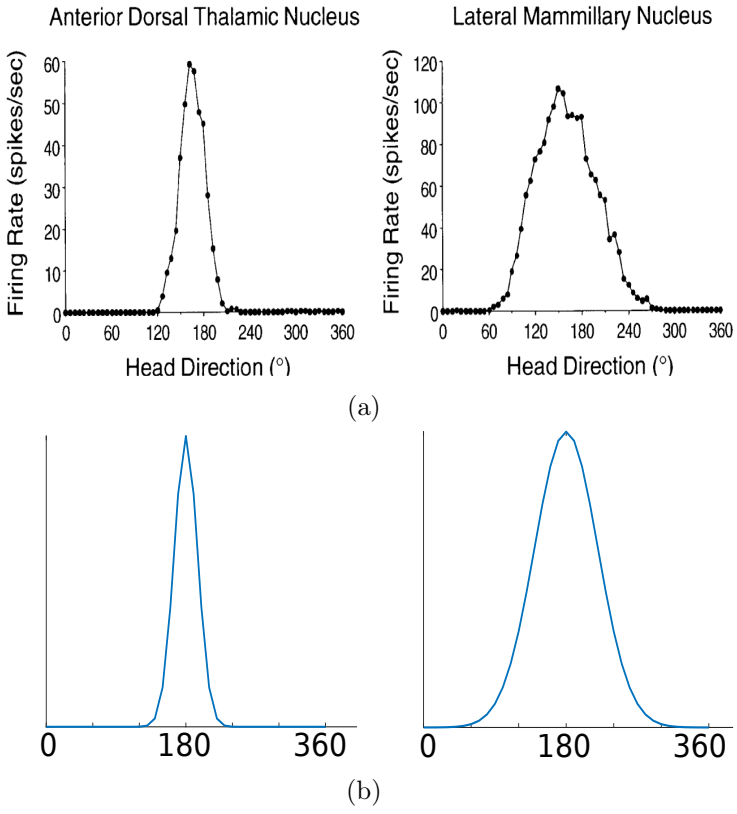


Figure 2.1: Comparison between the Gaussian shape and the firing range of HD cells found in biological experiments (Taube, 1998). a. biological results. b. left, Gaussian shape with $\sigma = 15$, firing range = 90 degrees. b.right, Gaussian shape with $\sigma = 40$, firing range = 240 degrees

## 2.3 Computational Model

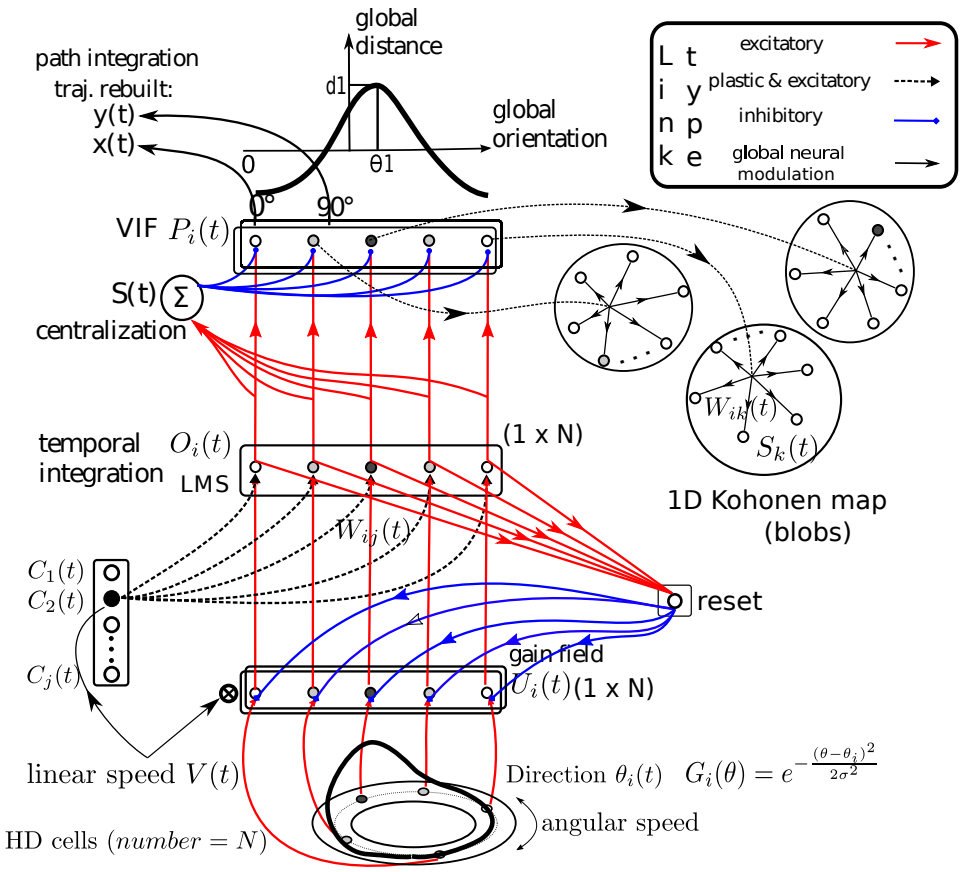


Figure 2.2: Model of the retrosplenial cortex with 1D field performing path integration and self-organizing blobs

Path integration (PI) is the integration of linear and angular movements of the animal. In our model, PI is constructed based on the integration of the activity of HD cells over time. As an input to our model, HD cells are modelled as a one-dimensional attractor network (McNaughton et al., 1991). The head direction is represented as a bump of activation on a ring of neurons. The movement of the bump and the head direction is controlled by the animal's angular speed. In our model, we take the HD cell activity as the input. Nevertheless, except for the HD cells input, visual landmarks and bidirectional HD cells (Jacob et al., 2017) could also be the input of our model.

Instead of using a cosine shape as the bump of HD cells in (Gaussier et al., 2007), we use a Gaussian shape which causes more errors but is more similar to the HD cells found in biological experiments (fig. 2.1). We take $G_i(\theta) = e^{-\frac{(\theta-\theta_i)^2}{2\sigma^2}}$ where $\sigma$ determines the width of the firing range of HD cells and $\theta_i$ is the absolute orientation of the animal with the common hypothesis that animals move in the direction where

their heads face.

The input of the model is the absolute orientation and the linear velocity of the animal. We suppose that a group of neurons is equally distributed to represent 360 degrees in order to simulate HD cells. Each neuron has a preferred direction depending on the amount (N) of total neurons. The interval between each preferred direction is $360/N$. The group of neurons can represent 360 degrees with good precision if we have enough neurons (e.g. a precision of 1.8 degrees if N = 200). A reset or recalibration mechanism is implemented to eliminate the accumulation of errors. There is no need of lateral interaction between neurons on the PI field.

To perform the HD vector integration, two solutions are possible: use STM (short-term memories) or modify the synaptic weights. In our initial works, we were using the STM but there is a potential issue with the biological plausibility of the STM time constant and the precision of the neurons' firing rate. In this paper, we use the second solution which is mathematically equal to the first one. A classical conditioning mechanism which is identical to (Rescorla, Wagner, et al., 1972; Widrow and Hoff, 1960) is implemented in the model. Using the following learning rule to modify the synaptic weights $W_{ij}$:

$$dW_{ij} = \lambda \cdot (U_i - O_i) \cdot C_j \tag{2.1}$$

where $C_j$ is a binary value associated to a spatial context $j$ (the conditional input). $O_i$ is the output:

$$O_i(t) = f(\sum W_{ij} \cdot C_j) \text{ , with } f(x) = \begin{cases} 0 & \text{if } x < 0 \\ x & \text{if } 0 \leq x < 1 \\ 1 & \text{if } x > 1 \end{cases} \tag{2.2}$$

The context $C_j$ is the output of a network shown in fig. 2.3. The origin of the computed PI starts at the moment the context $R_j$ is first activated. $R_j$ is triggered ON when the animal comes back near the learned location and activates an STM $M_j$ to maintain the context active even when the animal moves far away from the recalibration point. If another context was maintained in the STM, this context loses against the strong feedforward input $R_j$ which leads to updating the memory of the current context (see fig. 2.3). When the animal stops moving, the motionless state is active: S(t)=1 if V(t)=0 and 0 otherwise. We suppose this specific node inhibits the spatial context $C_j$.

Hence, the RSC output $O_i$ is set to zero. This accounts for the lack of RSC activation in (Mao et al., 2017) where the mouse stops moving on a treadmill to get the reward (sugar water) at the end of each lap.

$C_j$ is computed as follows:

$C_j(t) = H(M_j(t) - S(t))$ with $H(x)$ the Heavy-side function: $H(x) = 1$ if $x > 0$

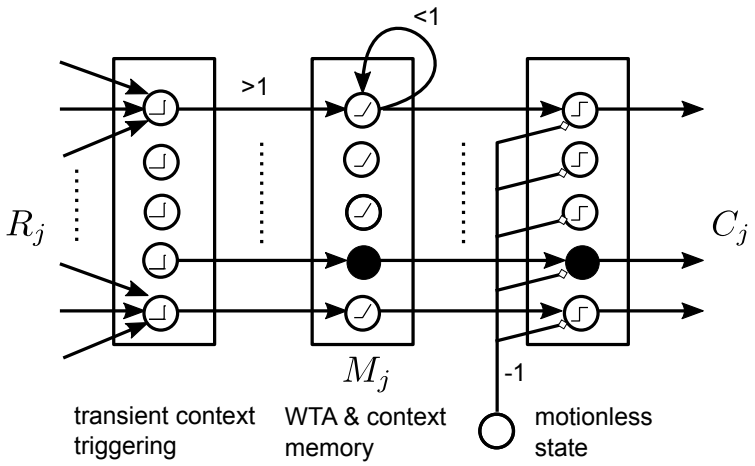


Figure 2.3: Schema of the contextual input $C_j$. $R_j$ represents the recognition of recalibration positions. $M_j$ is the STM.

and 0 otherwise. $M'_j(t) = f(\lambda_M.M_j(t-1) + R_j(t))$ with $0 < \lambda < 1$. $M_j(t)$ is the result of a competition mechanism between $M'_j$. $M_j(t) = M'_j(t)$ if $j = argmaxM'$ and 0 otherwise.

The firing rate of all RSC neurons is scaled to [0,1] interval. Hence, the maximum activity in our simulation corresponds to 160Hz, the maximum firing rate coming from the recordings of RSC neurons (Alexander and Nitz, 2015). In our model, most RSC neurons have a firing rate around $30Hz$ which is consistent with the results of biological experiments carried out by Alexander and Nitz (Alexander and Nitz, 2015).

The variation of the synapses $dW_{ij}$ relates to the difference between $U_i$ and $O_i$. Since $U_i$ is bounded between 0 to 1, with equations in the appendix, $W_{ij}$ and $O_i$ tend towards $U_i$ which is limited to 1 (the maximum of the firing rate).

$U_i$ represents the unconditional stimulus (one HD cell) which is modulated by $V$, the linear velocity of the animal and $G_i(\theta)$, the activity of the associated HD cell: $U_i = V \cdot G_i$

The modulation of the HD cells by the linear velocity of the animal can be explained by the speed-modulated cells found in different cortices. For instance, (Lozano et al., 2017) found the firing rate of the HD cells in RSC is correlated with running speed (Lozano et al., 2017). Speed cells in the medial entorhinal cortex (MEC) were also found by (Kropff et al., 2015).

As shown in the appendix, the output $O_i$ can be finally rewritten as:

$$O_i(t + dt) = (1 - \lambda) \cdot O_i(t) + \lambda \cdot U_i \tag{2.3}$$

This clearly shows our conditioning rule functions as a short-term memory or a first-order low pass filter.

Neurons perform a temporal sum of their inputs through synaptic plasticity, which approximates the PI (fig. 1.3) (Gaussier et al., 2007). The synaptic links from the context neurons $C_j$ to the $O_i$ neurons allow to update and store the value of the PI. When a context $C_j$ is activated ($C_j = 1$) and the learning rate is low, the synaptic weights between $C_j$ and $O_i$ work as short-term memories (STM) integrating the unconditional input $U_i$. With a high learning rate and a reset of $H_i$ the synaptic weights can be reset to perform a recalibration when coming back to a known place for instance.

At this stage, $O_i$ activity is not really homologous to PI since the $O_i$ neurons are only excited by the HD activity. The field of $O_i$ always increases and PI can not come back to the starting point because the activity of neurons can not be negative. We calculate the mean activity of every neuron in the field of $O_i$ and at each time step, the field is centred by subtracting the average value of the activity of all neurons. A global feed-forward inhibition $S(t)$ is added to obtain the output field $P_i(t)$ including positive and negative parts representing an approximation of the PI. The theoretical computation of the PI supposes the input pattern has a symmetric sine or cosine shape (with both positive and negative activities). Since the output of the neurons cannot be negative, we need to introduce a mechanism to come back to a symmetric computation otherwise the neuron's activity would only increase. Coming back to the starting location would not be correctly encoded as a global null activity. Hence, the integral over the different angles of the sum of the instantaneous movements has to remain constant (moving of a distance d in the direction $\theta_i$ also implies moving of a distance -d in the direction $\pi + \theta_i$. This can be obtained by applying a feedforward inhibition on $O_i$ activities:

$$P_i(t) \quad = \quad O_i(t) - \gamma.S(t) \tag{2.4}$$

with $S(t) = \sum_{i=0}^{N} O_i(t)$ and usually $\gamma = \frac{1}{N}$. Because $P_i$ activities are centred, the activity of $P_k$ with $k = argmax(V_i)$ is proportional to the distance travelled in direction $i$ from the reset point. The neural field $P_i$ is entitled the vector integration field (VIF).

In our model, the direction of the animal's instantaneous movement and the result of PI are coded on a neural map covering 360° (similar to a 1D neural field (Amari, 1977a; Schöner et al., 1995a)), besides that, there is no need of lateral interaction between the neurons in the vector integration field. Each neuron codes for a given direction $\theta_i$ relative to an arbitrary reference possibly obtained from vestibular or visual information. Since in our integration fields each neuron is coding for a specific direction, the field activity can also be seen as a memory to store one vector. In fact, each neuron codes for the projection of one vector onto its associated direction. The other models introduced in this thesis are all extended from this original model.

The integration of the activity modulated by the linear speed and the absolute orientation of the animal is proportional to the path the animal moved (Alexander and Nitz, 2015).

Our model can adapt to different sizes of environment using different $\lambda$. In the following simulation, we suppose the size of the environment for training the animal is 2m x 2m. A learning rate = 0.001 is sufficient to build a correct PI within this environment.

Our PI model has a limitation for a long travelling time when the animal moves in the same direction at a constant speed. Our system of PI can be considered as a linear time-invariant system with a time constant ($\tau$) depending on the learning rate. $\tau$ is inversely proportional to the learning rate. The quicker the animal learns, the faster the system arrives at the saturation state, which means PI can no longer represent precisely the variation of the distance. The time constant of the system using two different learning rates is illustrated in (fig. 2.4).

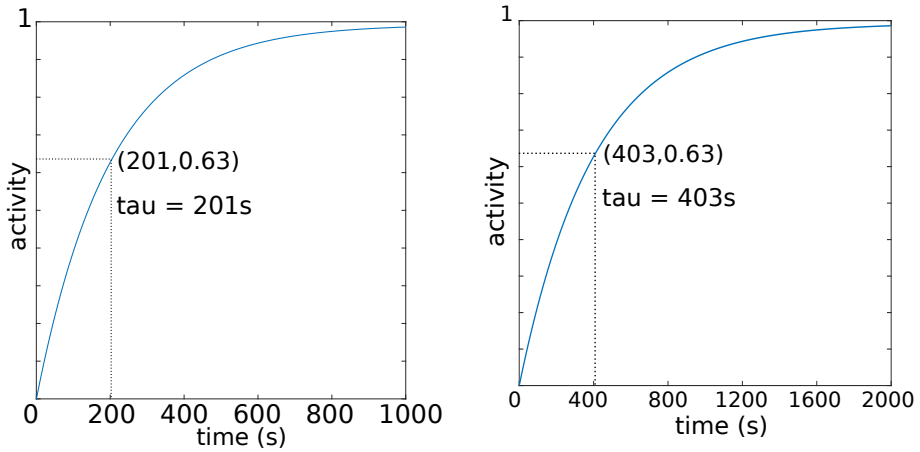


(a) (b)

Figure 2.4: Activity of one neuron in PI field when the animal moves in one direction at a constant speed. Left, time constant = 201s when the learning rate is 0.001. Right, $\tau = 403s$ when $\lambda = 0.0005$

Our PI saturates if the animal moves too far away from the initialization point. To avoid the accumulation of errors, a general reset mechanism should be implemented. Nevertheless, the animals' movement patterns can be variable when the speed or the direction changes. With the learning rate alone, we can not predict when the system reaches saturation, while in classical grid cell models, this issue is avoided thanks to the precise toroid shape of the underlying 2D map. In our model, the general reset can be realized by the detection of the novelty (Markou and Singh, 2003; Jauffret et al., 2013). The reset of PI is activated when the gradient of novelty becomes flat. In our simulation, we define novelty as the distance of the path integration updated

at each time step. One time step after the reset mechanism activates, the conditional input $C_j$ and the reset learning rate ($\lambda_{reset} = 1$) are activated and the unconditional input of the PI is inhibited to 0. By substituting the parameters in (eq. 2.3) with their reset values, we have $O_i(t + dt) = U_i$ so that PI is reset to 0.

Although the time constant of the system is much longer than that of neurons (Rall, 1960). The activity of neurons on PI field with a low learning rate (long time constant) can be achieved by several fields connected in cascade with a higher learning rate (shorter time constant). If we connect several fields in cascade, we can have a system with lower $\lambda$. Hence, neurons with a short time constant (10ms-1s) can be used to build PI system with a higher time constant by increasing the number of fields in the cascade.

We suppose that the approximated PI could be built in RSC. The 'place cell' activity can be discretized by the activity of neurons on PI field. Hence, to simulate the representation of spatial context in RSC, we project the activity of PI field to the Kohonen maps (blobs on fig. 2.2). Instead of using the distance between the vector of the input activity and the vector of weight pointing to each neuron on the Kohonen map, we use the dot product which is considered as a more plausible way to determine which pattern of weights is the most similar to the vector of input activity. The normalization is not necessary when the dimension of the input space is high enough (Blayo, 1992).

Following simulations are designed to show the performance of the approximate PI and the representation of the spatial context in RSC using our model.

## 2.4 Simulations

The animal is simulated according to its (x,y) coordinates, its head direction and its instantaneous linear speed. At each time step, PI field receives an input composed of the direction and linear velocity of the current movement of the animal.

The quantitative analysis is not studied in this paper. We focus on the qualitative proof for our model. The quantitative analysis relating to the selection of the appropriate decay rate $\lambda$ will be discussed in future works.

### 2.4.1 Simulation in a spiral maze

To test the performance of PI mechanism, we simulate a rat moving at 10 cm/s inside a square spiral maze (fig. 2.6a). The external length of the maze is 80 cm and the distance between parallel corridors is 8 cm. The turning angle between two corridors is 90 degrees. The duration of the simulation is 880 time steps (88 seconds) with a learning rate = 0.001 ($\tau = 201s$). We use 200 neurons for the HD cells so the precision of orientation is 1.8 degrees. The number of neurons can be increased

if higher precision of the orientation is needed. However, for animals, the balance between precision and the consumption of energy should be maintained.

To visualize the meaning of the PI field, we record the activity of two neurons with an interval of $N \cdot \frac{90}{360} = \frac{N}{4}$. $x(t) = P_i(t)$ and $y(t) = P_{i+N/4}(t)$. If we use the activity of the first neuron as the x coordinate and the activity of the second neuron as the y coordinate, we can artificially rebuild the trajectory (fig. 2.6a) of the simulated animal. Since the field represents a projection of PI, taking the activity of 2 neurons distant from 90 degrees is equal to taking the cosine and sine of the associated PI vector (Gaussier et al., 2007). More neurons can always be used to rebuild more precisely the trajectory. In fig. 2.15 we will show neurons having access to the whole field or to 10% of the field can easily learn to rebuild specific places.

For the size of HD bumps, we take $\sigma = 60$ degrees. The sum of the two Gaussian shapes has one peak which presents the orientation of the path integration (fig. 2.6b). The red and green curves represent PI field when the rat's orientation is 0 and 90 degrees respectively (when the animal moves from one corridor to the next in the spiral maze). The black curve is the sum of two previous curves representing the updated homing direction and distance of PI.

Fig. 2.5c and 2.5d show the temporal activity of two neurons on PI field which is consistent with the recordings of RSC neurons (Alexander and Nitz, 2015). Intuitively, the temporal activity of these two neurons can not remind us of PI or the trajectory the animal moved. However, we can rebuild the animal trajectory by the activity of these two neurons (fig. 2.6a). The activity of all the neurons on PI field should correspond to a one-peak bump (fig. 2.6b) of PI pointing to the starting position as long as PI mechanism works well. In brief, a simple low-pass filter mechanism is adequate to generate PI field in RSC.

To test the effect of the noise on the performance of PI. We add a white noise with an amplitude of 10% and 40% of the maximum neuronal activity to the bump of the HD cells. The unconditional stimulus $U_i$ is thereby written as $U_i = V \cdot G_i + noise$. In (fig. 2.7a), PI mechanism stays robust to the white noise of 10%. For a noise level of 40%, the effect on the trajectory is more important (fig. 2.7b). However, in both cases, PI always maintains the general space information. Our model is robust to the white noise because PI mechanism in our model acts as a low pass filter. In the next section, the effect of noise on the output of PI mechanism is discussed.

PI performs well when the firing range spreads over 360 degrees with an animal performing an instantaneous rotation of 90 degrees. However, the real firing range of the HD cell is not that large. The largest firing range found in the LMN (Lateral Mammillary Nucleus) is about 240 degrees (fig. 2.1a). In the following simulations, we test PI with a smaller size for the HD cells to be more similar to those observed in biological experiments. We still use the square spiral maze but with the bump size of 240 degrees, $\sigma$ of the Gaussian shape $= 240/6 = 40$. We use neurons 25 and

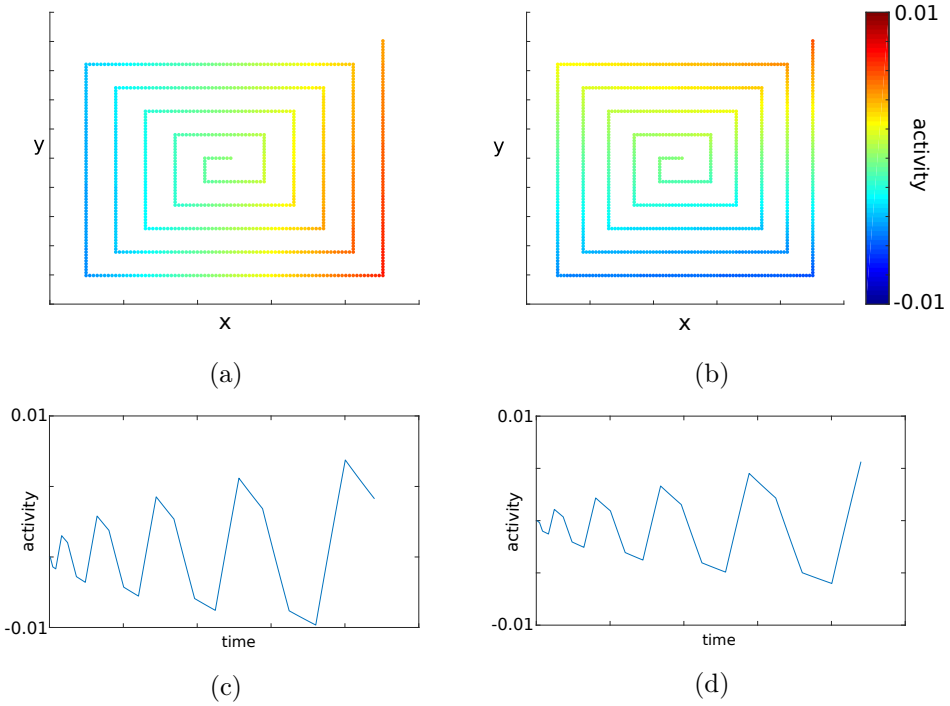


Figure 2.5: Activity of neurons on PI field when the rat moves in a square spiral maze with $\sigma$ of the Gaussian shape = 60 degrees. a, b. Activity of neurons 100, 150 along the trajectory. c, d. Temporal activity of neurons 100 and 150 during the locomotion of the simulated rat.

75 (fig. 2.8a, b) from PI field to rebuild the trajectory. If PI field is working well, we should be able to rebuild the trajectory up to a rotation factor related to the choice of the 2 neurons used in the reconstruction. Fig. 2.9b shows the overlap of two bell curves associated with the sum of the activity of 2 HD cells. The peak of the curve is no longer in the middle. In spite of the error in PI (fig. 2.9a), the model is still quite useful to navigate in 3/4 of the cases which means our model is robust to the error in the direction of PI.

To discover the relationship between the turning angle of the movement and the size of bump, we simulate a rat moving at 10 cm/s in a triangle spiral maze, the external length of the maze is 136 cm and the distance between parallel corridors is 8 cm. The turning angle between two arms is 120 degrees. The duration of the simulation is 928 time steps (92.8 s) with a learning rate = 0.001 ($\tau = 201s$).

We use neurons 100 and 150 (fig. 2.11a, b) from PI field to rebuild the trajectory. In this case, PI tends to be inaccurate even using the HD cell with the largest firing range observed from biological experiments. Hence, our model has the constraint that the instantaneous turning angle should not exceed twice the size of the bump to ensure the accuracy of PI. It is coherent with what we see in animals and humans that

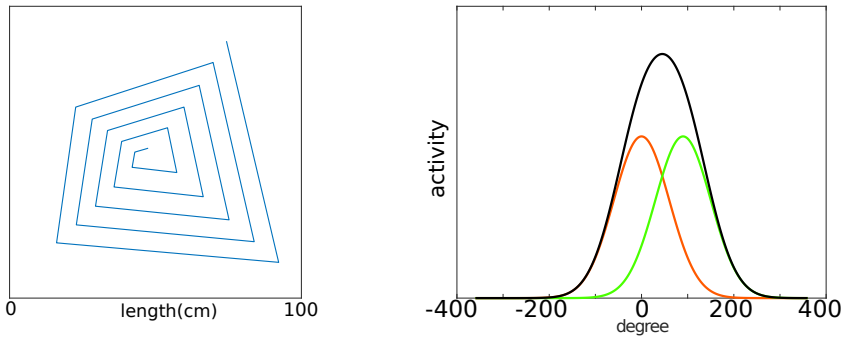


(a) (b)

Figure 2.6: The rat moves in a square spiral maze with $\sigma = 60$ degrees and learning rate = 0.001. a) Trajectory rebuilt by neuron100 and 150. b) Overlap of two Gaussian shapes distant from 90 degrees, showing the path integration is done correctly.

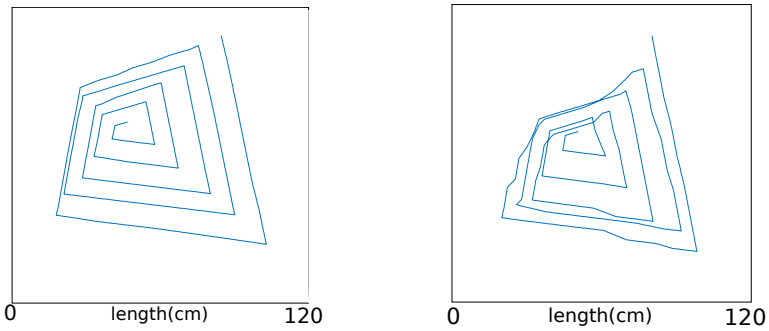


(a) (b)

Figure 2.7: Performance of PI mechanism under the perturbation of a white noise added to all the neurons on the input field of PI mechanism. a. PI under a 10% white noise. b. PI under a 40% white noise.

are disoriented under too fast rotations. We don't adapt to the too-sharp turning.

### 2.4.2 Simulation in W mazes

The following simulation will show that our model is capable to reveal the ability of RSC to 'map the conjunction of internal and external space' which is discovered in (Alexander and Nitz, 2015). We simulate a W maze whose corridor is 66cm and the angle between two conjoint corridors is 90 degrees. The animal moves at 10cm/s in the maze with a learning rate = 0.001. We record simulated neurons' activity of the PI field and compare them with the results found in biological experiments. Neurons in PI field are equally distributed to the orientation and react not strictly to only one direction because of the wide firing range of HD cells which is supposed to be 240 degrees in our simulation. The activities of neurons can be considered as the

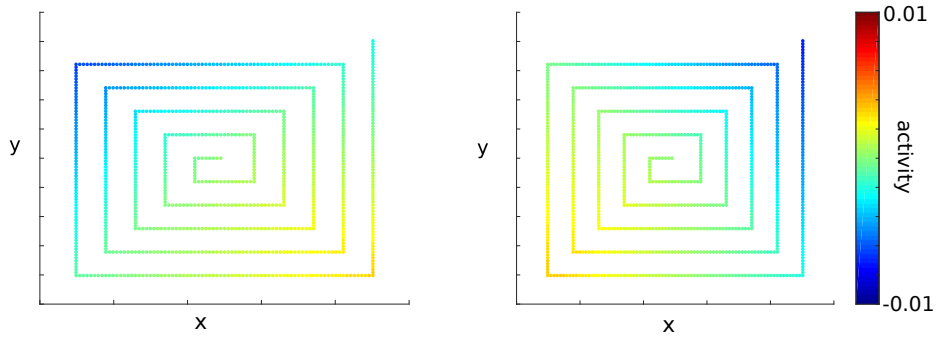


(a) (b)

Figure 2.8: Activity of neurons on PI field when the rat moves in a square spiral maze with $\sigma$ of the Gaussian shape = 40 degrees. a, b. Activity of neurons 75, 25 along the trajectory.

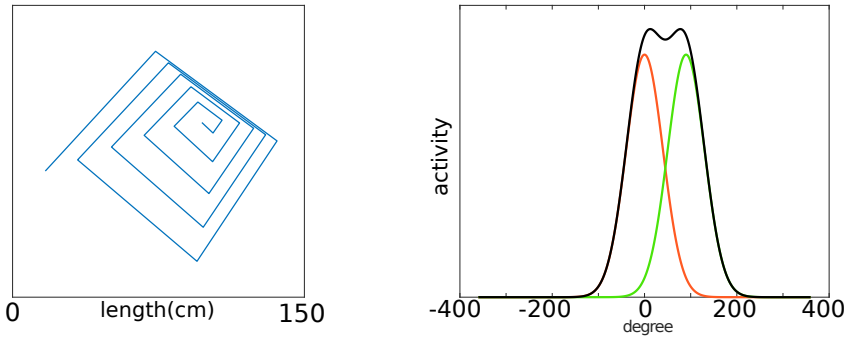


(a) (b)

Figure 2.9: PI with $\sigma = 40$ and learning rate = 0.001 in the square spiral maze. a) Trajectory rebuilt by neurons 25 and 75. b) Overlap of two Gaussian shapes distant from 90 degrees, showing the path integration is not done correctly.

projection of the trajectory to a different axis. 200 neurons are equally distributed to represent 360 degrees. During the w maze simulation, about half of the neurons have no action specificity which accords with the results from (Alexander and Nitz, 2015).

To compare the properties of our VIF to the neurons in RSC, we plot the activity of neurons selected on a VIF while the agent follows a predefined trajectory corresponding to a W maze used for rodent recordings in the RSC (Alexander and Nitz, 2015). The impact of the learning rate will be enlightened using 3 different time constants showing the model's ability to encode allocentric, egocentric, and PI information.

Fig. 2.12 (upper part) shows the temporal activity of few neurons on the field according to the decay rate $\lambda$ used and to the direction of displacement in the maze.

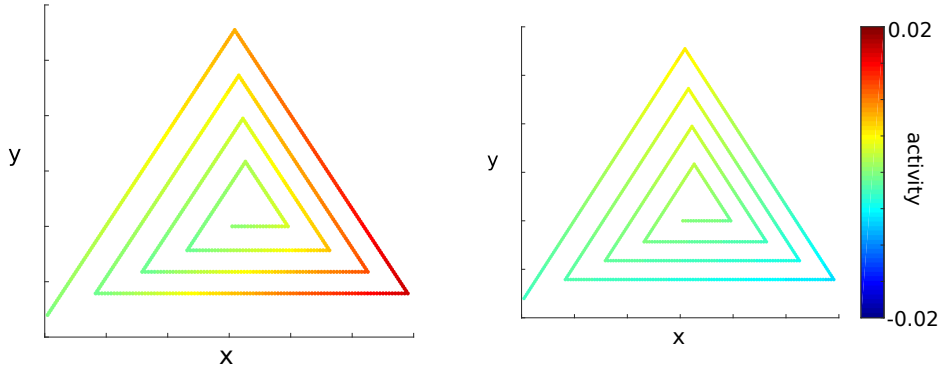


(a) (b)

Figure 2.10: Activity of neurons on PI field when the rat moves in a triangle spiral maze with $\sigma$ of the Gaussian shape = 40 degrees. a, b. Activity of neurons 100, 150 along the trajectory.

In fig. 2.12 a), the recording looks like a head direction cell with the cell active for a given branch (and direction) in the W maze.

With a very fast decay $\lambda = 0.2$ ($\tau \simeq 70$ ms), the cell activity looks like the activity of the HD cells with a small temporal filtering (see fig. 2.12 a). Using a mirror W shape or entering from the opposite side of the maze (blue RLR instead of black LRL rotations) shows that half the cells are more active for either the right or the left turn. These cells are "turn-related" cells. With $\lambda = 0.02$ ($\tau \simeq 0.7$ s), the cells capture the global direction of the motion and can be active all along the W maze.

Most of the neurons in fig. 2.12 seem as if they are reacting to a specific turn in the maze but as soon as $\lambda$ is small enough (long time constant) the neuron activity is modulated by the animal's position in the maze. When the neuron direction is not well aligned with the main direction of the maze, the neuron is only active for the parts of the trajectory pointing in its preferred direction and when the integration is high enough. Otherwise, the global feed-forward inhibition $S(t)$ suppresses its activity. Hence, our model can explain the responses of neurons in the rat's RSC (Alexander and Nitz, 2015) showing differences in neuronal activity for the first and the second turn (see lower part of fig. 2.12). This could be the result of the temporal integration performed by leaky integrators according to the preferred orientation of the recorded cell.

In our simulations, if a high value is used to preset the field (HP) we see a decreasing activity for the neurons having previously an increasing activity because the initial vector was high (in a given direction) and is decreasing. With a decay $\lambda = 0.02$ the neurons are "turn-related" but not "complete route-modulated" since

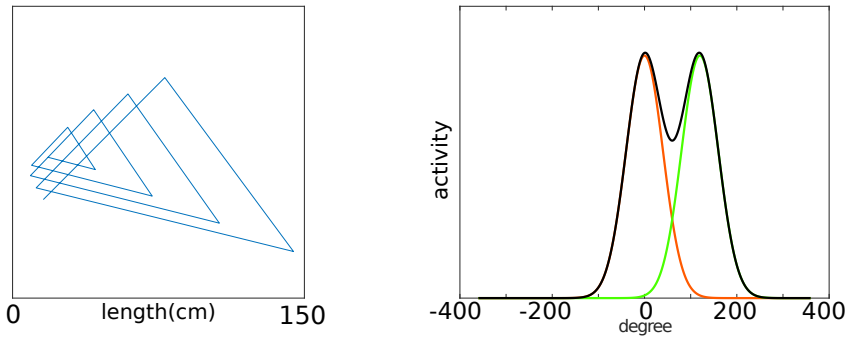


(a) (b)

Figure 2.11: The rat moves in a triangle spiral maze with $\sigma = 40$ and learning rate = 0.001. a) Trajectory rebuilt by neuron 100 and 150. b) Overlap of two Gaussian shapes distant from 90 degrees, showing the path integration is not done correctly.

the decay is too fast (no difference can be seen because no activity/memory remaining of the first turn in the field). The neurons only provide a trace of the local trajectory.

For a decay slow enough ($\lambda = 0.005$ or $\tau \simeq 2.8$ s) the cells in our model are also "complete route-modulated" since their activity level is different for the first and the second right turn for instance. Their activity looks much more like one would expect from PI. Most of these cells are either always active or inactive, which may explain why they are oftentimes overlooked. Fig. 2.12 f shows an extreme case of one neuron with a single peak activity for the last turn. It is clearly route related and could even be seen as a place cell.

Route-centric responses could be in the form of 1) stronger responses to one turn in a series of turns, or 2) ramped activity with the animal's progression along a route. Responses that have both of the two forms in the W maze experiment can be considered as "complete route-modulated". In both cases, these responses will be informative of the animal's position along route space, as opposed to place specific or allocentric space. Bicanski and Burgess, 2018 and Byrne et al., 2007 suggested that the RSC transformed an egocentric reference frame to an allocentric frame. Here instead, we suggest that RSC responds in all three frames, as Alexander and Nitz, 2015, by varying the temporal integration time constant. It could be related to the use of different kinds of synapses or a push-pull cascade of fields having the same time constant. Table 1 summarizes the properties that can be exhibited by our VIF according to the value of the decay and the kind of context used.

In the simulation, both allocentric and egocentric references can be built by using distant or local landmarks to recalibrate the field of HD cells. For instance, when the animal moves in the w maze located in two different locations in the environment. The activity of neurons can be allocentric when the animal uses a distant visual landmark to recalibrate. The local cue(orientation of the entrance of the w maze)

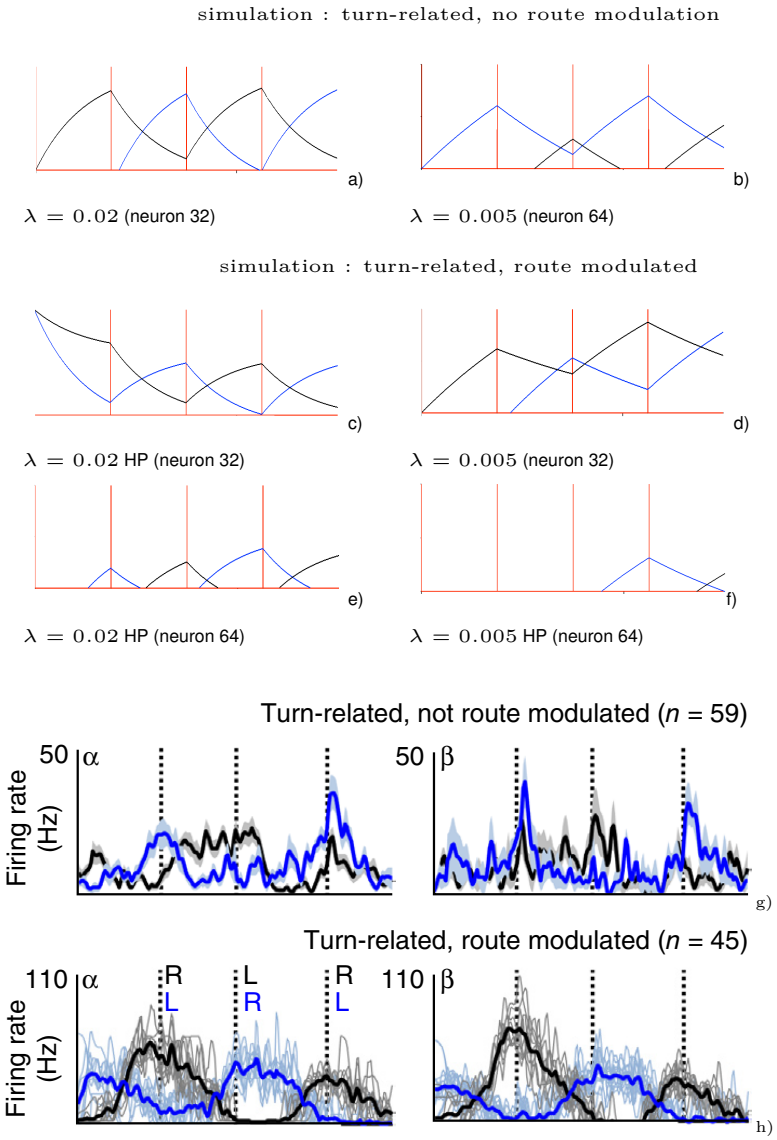


Figure 2.12: Representative neural activity from the W maze simulations using different decay constants (or learning rate). The temporal activity of 2 cells from the field of 100 neurons according to the direction used in the W maze (blue RLR, black LRL). a) to f) correspond to simulated neural activity. The x-axis represents time travelling on a trajectory. Vertical lines in red represent the right or left turn in the W maze. HP (High Preset) represents cases where the simulated field is preset with a high value. Lower decay/learning rate $\lambda$ induces more route-related behaviour but it depends also on the neuron's preferred direction. g) and h) Temporal activity of neurons recorded by (Alexander and Nitz, 2015) in the RSC during experiments in a "W" maze showing route-sensitive neurons.

| learning rate / Recalibration | fast ($\tau < 100$ ms) | slow ($\tau > 500$ ms) |
|---|---|---|
| egocentric (local landmark) | egocentric heading dir. | route-centric path integration |
| allocentric distant landmark(s) and place recognition | allocentric heading dir. | allocentric path integration |

Table 2.1: Comparison of the properties of the neurons in a VIF according to the learning rate or decay value and the recalibration method used

can be used for the recalibration to have the egocentric activity of neurons in the field of HD cells.

However, the geometrical representation is precise only when the bump of the HD cells is a cosine shape with a size of 180 degrees. The centralization mechanism will also cause a shift in the projection. Despite all these effects, the activity of simulated neurons will always maintain the tendency to increase or decrease.

Our model performs PI in RSC using only the HD cell activity as input. It fits with the results obtained by (Alexander and Nitz, 2015). In the next section, we will show our model can also simulate some particular results obtained in (Mao et al., 2017) showing place cell-like activities while usual recordings show no place cell activity in RSC.

### 2.4.3 Simulation on a treadmill

To reproduce the experiment done in (Mao et al., 2017), we simulate a mouse running on a treadmill whose length is 150cm. The mouse is head-fixed on the treadmill so the position of the mouse doesn't change. The travelling distance of the mouse is recorded by the movement of the belt. A reward (a drop of sucrose water ) is delivered to the mouse at the end of each lap. In our simulation, before being fixed on the treadmill, the mouse moves freely in an open wide space. To avoid any problem caused by the environment, we ensure the longest distance in one direction in an open space is longer than the longest path on the treadmill.

In our model (fig. 2.2), each neuron on the 1D PI field projects to one particular 1xM Kohonen map. So we can have up to N 1D Kohonen map representing N blobs or hypercolumns. Our model supports the hypothesis that RSC should be a cortex with the same organization as V1 (blobs) (Crawford et al., 2001). The mouse's PI is reset at the beginning of the simulation. After learning, the activities of our cortical columns in RSC are similar to the 'place cells' recorded in (Mao et al., 2017). Distinct neurons are active when the mouse crosses the distinct positions on the treadmill. When the mouse stops running, the PI field activity is null because $C_j$ is null (see fig. 2.3). Hence, the same neuron will be active no matter how long

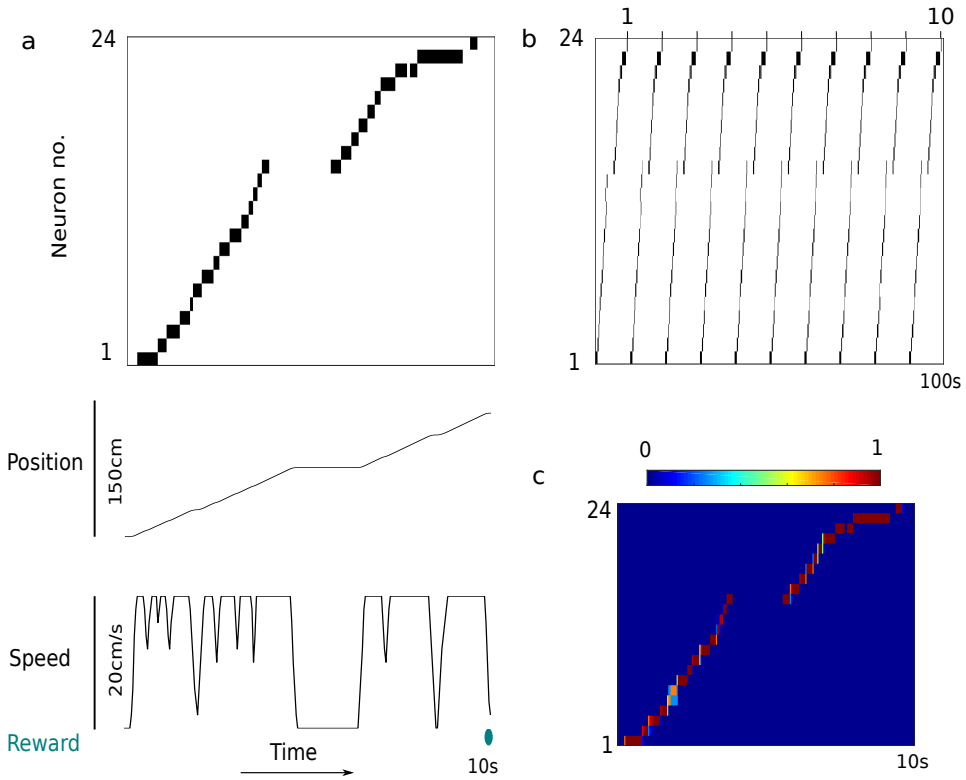


Figure 2.13: Simulation where the mouse is head-fixed and running for 150cm on a treadmill. (a.top) Plot of recorded activity of 24 neurons on a one-dimensional Kohonen map. (a.mid) Position of the mouse on the treadmill. (a.bottom) Speed of the mouse during one lap on the treadmill. Reward (blue) is placed at the end of each lap. (b) Activation time points of 24 neurons in 10 consecutive laps. (c)Average activity of 10 laps for 24 neurons from b

the mouse has moved. No specific place-oriented neuron is active when the mouse stays still (fig. 2.13a.top). Thereby, the representation of the spatial context in RSC is realized using PI field as the input. However, this experiment is very specific since the mouse moves always in one direction. In many other biological experiments, animals move in a two-dimensional environment. In that case, biologists do not find 'place cells' in RSC. Therefore, we simulate the random movements of the mouse in a 2D environment with the same network and record the activity of all the neurons in the Kohonen maps to test if we still find 'place cells' in RSC (in the same region that we recorded the activity of neurons in the treadmill simulation).

From (fig. 2.14a), we can see that the mouse has explored almost everywhere in the 2D environment. In (fig. 2.14b, c, d), each neuron in 3 different blobs is active in many different places on the trajectory. The non place-cell activity is not observed coincidentally. There is no apparent spatial correlation between the cell activity and the animal's position. We find no more place cell-like activity. No cluster of

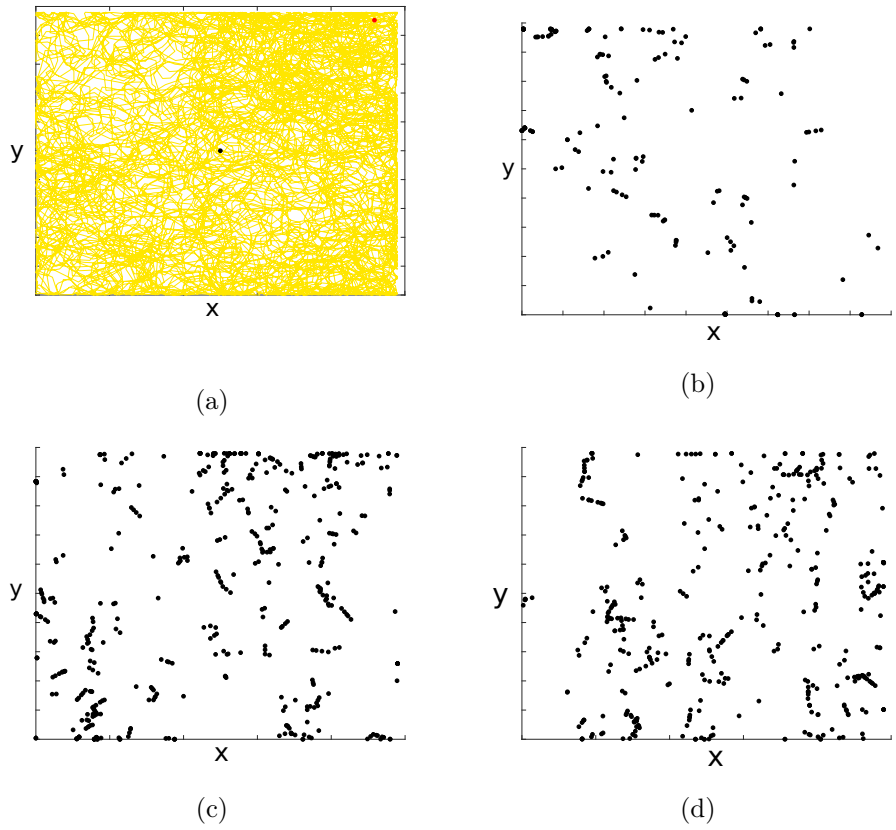


Figure 2.14: a. The trajectory of the mouse. The mouse starts moving from the middle of the environment indicated by a blue point and the stop position is marked by a red point. b, c, d. Activity of three neurons on 3 different 1D Kohonen maps (blobs).

activity is observed. This is quite normal since we are using local self-organizing maps focusing on quantifying the distance in a given direction. The neurons on the Kohonen map are associated only to a local neighbourhood of PI field to quantify one part of the bump (i.e. PI). They cannot access to the 2D information on PI field.

However, if the neurons on the Kohonen map can access to the whole PI field (global self-organization), place cells can be rebuilt in a 2D environment (fig. 2.15a, b) like it is done in the hippocampus after the entorhinal cortex (EC) merging.

Moreover, the place cell activity emerges as well using the global self-organizing map with random connections to a small part of the neurons on the path integration (fig. 2.15c, d) because even random connections can capture the spatial property of the bump of PI field as long as a "global" access to PI field is ensured.

That's totally different from what we got from a Kohonen map connected only to neighbour neurons on the PI field. The local self-organizing map is good enough to simulate a place cell-like activity in RSC when the animal moves in one single

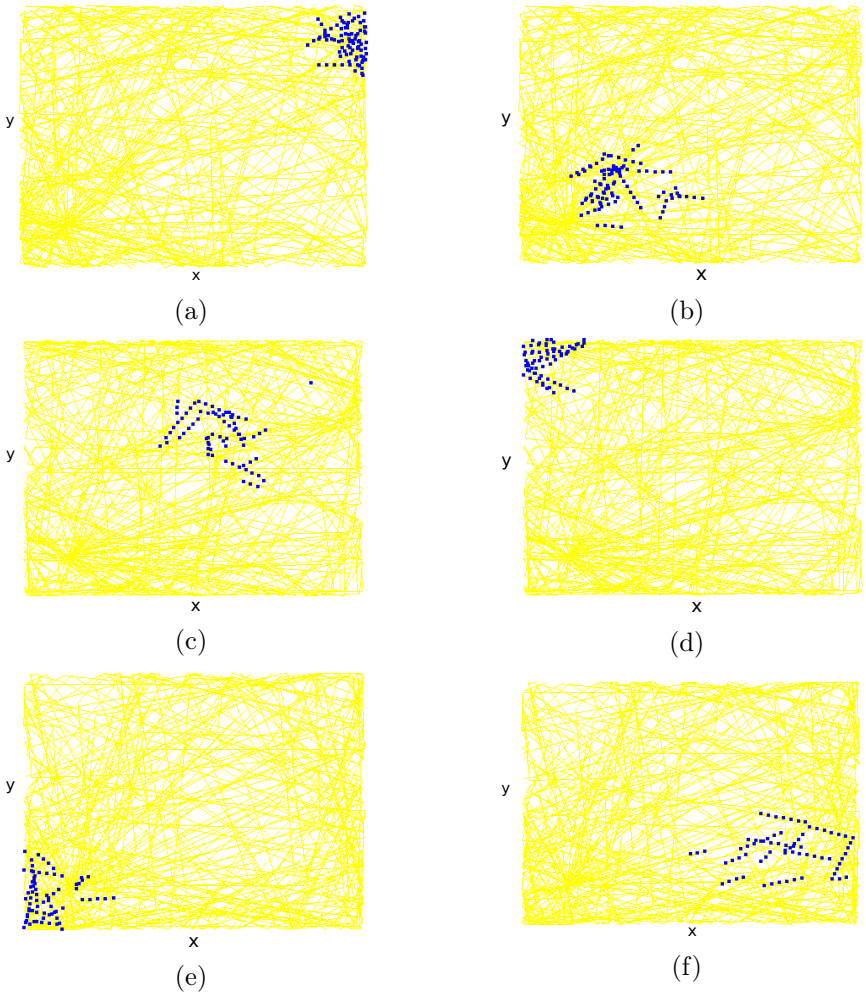


Figure 2.15: Place cell-like activity recorded from a global self-organizing map. Yellow line is the trajectory of the simulated animal. Blue points in each figure are the activity of one neuron on the global self-organizing map representing one place. a, b. Activity of two different neurons on one global self-organizing map with a complete connection to PI filed. c, d. Activity of two different neurons on one global self-organizing map with a random connection to 6% of the neurons on PI field. e, f. Activity of two different neurons on one global self-organizing map with a random connection to 10% of the neurons on PI field. Activity of 25% neurons in PI field is killed.

direction on the treadmill (Mao et al., 2017). When the animal moves freely, the connectivity from PI field to the self-organizing map is not sufficient to access to the 2D information for generating place cells in RSC.

The effect of the noise on PI mechanism is also shown by killing the activity of 25% neurons in PI field (fig. 2.15e, f). Place cell-like activity can still be observed in RSC thanks to the connection with full access to PI field. The spatial information

in RSC simulated in our model is robust to the noise from the input (fig. 2.7) and the output of PI mechanism.

Our model also supports the idea that RSC projects onto EC and the hippocampus to build grid cells and place cells.

## 2.5 Conclusion

In this paper, we show the capability of our model to approximate PI using the bumps of HD cells as inputs. The robust PI built by our low pass filter mechanism therefore supports the representation of the spatial context in RSC via local self-organizing maps.

The learning rate plays a crucial role in our model. Different learning rates can be used cooperatively to have a variable resolution for representing environments of different sizes. Using different amounts of PI fields connected in cascade with the same learning rate can also provide the variable scale of the environment (Gaussier et al., 2020)

In the spiral maze simulation, we tested our model with different learning rates and sizes of HD cell bumps. A correlation between the performance of PI and the size of the bump of HD cells is predicted. The size of the bump should be larger enough than the turning angle to ensure the precision of PI. We hypothesize that the rodent will be disoriented under too sharp rotation (e.g. turn more than 90 degrees within a short time). Hence, if our model is correct, according to the width of the HD cells, we should be able to predict when an animal will be disoriented.

Our model also has the capability to build the grid cell activity recorded in the dorso Medial Entorhinal Cortex (Sargolini et al., 2006). We suppose the grid cell activity can be the compression of the cortical activities on the 1D discretization of PI field in RSC (Gaussier et al., 2007). As illustrated in (fig. 2.16), the activity of neurons in PI field is discretized by the Kohonen maps. The activity of each neuron on the Kohonen map represents the distance of PI in their respective preferred orientation on a Cartesian plane. By adding a modulo projection, the neurons on the 1D Kohonen map will be active recurrently with the same distant interval depending on the modulo operator. The activity of two different neurons on the Kohonen map is projected separately onto two modulo fields which can be considered as 1D vectors. The grid cell activity can be built by the activity of neurons on these two modulo fields using conjunctive cells. The grid orientation is determined by the selection of two neurons distant from 60 degrees. Ongoing works focus on how a learning process can be used to build at the same time modulo mechanism and the preference for 60 degrees.

Our work advocates the hypothesis that the path integration could pre-exist before EC 'grid cells' and hippocampal 'place cells' as proposed by (Gaussier et al.,

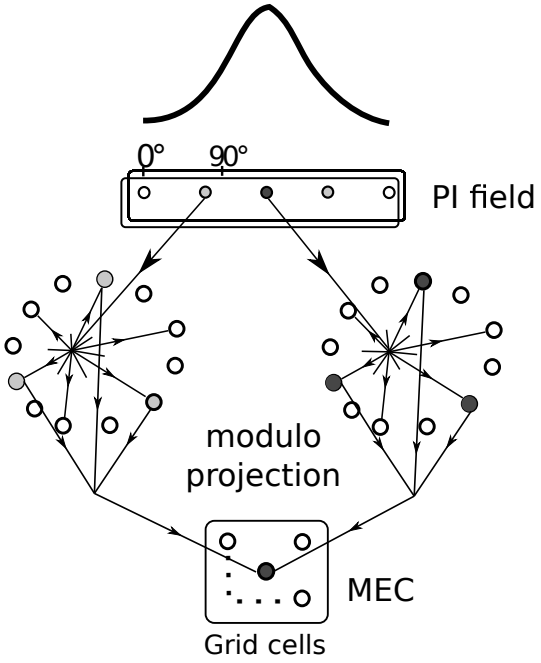


Figure 2.16: Building MEC grid cells from the projection of RSC blob activity using a modulo operator

2007). In our model, RSC is nothing more than a classical cortex performing a low pass filtering to its inputs related to HD cells and using blobs of neurons to 'recognize' or quantify those activities. In the treadmill simulation, the mouse is head-fixed on a linear treadmill rewarded once per lap. The activity of neurons on the Kohonen map shows similarity with the activity of RSC 'place cell' found in (Mao et al., 2017). Our model also explains why (Mao et al., 2017) were able to find 'place cells' in their treadmill experiment while nobody else found such an activity in the case that the animal is moving in a 2D environment. Restricted movements in a spiral maze however allow obtaining cells that react to the followed route (Nitz, 2012) and correspond to what we expect from the recording of some neurons in our PI fields.

The spatial navigation at different scales can be realized by using high or low learning rates in our model. This model can also realize both allocentric and egocentric tasks by using distant or local cues as the landmark to recalibrate HD cells and/or PI as long as the visual information is added. RSC in our model could play a role as a hub where the visual and proprioceptive information can be merged. The interaction of the allocentric and egocentric information should allow the animal to switch between different reference frames for complex spatial navigation tasks.

# Appendix of chapter 2

## Classical conditioning mechanism used as an STM

In the classical conditioning mechanism, $dW_{ij} = W_{ij}(t + dt) - W_{ij}(t)$, we substitute $dW_{ij}$ in (eq. 2.1). Thereby, the conditional output (vector field) $O_i$ can be represented as:

$$O_i(t + dt) = C_j \cdot W_{ij}(t) + \lambda \cdot C_j^2 \cdot (U_i - O_i) \tag{2.5}$$

$O_i(t + dt)$ is inhibited to 0 when $V_i(t - dt) = 0$, otherwise,

$$O_i(t + dt) = W_{ij}(t) + \lambda \cdot (U_i - O_i) \tag{2.6}$$

when $C_j = 1$, $O_i = C_j \cdot W_{ij} = W_{ij}$. Finally, the output can be rewritten as:

$$O_i(t + dt) = (1 - \lambda) \cdot O_i(t) + \lambda \cdot U_i \tag{2.7}$$

where $\lambda$ is the learning rate altered between no stimulated rate 0.001 and strong stimulated rate 1 (when the animal meets the reward or the reset mechanism is triggered. When $\lambda$ is small enough as the one we use for the simulation ($\lambda = 0.001$), the animal reserves most of the state of the past PI and updates PI field step by step. While the reset is activated ($\lambda = 1$), the animal erases all the past PI and updates to the current state immediately.

## Approximation of path integration with the LMS

We suppose the animat is moving from position 0 (at time $t_0$) to position C (at time $t_C$) with a reset in 0. So $\forall i \in [0, N-1], O_i(t_O) = 0$. Using a constant speed of 1, we have $C = 1$. The cumulative activity of any neuron i of the Vector Integration Field with a cosine bump of activation for $U_i$ is $O_i(t) = (1 - \lambda)O_i(t - dt) + \lambda U_i(t - dt)$ because of the equivalence between STM and classical conditioning demonstrated earlier. If we recursively replace $U_i(t)$ by its value at time $t - 1$, we obtain:

$$U_i(t) = \sum_{t=t_O}^{t_C} \lambda(1 - \lambda)^{t_C - t} U_i(t) = \lambda \sum_{t=t_O}^{t_C} (1 - \lambda)^{t_C - t} U_i(t)$$

$$O_i(t) = \sum_{t=t_O}^{t_C} \alpha(t) U_i(t)$$

with $\alpha(t) = \lambda(1 - \lambda)^{t_C - t}$ an exponentially decreasing function. Since $U_i(t)$ is a discretized positive cosine function over i with a maximum for the angle $\theta_i$. We can

write $U_i(t) = 1 + \cos(\Phi(t) - \theta_i)$ and then

$$\begin{aligned} O_i(t) &= \sum_{t=t_O}^{t_C} \alpha(t)(1 + \cos(\Phi(t) - \theta_i)) \\ &= \sum_{t=t_O}^{t_C} \alpha(t) + \sum_{t=t_O}^{t_C} \alpha(t) \cos(\Phi(t) - \theta_i)) \end{aligned}$$

We note $A = \sum_{t=t_O}^{t_C} \alpha(t)$, then

$$O_i(t) = A + \sum_{t=t_O}^{t_C} \alpha(t) \left(\cos \Phi(t) \cdot \cos \theta_i + \sin \Phi(t) \cdot \sin \theta_i\right)$$

Using the classical trigonometrical transform: $cos(a-b) = cos(a)cos(b)+sin(a)sin(b)$, we obtain:

$$O_i(t) = A + \cos \theta_i \sum_{t=t_O}^{t_C} \alpha(t) \cos \Phi(t) + \sin \theta_i \sum_{t=t_O}^{t_C} \alpha(t) \sin \Phi(t)$$

On a short time scale, with $\lambda$ small enough, we can consider $\alpha(t) \approx \alpha$ then

$$O_i(t) = A + \alpha(\cos \theta_i \sum_{t=t_O}^{t_C} \cos \Phi(t) + \sin \theta_i \sum_{t=t_O}^{t_C} \sin \Phi(t)) \tag{2.8}$$

If we note $\Phi_T$ and $D$ the direction and the distance of the straight line displacement from $O$ to $C$ then we have also $D \cos \Phi_T = \sum_{t=t_O}^{t_C} \cos \Phi(t)$ and $D \sin \Phi_T = \sum_{t=t_O}^{t_C} \sin \Phi(t)$ (projections of all the displacements on the x and y axis respectively if the angles $\Phi(t)$ are always relative to the same absolute or allocentric direction). Hence eq. 2.8 can be rewritten as follow:

$$\begin{aligned} O_i(t) &= A + \alpha \left(D \cos \theta_i \cos \Phi_T + D \sin \theta_i \sin \Phi_T\right)) \\ &= A + \alpha D \cos(\theta_i - \Phi_T) \end{aligned}$$

The average activity on the whole field $O_i t()$ is A since $\int \cos(\theta_i - \Phi_T) dT = 0$ and $1/N \sum_{i=1}^{N} A = A$. If as proposed in our model, we use a feedforward inhibition to suppress the average activity over the field the resulting field $O_i$ is:

$$O_i(t) = \alpha D \cos(\theta_i - \Phi_T)$$

As a result, the winning neuron in the path integration field corresponds to the final direction of the movement $\Phi_T$ since the last reset of the field activity. Its activity level corresponds to the distance travelled in this direction from the starting point if

we suppose the decay can be neglected.

In practice, because of the decay, the result is not exactly a path integration. It is similar to a path integration with the strength of the first movements lower than the strength of the most recent movements. Hence, with a cosine bump, we have a correct approximation of the path integration if the learning rate is sufficiently small. For a Gaussian bump similar to a cosine the error is quite limited as shown by the experimental results. If the size of the bump is sharper than the cosine shape the approximation is still correct if the rotation speed is sufficiently slow so that the bump can continuously move on the field. This is verified by our different simulations.

### Kohonen map algorithm using scalar product

The activity of neurons on the Kohonen map $S_k(t)$ is discretized from the PI field. To cluster the activity on the map, we use the dot product to determine which pattern of weights $W_{ik}(t)$ is the most similar to the vector of input activities $P_i(t)$ (fig.2.2). The number of the winner neuron $k^w$ is defined by :

$$k^w(t) = arg\ max(\frac{P_i(t) \cdot W_{ik}(t)}{\sqrt{P_i(t)^2 \cdot W_{ik}(t)^2}}), k \in \{1, .., M\} \tag{2.9}$$

M is the number of neurons on a 1D Kohonen map. The weight between the neurons on the PI field and the Kohonen map is updated by:

$$W_{ik}(t + dt) = \epsilon \cdot (P_i(t) - W_{ik}(t)) \cdot S_k(t) \tag{2.10}$$

$\epsilon$ is the learning rate of self-organizing. With a neighborhood function $h_{kk^w}(t)$, we have the activity on the Kohonen map :

$$S_k(t + 1) = h_{kk^w}(t, d) \tag{2.11}$$

d is the coordinate distance between the winner neuron $k^w$ and other neurons on a 1D Kohonen map. Fig(2.17) shows the shape of the neighbourhood function.

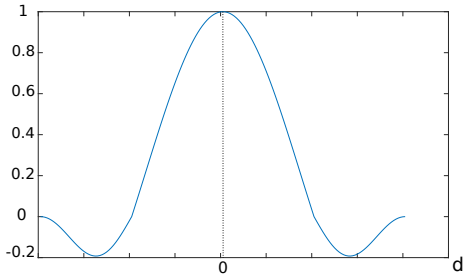


Figure 2.17: Shape of the lateral interaction function

## Perspective

Our model could be further extended to recalibrate and generate the bi-directional cells observed in (Jacob et al., 2017) by merging visual information and proprioceptive information. RSC is known to manipulate visual information and to translate between egocentric (self-centred) and allocentric (world-centred) spatial information (Alexander and Nitz, 2015). Visual information could be very important for the recalibration of HD cells in RSC. However, further study in the bi-directional cells has not been conducted due to time limitations. In the next chapter, we will focus on the important contribution of the RSC in conveying information of path integration. Complementary simulations will be made to prove our proposed hypothesis that the RSC only has a local connection to the path integration field. Modulo connectivity between the RSC and the EC will be introduced to explain the compression role of the EC and the grid cells generated by self-motion. Notably, no specific mechanism is used in our RSC model. Therefore, it could be a general model not only for PI but also for modelling sensory information or other cortical areas.

# Chapter 3

# Contribution of the retrosplenial cortex to path integration and spatial codes [1]

## 3.1 Abstract

In the proposed model, we suppose the retrosplenial cortex(RSC) conveys path integration(PI) information to the hippocampal system. Our model shows the potential of the PI field in reproducing diverse neuronal activities involved in the spatial representation of animals. We explain the absence of places cells in RSC because of the difficulty of neurons accessing the whole PI field. The simulated activity with only local connections fits with the recorded activities in RSC. Moreover, we emphasize the importance of the entorhinal cortex(EC) as a hub to merge the different afferent cortical activities in order to build an efficient hash code for complex pattern recognition and novelty detection at the level of the hippocampus. The grid cells could be an epiphenomenon of this compression mechanism in EC.

**Keywords:** path integration, retrosplenial cortex, entorhinal cortex, head direction cell, place cell, grid cell

## 3.2 Introduction

Path integration(PI) is the estimation of distance and direction as a function of velocity and time. It enables animals to return to a starting point even in the absence of visual cues. Many different species, from insects (Collett et al., 1996)) to mammals (Etienne and Jeffery, 2004)), have the ability to perform PI. However, it

[1] Ju, Mingda, and Philippe Gaussier. "Contribution of the Retrosplenial Cortex to Path Integration and Spatial Codes." International Conference on Simulation of Adaptive Behavior. Springer, Cham, 2022.

remains unknown where and how this information is integrated. Various recordings in the retrosplenial cortex (RSC) (Cooper and Mizumori, 1999; Save et al., 2001; Czajkowski et al., 2014) suggest that RSC might play an important role in PI (Cooper et al., 2001; Elduayen and Save, 2014). The place cell-like activity found in RSC (Mao et al., 2017) could also be a sign of the PI information conveyed via RSC. Many prior models (McNaughton et al., 1996; Redish et al., 1996) propose that PI is performed in the hippocampus (Hipp). Some of the models adapted to the findings of grid cells and head direction(HD) cells in the entorhinal cortex (EC) by reclaiming that the PI takes place inside EC. Grid cell models including oscillatory interference model (Burgess et al., 2007; Hasselmo, 2008) and attractor models (Fuhs and Touretzky, 2006; McNaughton et al., 2006; Burak and Fiete, 2009; Bonnevie et al., 2013) rely on velocity input consisting of the movement direction and the linear speed. These models take the movement direction calculated from sequential positions in the experimental data comprising the velocity input, rather than the HD at each position while citing HD recordings as the justification for velocity input (Fuhs and Touretzky, 2006; McNaughton et al., 2006; Burgess et al., 2007; Hasselmo, 2008; Burak and Fiete, 2009) Recordings in EC (Raudies et al., 2015) indicate that coding of MD is not prominent in the medial EC, and HD cannot directly replace MD in the mentioned models using PI to build the grid cells. Cortices such as RSC and the parietal cortex could be candidates for the seeking of the moving directional tuning and as the potential origin of the PI. Our model of the PI is independent of Hipp or the HD cells in EC. We suppose grid cells (Hafting et al., 2005) is the result of a generic compression mechanism of the cortical activities when applied on PI fields primarily computed outside Hipp (Gaussier et al., 2007; Ju and Gaussier, 2020). The hippocampus could play a role of indexing or building hash codes of the cortical activity (Teyler and Rudy, 2007) in order to detect new events or patterns that have to be stored in the cortex (Eichenbaum et al., 1994; Bunsey and Eichenbaum, 1996; Buzsáki and Moser, 2013). In this research, we used a simple learning rule(classical conditioning) (Rescorla, Wagner, et al., 1972) as a low path filtering to directly compute PI from movement direction cells. Following the biological recordings of the place cell-like activity in RSC (Mao et al., 2017) which has been successfully simulated using our PI model (Ju and Gaussier, 2020), our model of PI is also able to account for diverse neuronal activities in the corticohippocampal circuit including activities of place cells, grid cells and movement direction-modulated cells. We emphasized in our simple model the potential of the PI as the substrate of the spatial representation of animals and the richness of the spatial information conveyed by the PI might have been underestimated.

## 3.3 Computational model

The preliminary inputs to our PI model are the HD cells simulated by a one-directional ring attractor (McNaughton et al., 1991) with the presumption that the moving direction is consistent with the HD while recordings (Raudies et al., 2015) proved the contrary. We thereby replace the HD cells with the movement direction cells as the input to our model and hypothesize that the MD cells share common properties as the HD cells. To simplify, the potential MD cells are simulated by the one-directional ring attractor.

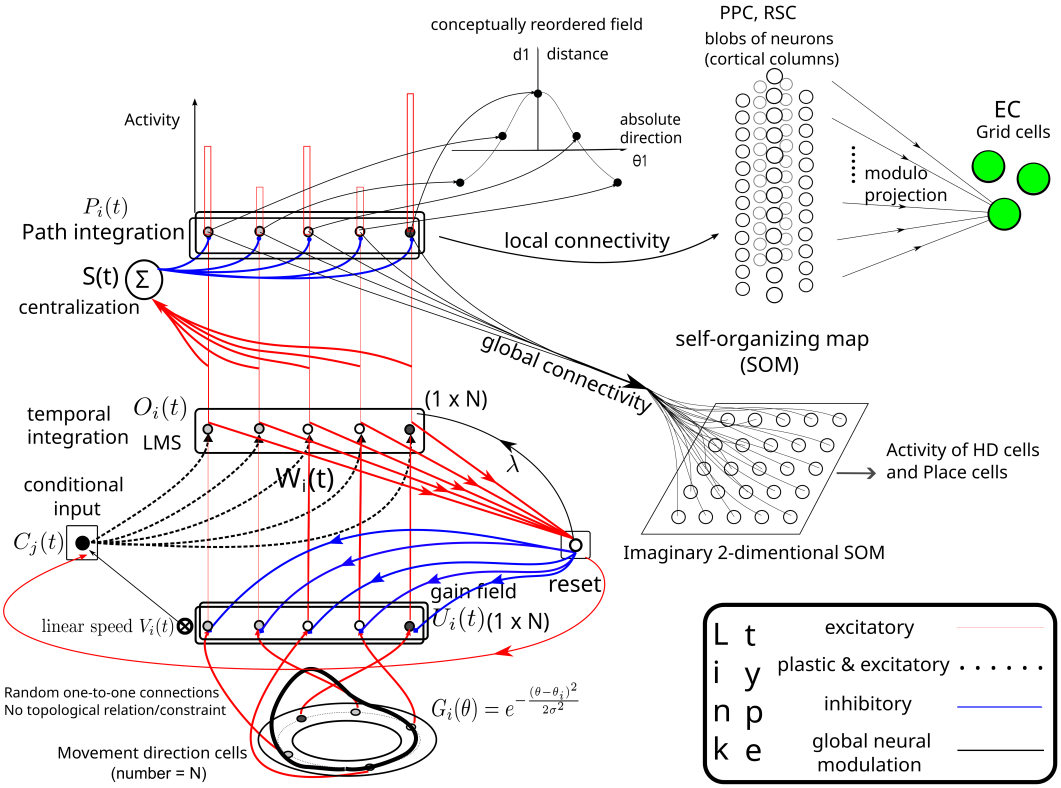


Figure 3.1: Computation model of path integration (PI) in the retrosplenial cortex. Since there is no need of lateral interaction between the neurons on the PI field, the global bump of activation is only visible if neurons are reordered according to their preferred direction. Self-organization properties in RSC with local or global connections to some neurons in the PI field allow the building of different spatial signatures. Compression of this information at the level of EC allows the building of a compact code (grid cells). Hippocampal neurons having global access to the whole PI field from EC grid cells can recognize associated places to PI information.

The activity of MD cells is represented as a bump of activity of a ring of neurons: $G_i(\theta) = e^{-\frac{(\theta-\theta_i)^2}{2\sigma^2}}$ where $\sigma$ determines the width of the firing range of MD cells and $\theta_i$ is the absolute orientation of the animal.

The input of the model (Fig. 3.1) is the absolute orientation and the linear velocity of the animal. We suppose that a group of neurons is equally distributed to represent 360 degrees in order to simulate MD cells. Each neuron has a preferred direction depending on the number(N) of neurons. The interval between each preferred direction is 360 degrees divided by N. This group of neurons can represent 360 degrees with good precision if we have enough neurons. Visual place recognition of the starting location for PI is used to reset the PI field and limit the error accumulation. Each time the animal comes back in the vicinity of this location the reset is performed. Using border cells could also be useful for the recalibration of animals during navigation tasks. For the following simulations, the reset point is in the middle of the environment. No movement constraint is introduced after the reset while the movement is limited to half of the environment if the reset point is near the border of the environment. There is no lateral interaction or adjacency among neurons on the PI field.

Now we will describe how a simple condition mechanism can be used to perform path integration if the input activity is a bump of activity of a ring of neurons. Starting from the linear velocity of the animal $V$ and a field of neurons $G_i(\theta)$ representing the M cells, conjunctive cells are used to build the field $U_i$ defined as $V \cdot G_i(\theta)$. $U_i$ is used as the unconditional stimulus to perform temporal integration on $O_i$ neurons.

$$O_i(t) = f(\sum W_{ij} \cdot C_j) \text{ , with } f(x) = \begin{cases} 0 & \text{if } x < 0 \\ x & \text{if } 0 \leq x < 1 \\ 1 & \text{if } x > 1 \end{cases} \tag{3.1}$$

The update of the synapses $dW_{ij}$ is subject to the least mean square algorithm which is identical to a classical conditioning (Widrow and Hoff, 1960; Rescorla, Wagner, et al., 1972):

$$dW_{ij} = \lambda \cdot (U_i - O_i) \cdot C_j \tag{3.2}$$

where $\lambda$ is the learning rate of classical conditioning. $C_j$ is a binary value associated to a spatial context $j$ (the conditional input). To simplify, we maintain the environmental context which is the conditional stimulus $C_j$ constant and equal to 1 during the simulations in this work. However, replacing this constant neuron with a set of neurons representing different contexts might be used to compute in parallel different path integration according to different positions or contextual goals in the environment.

The output $O_i$ can be finally written as:

$$O_i(t + dt) = (1 - \lambda) \cdot O_i(t) + \lambda \cdot U_i \tag{3.3}$$

We obtain the path integration field composed of positive and negative values by

subtracting the average activity of all neurons:

$$P_i = O_i - \sum_{i=0}^{N} O_i/N \tag{3.4}$$

The integration of the activity modulated by the linear speed and the absolute orientation of the animal is proportional to the path the animal moved (Alexander and Nitz, 2015).

The reset of the PI can be realized by the detection of the novelty (Markou and Singh, 2003; Jauffret et al., 2013) in order to avoid the overloaded accumulated error. This reset is activated when the gradient of novelty becomes flat. In our simulation, we define novelty as the difference between PI fields updated at sequential time steps. During the reset, the learning rate $\lambda$ is set to 1 and the unconditional input of the PI is inhibited to 0 one time step after the reset mechanism activates. By substituting the parameters in (eq. 3.3) with their reset values, we have $O_i(t + dt) = U_i$ so that PI is reset to 0 in one time step.

The activity of PI field is projected to a set of Kohonen self-organizing maps (SOM) (blobs on Fig. 3.1). Each neuron on the PI field projects selectively to every neuron on the SOM depending on the connectivity (local or global) from PI field to the SOM. The activity of neuron k on the SOM is the following:

$$E_k = \left( \frac{\sum P_i(t) \cdot W_{ik}(t)}{\sqrt{\sum P_i(t)^2 \cdot \sum W_{ik}(t)^2}} \right), k \in [1, .., M] \tag{3.5}$$

The index of the winner neuron $k^w$ is defined as:

$$k^w(t) = arg\ max\left(E_k\right), k \in [1, .., M] \tag{3.6}$$

M is the number of neurons on the SOM. The synaptic weights between neurons on the input field $P_i$ and neurons on the SOM is updated by:

$$W_{ik}(t + dt) = \lambda_{som} \cdot (P_i(t) - W_{ik}(t)) \cdot S_k(t) \tag{3.7}$$

$\lambda_{som}$ is the learning rate of self-organization. The potential of neurons on the self-organizing map is subject to a Mexican hat function $h_{kk^w}(t)$ such as:

$$\begin{gathered} S_k(t) = h_{kk^w}(d_k) \cdot S_{k^w}(t),\ k \in [1, Q] \text{ with} \\ h_{kk^w}(d_k) = \left(\frac{1}{\sigma_1 \cdot \sqrt{2 \cdot \pi}} \cdot exp^{-\frac{d_k^2}{2 \cdot \sigma_1^2}} - \frac{1}{\sigma_2 \cdot \sqrt{2 \cdot \pi}} \cdot exp^{-\frac{d_k^2}{2 \cdot \sigma_2^2}}\right) \cdot 15 \end{gathered} \tag{3.8}$$

Here we take $\sigma_1$ equals to 3 and $\sigma_2$ equals to 6 for the SOM containing 36 neurons.

$S_k(t)$ is the potential of the k-th neuron with $Q$ the size of the Mexican hat. $d_k$ represents the distance between the winner neuron $k^w$ and other neurons $k$ on the SOM.

In the next section, we discuss in detail the potential of our PI model to simulate diverse neuronal activity related to the PI in RSC according to the learning rate of the temporal integration field.

## 3.4 Parameters and moving pattern

In the following simulations without special indication, the animal moves freely in a 2x2 metres square arena for 40000 time steps. One iteration in the simulation corresponds to 0.1 seconds. The product of the learning rate $\lambda$ and its associated time constant $\tau$ equals 0.1 seconds in order to scale the simulation from time steps to seconds. The moving pattern of the animal is adjusted to be biologically plausible. The acceleration of linear and angular speed has been introduced. The linear speed varies from $10cm/s$ to $40cm/s$. The acceleration of linear speed is $20cm/s^2$ (Høydal et al., 2007) while the angular speed of the animal's body is $90°/s$ (Pasquet et al., 2016).

The (x,y) coordinate of the animal are updated as follow:

$$\begin{aligned} x(t+dt) &= x(t) + d.cos(\theta(t)) \\ y(t+dt) &= y(t) + d.sin(\theta(t)) \end{aligned} \tag{3.9}$$

with $\theta(t)$ the animal's MD according to an absolute referential and $d = v \cdot dt$ with v its instantaneous speed.

Simulations are conducted using bumps of activity of MD cells as the input. The bump is simulated by a Gaussian function with $\sigma = 60°$. MD is analyzed with a 6 degrees bin width. The metric to characterize the MD cells (Taube et al., 1990a) is the directional information rate:

$$MD_{score} = \sum_{i}^{N} p_i \frac{\lambda_i}{\lambda} log_2 \frac{\lambda_i}{\lambda} \tag{3.10}$$

where N equals 60, $\lambda_i$ is the mean firing rate of a neuron in the i-th bin, $\lambda$ is the overall mean firing rate, and $p_i$ is the probability that the animal's MD pointed to the direction which is represented by the i-th bin. The spatial information rate is calculated to characterize the place cells:

$$PC_{score} = \sum_{j}^{M} p_j \frac{\lambda_j}{\lambda} log_2 \frac{\lambda_j}{\lambda} \tag{3.11}$$

where the environment is divided into 100 non-overlapping spatial bins which means M equals 100, $p_j$ is the occupancy probability of bin j,$\lambda_j$ is the mean firing rate of bin j, and $\lambda$ is the overall firing rate of the cell.

The sparsity of cells (Skaggs et al., 1996) measures the fraction of the environment in which a cell is active:

$$Sparsity = \sum(p_j \cdot \lambda_j)^2 / \sum p_j \cdot \lambda_j^2 \tag{3.12}$$

Intuitively, a sparsity of 0.1 means that the place field of the cell occupies 1/10 of the area the rat traverses. The selectivity measure is equal to the spatial maximum firing rate divided by the mean firing rate of the cell. The more tightly concentrated the cell's activity, the higher the selectivity is. A cell with no spatial tuning at all will have a selectivity of 1. The main variable modulated during all the simulations is the learning rate $\lambda$ used for the temporal integration of the gain field in Fig. 3.1 and in Eq. 3.2, 3.3. The performance of the PI model with learning rates ranging from 0.1 to 0.001 ($\tau$ from $1s$ to $100s$) will be tested.

### 3.4.1 Recording of neurons learning MD activities in RSC

The first simulation tests the capability of our path integration to retrieve the activity of MD or HD cells by using a high learning rate $\lambda$ equal to 0.1. The activity of one neuron on a SOM showing MD cell's activity is recorded in Fig. 3.2.

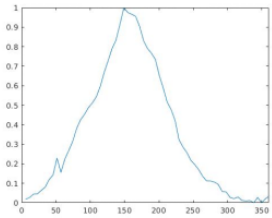

(a) activity of one neuron as a function of MD

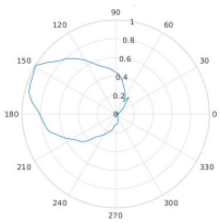

(b) activity of the same neuron as a function of MD in polar coordinates

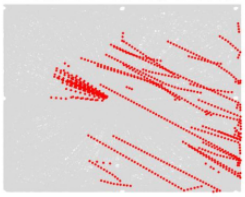

(c) winner position of the same neuron along the trajectory

Figure 3.2: Example of one activated neuron showing MD cell activity on the SOM when $\lambda$ equals to 0.1

The mean values of the directional and spatial information rates are 2.35 and 2.43 with STD of 0.73 and 1.41 respectively. MD cells present a high directional information rate but a very random spatial information rate. The high standard derivation in the spatial information rate is related to the freely moving pattern in which the probability of the animal facing each direction can be different. The width of the bump of activity of MD cells before the competition depends on the shape of

the bump of activity of the initial MD cells which are the input to our model. The dependency between the retrieval MD cells and the original MD cells as the input to the PI model leads to a hypothesis that the HD or potential MD cells in RSC could be homogeneous to the ones found in Hipp. A high learning rate leads to the early saturation of the PI field and realizes the retrieval of the MD cells homogeneous to the input MD cell.

### 3.4.2 Building place cells from PI information

The involvement of the spatial information conveyed by the PI in the generation of place cells is tested using a comparatively low learning rate equal to 0.001 with neurons fully connected to the virtual PI field. The activity of one neuron on a SOM is shown in Fig. 3.3.

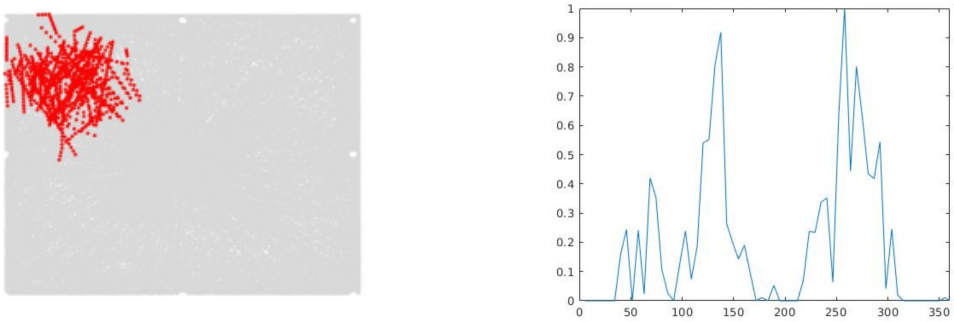


(a) winner position of one neuron along the trajectory

(b) activity of the same neuron as a function of MD in polar coordinates

Figure 3.3: Example of one activated neuron showing place cell activity on the SOM when $\lambda$ equals to 0.001 when using connections to the whole path integration field

The mean values of the directional and spatial information rates are 1.08 and 4.44 with STD of 0.62 and 0.66 respectively. No MD cell activity is observed. By accessing the whole PI field, our model is able to build place cell activity by simply using a low learning rate. Classical conditioning thereby plays a role of short-term memory or a low pass filter.

The average directional and spatial information rates of the activity of neurons using different learning rate is shown in Fig. 3.4. Our PI model is capable of building a wide range of neuronal activity by exclusively modulating the learning rate as long as the downstream region gets full access to the upstream cortex conveying the PI information.

Notably, no place cell in an open environment was found in RSC. It means the connectivity from the PI field to the SOM in RSC is not global but only local as is the case for the classical cortical column.

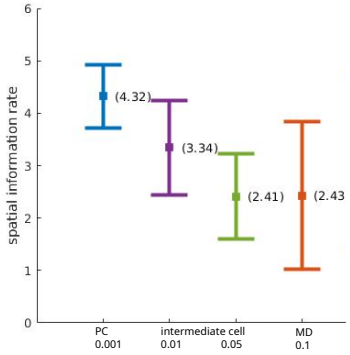


(a) spatial information rate

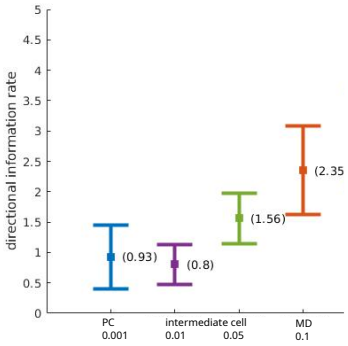


(b) directional information rate

Figure 3.4: The average directional and spatial information rates of the activity of neurons using different learning rates. The square indicates the mean value. The interval of STD is represented by horizontal lines.

### 3.4.3 Robustness of the model

#### High frequency recalibration

To test the robustness of our model, the uniform white noise with an amplitude of 10 percent of the value of linear and angular speed is implemented at the stage of the gain field. The learning rate is fixed at 0.001. The animal is forced to go through the recalibration point once per 10 seconds. The activity of neurons is recorded when the animal moves freely in a 2x2 metres square environment for 7500 seconds(1 iteration = 0.1s).

The equation of the gain field in Fig. 3.1 can be rewritten as:

$$\begin{aligned} U_i(t) &= speed(t) \cdot (1 + speed\_noise) \cdot f_{\theta_i}(\theta(t)) \\ \text{with } \theta(t+1) &= \theta(t) + angular\_s \cdot (1 + angular\_noise) \end{aligned} \tag{3.13}$$

This noise will accumulate during the PI until the animal moves to a point of recalibration. The activity of one neuron is illustrated in Fig. 3.5. top.

The mean values of the directional and spatial information rates are 1.19 and 4.16 with STD of 0.83 and 0.92 respectively.

#### Low frequency recalibration

To test the limit of our model, the frequency of the recalibration is decreased tenfold to once per 100 seconds. The duration of the free movement of the animal is still

7500 seconds. The activity of one neuron is illustrated in Fig. 3.5. bottom.

The mean values of the directional and spatial information rates are 1.12 and 3.27 with STD of 0.99 and 1.71 respectively. The spacial information rate decreases significantly along with the destruction of the place cell activity.

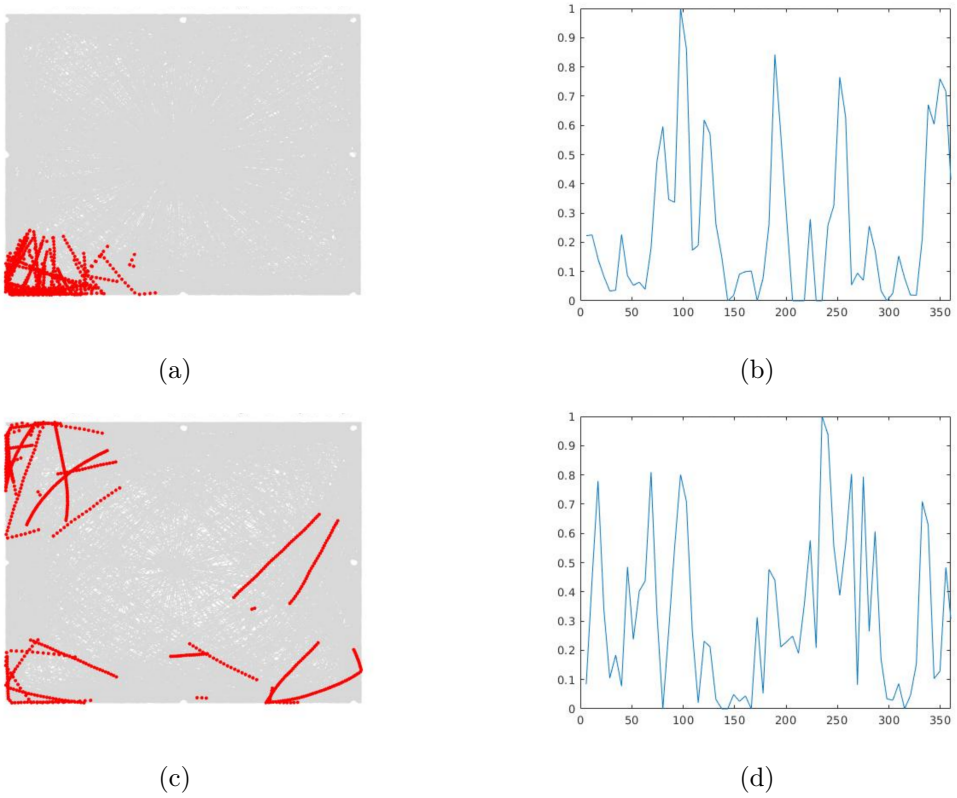


Figure 3.5: Activity of two neurons under the situation of High(top) and low(bottom) frequency recalibration. a and c show the winner position of the two neurons along the trajectory. b and d show the activity of the same two neurons as a function of MD in polar coordinates.

Under a high-frequency recalibration, the mean activity and the standard deviation of neurons are consistent with the values obtained without the interference of the noise. Our model is robust to convey information of different spatially related neuronal activities using different learning rates even under the interference of considerable noise. Nevertheless, the generation of the spatial activity is destructed due to the accumulated error of the PI caused by the lack of a solid recalibration mechanism. The recalibration of the path integration field could be realized by visual cues or other sensory inputs such as olfactory or tactile stimuli.

**Grid cells in EC from RSC activities**

We have shown in our prior works the capability of reproducing the place cell-like activity (Mao et al., 2017) in RSC when the animal runs on a treadmill using our PI model (Ju and Gaussier, 2020). Notably, place cells can be obtained even in a 2D environment with a global connection from the PI field to a SOM. However, biologists didn't find place cells in RSC when the animal moves freely instead of running in a fixed direction on a treadmill. We thereby suppose the connectivity between neurons performing PI and the SOM is local and define blobs of neurons working as local Kohonen maps. Neurons in EC could have global access to the PI field and compress the PI information using a simple modulo operation. To build grid cells, one pair of neurons $(P_{i1}, P_{i2})$ distant from 60 degrees ($i2 = i1 + [\frac{N}{360} \cdot 60]$) on the path integration field is selected as the input to two Kohonen maps ($E_j$ and $E_k$ calculated by eq. 3.5) which are compressed by two modulo layers ($MO_l$ and $MO_n$) according to the equation:

$$MO_l = \begin{cases} 1 & \text{if } l = 1 + argmax(E_j) \; mod \; Q \\ 0 & \text{else} \end{cases} \tag{3.14}$$

A population of grid cells ($F^{GC}$) can be built from the tensor product of the activity of neurons on the two modulo layers in EC:

$$F^{GC} = MO_l \otimes MO_n \tag{3.15}$$

A simple illustration of the modulo operation and an example of the activity of one grid cell are shown in Fig. 3.6.

For sake of simplicity, the self-organization of the Kohonen maps used to discretize the path integration field was done during a long random walk limited to the arena. It is therefore normal the same cell is activated 4 times (compression ratio $Cr = M : Q$) in the diagonal direction (longest distance in our environment) when Kohonen maps recruit 32 neurons ($M$) and the divisor $Q$ equals to 8 in the modulo operation.

It is known that one of the most important roles of Hipp is the detection of the novelty and the recognition of complex states, but the number of neurons in Hipp is very limited. EC could play the role of a compression mechanism providing Hipp with the capability to detect and learn quickly complex cortical patterns.

## 3.5 Conclusion

The potential of the PI to convey spatial information is studied in this work. Due to the local connectivity between cortices, the place cell-like activity can be only observed in RSC when the animal moves in one direction on the treadmill with its

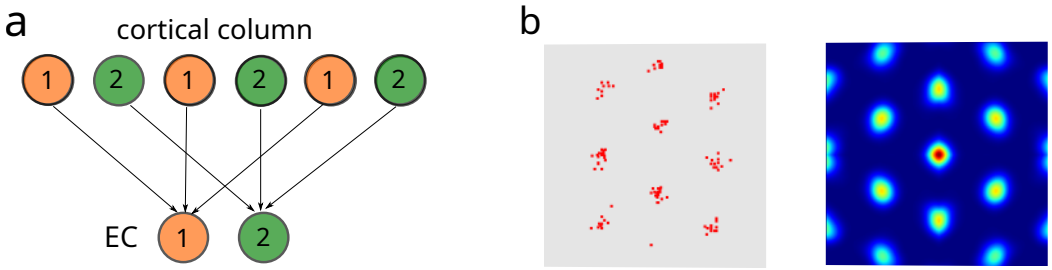


Figure 3.6: a, a simple illustration of the modulo operation. Neurons in EC(bottom) connect alternately to neurons in one cortical column(top) representing the discretization of the activity of one neuron on the path integration field. b, an example of the firing field of one grid cell built by our PI model applied the modulo operation. Left, firing field of a grid cell built by our PI model. Right, auto-correlation of the activity of the grid cell in b. left. Kohonen maps have 32 neurons ($M$ in eq. 3.5) and the divisor $Q$ equals to 8 in the modulo operation (eq. 3.14).
.

head fixed (Mao et al., 2017). A wide range of spatially involved neuronal activity such as place cells and head direction cells has been produced by our PI model assuming the brain area has full access to the upstream cortex or subcortex where the PI could originate. We have shown in our simulation that a global connection to the path integration neural field requires a large number of neurons and synaptic connections. The cost even increases if we consider the need for redundant neurons for robust coding in case of perturbation and malfunction of neurons. Therefore, the global connectivity between cortices and Hipp lacks biological plausibility considering the limited number of neurons and synaptic connections of each neuron in Hipp, not to mention numerous afferent signals to Hipp including the proprioception of self-motion and the information of different types of perceptions. Considering the rich innervation between EC and Hipp, we thereby propose that EC could play the role of a hub to compress the cortical information involved in navigation, vision, and other recognition tasks and interact with Hipp to generate place cells. EC could maintain the global feature of the cortical information with sparse connectivity to the afferent cortices owing to the modulo projection. The grid cell activity in EC could be an epiphenomenon of this general compression mechanism.

## Perspective

We will present in the next chapter the mathematical basis to build the grid cells from the compressed afferent cortical activity and how the reciprocal connectivity between Hipp and EC could play a crucial role in the self-organization of both spatial and visual grid cells. The place cells activity from Hipp could be the teaching signal to the medial entorhinal cortex (Bonnevie et al., 2013) during the early development.

The place cell activity in Hipp could be generated by a provisionally global connection to the path integration neural field or neural fields processing other types of perception such as saccade. This global connection could exist during the early development and become obsolete after the maturity of grid cells.

The recruitment of place cells could be controlled by a constant vigilance parameter with the adaptation maximizing the distance between firing fields of different place cells. Each recognized place area should have the same size and be surrounded by other place areas (i.e., the place area which is near the learned area will not activate the same cell. There exists a competition between cells learning place areas). This process could be modulated by the medial septum as the ACh modulation related to the loop between CA and the medial septum (Hasselmo et al., 1995). We suppose neurons activated by the peak activity of a set of place cells will show a grid pattern of activation that modulates the learning of grid cells in EC. During the early development, Place cells could also emerge by a threshold summation of the non-grid activity of immature grid cells from EC. The immature grid cells during the early development could still emerge non-grid activity having random conditional synaptic connections with the cortical columns in the PPC or RSC. This reciprocal mechanism between place cells and grid cells is consistent with the biological recordings where place cells emerge before the maturation of the grid cell (Langston et al., 2010; Wills et al., 2010).

# Chapter 4

# Self organization of the entorhinal cortex grid cells: impact of the hippocampal feedback

## 4.1 Introduction

The debate about the causal relationship between place cells and grid cells has been conducted during decades (Langston et al., 2010; Wills et al., 2010; Bonnevie et al., 2013; Bush et al., 2014; Gaussier et al., 2019). Biological experiments in 2.5–3-wk-old rat pups suggest that place cells (PC) can be generated by self-motion proprioception in the absence of fully mature grid cells (GC) whose firing field is not yet a regular hexagonal pattern (Bjerknes et al., 2018). Compromised grid-cell-like representations along with path integration (PI) deficits have been found in the human entorhinal cortex (EC) in old age. This recording suggests that impaired grid cell function or PI deficits might predict an age-related decline of cognitive functions (Stangl et al., 2018). In this chapter, we address the causal dilemma between place cells and grid cells by introducing the reciprocal connections between the hippocampus (Hipp) and EC. This connection could be modulated by the medial septum as the acetylcholine modulation related to the loop between CA and the medial septum (Hasselmo et al., 1995). In our model, grid cells could emerge as a correlate to PC peak activities. In addition, PC could also be generated by combining the activity of mature grid cells (Jauffret et al., 2015) or even benefits from the immature GC whose firing field is not yet following a stable periodic hexagonal pattern. Considering the limited number of neurons in Hipp compared to that of input cortices, a compression mechanism is required at the level of Hipp in order to form an efficient coding. In our model, EC could receive compressed information afferent from different cortical regions such as RSC and PPC. In this chapter, we will explain how to generate grid cells by our ad

hoc computational model. Some learning processes will be introduced for biological plausibility. Simulations will be conducted under a scenario where an animal moves randomly in an enclosure. Grid cells taking input derived from the path integration field can be learned from the septal signal. Due to time constraints, some of the results are still preliminary.

## 4.2 Ad hoc computational model of grid cells

The computational model of the path integration (fig. 4.1, left) in this chapter is identical to the ones in the preceding two chapters.

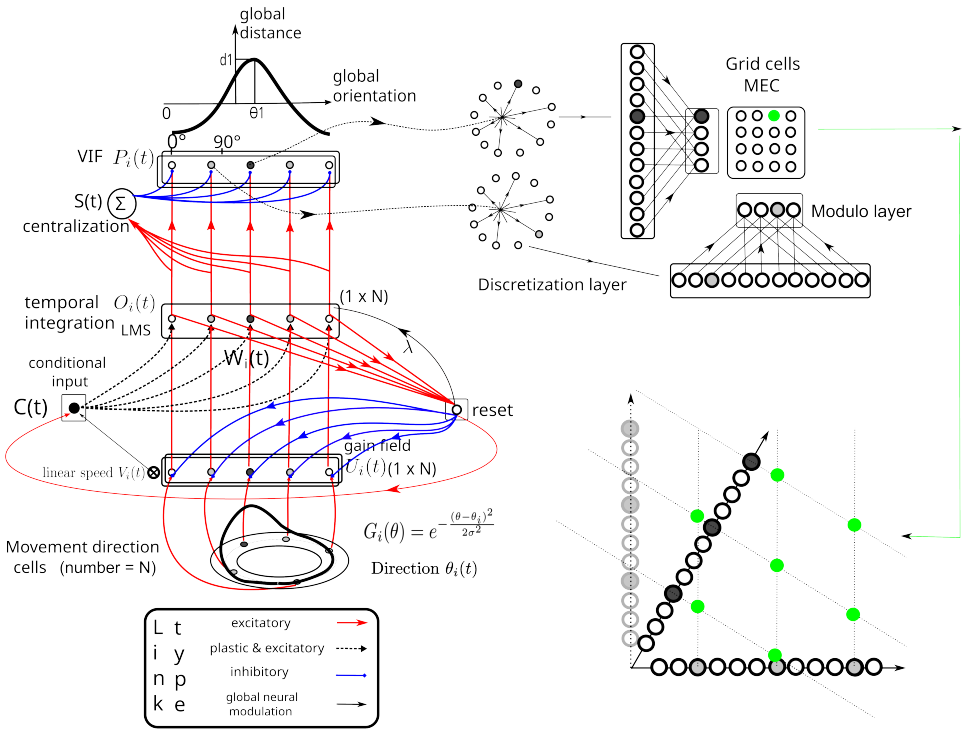


Figure 4.1: Architecture of a computational model to build grid cells from path integration fields

The main input of our model is a ring of neuron modelling movement direction (MD) cells. Each MD cell has a peak activity when the animal moves to a precise direction $\theta_i$ and the cell activity decreases as a bell function modelled as a non-normalized Gaussian shape, with $\sigma$ a parameter defining the width of the bump and $\theta$ being the absolute orientation of the animal at time t. The gain field Ui is modulated by the bump of MD cells and the linear velocity of the animal. We implement a classical conditioning mechanism with the least mean square rule to

calculate the path integration. Oi is the output which is the product between W and C in a ramp function. C represents a bunch of binary values associated with different spatial contexts (the conditioned input). At this stage, Oi activity is not really homologous to PI since the Oi neurons are only excited by the MD activity. A global feed-forward inhibition S(t) is added to obtain the PI neural field Pi(t) including positive and negative parts representing an approximation of the PI.

We suppose the grid cell activity can be the compression of the cortical activities on the 1D discretization of PI field in RSC (Gaussier et al., 2007). As illustrated in (fig. 4.1, right), the activity of neurons in PI field is discretized in the discretization layer. The activity of each neuron in the discretization layer represents the distance of PI in their respective preferred orientation on a Cartesian plane. By adding a modulo mechanism (fig. 4.2), neurons in the discretization layer will be connected recurrently to the neurons on the modulo layer. The modulo layer can be considered as a ring of neurons where the first neuron is adjacent to the last one so that each neuron of the discretization layer can link to one neuron of the modulo layer in succession even if the number of neurons of the afferent and efferent layer is not identical. In other words, neurons of the modulo layer will be activated periodically by neurons of the discretization layer. The connection pattern depends on the ratio between the number of neurons in the discretization layer and the number of neurons in the modulo layer. This ratio is the compression ratio of the cortical information in our model.

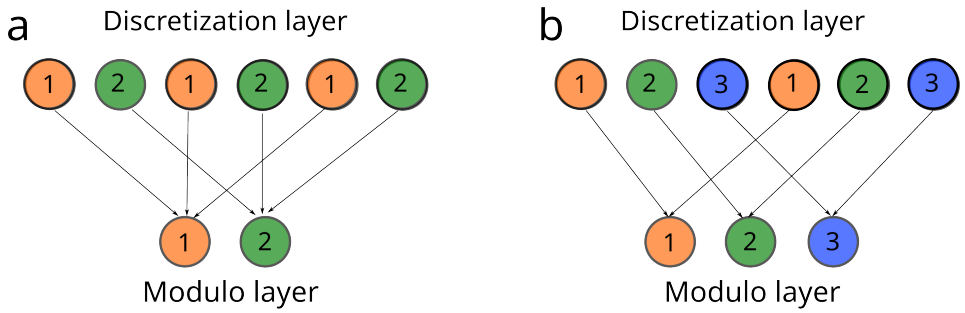


Figure 4.2: Illustration of the modulo mechanism between neurons of the discretization layer and of the modulo layer. The modulo layer can be considered as a ring of neurons where the first neuron is adjacent to the last one so that each neuron of the discretization layer can link to one neuron of the modulo layer in succession. a, compression ratio equals 3. b, compression ratio equals 2.

The activity of neurons in the two discretization layers is projected respectively onto two modulo layers which can be considered as 1D vectors. The grid cell activity can be built by the activity of neurons on these two modulo layers using conjunctive cells (fig. 4.1, left). The grid orientation is determined by the selection of the pair of neurons of the path integration field. However, the activity of the PI neural field

could be negative due to the global feed-forward inhibition S(t). From the biological point of view, the negative firing rate of neurons doesn't exist. We need to transfer the information on the negative field to the positive part without destroying the geometric properties.

Our field covers 360 degrees which means the value of one neuron representing orientation 0 equals the inverse value of the neuron representing orientation 180 (mathematical proof of the calculation of PI field can be· found in the appendix of chapter 2). This property allows us to use the field of only positive activity of neurons to represent the PI when the animals move freely in a 2D environment. In the following simulations without specific indication, the animal moves freely at 10 cm/s in a 2x2 metres square arena for 20000 time steps. One iteration in the simulation corresponds to 0.1 seconds. The product of the learning rate $\lambda$ and its associated time constant $\tau$ equals 0.1 seconds in order to scale the simulation from time steps to seconds. The animal is simulated according to its (x,y) coordinates, its movement direction, and its instantaneous linear speed. At each time step, the PI field receives an input composed of the direction and linear velocity of the current movement of the animal. We use 360 neurons for the HD cells so the precision of orientation is one degree. The number of neurons in the modulo layer is 18. To test the feasibility of our concept in a fast way, we replace the Kohonen map with a simple algorithm without learning for the discretization of the activity of the PI neural field. The number of neurons in the discretization layer is 90.

We use two homologous fields each covering 360 degrees. Neurons in these two fields only have positive activities. Instead of taking one pair of 2 neurons distant from 60 on the global VIF, we need to take two pairs of the same two neurons in the two fields respectively.

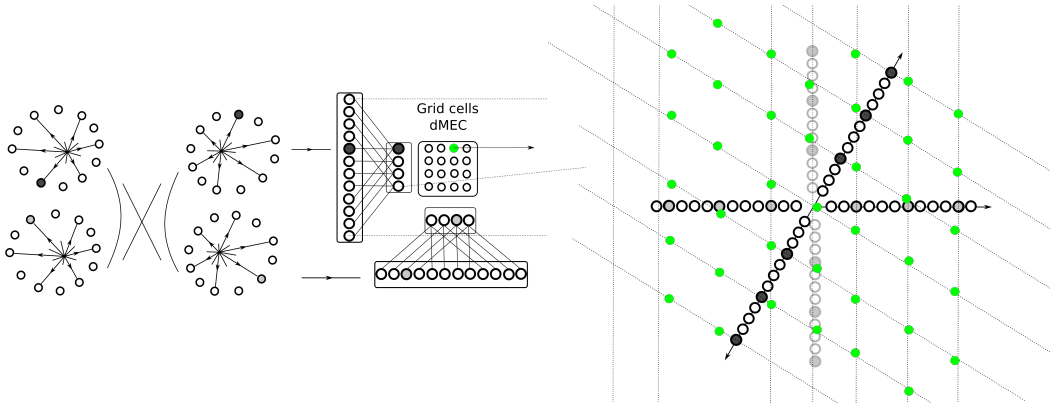


Figure 4.3: Ad hoc selection of four grid cells each representing one quadrant of the environment.

The activity of these 4 neurons needs to be discretized before being conducted product operations in pairs. Then we have 4 different grid cells each representing

one quadrant of the environment. Grid cell activities in two symmetric quadrants are shown in (fig.4.4a) and (fig.4.4b). We then moved the origin of the animal to the middle of the environment. The merged grid cell activity in the complete environment is shown in (fig.4.5). A reset mechanism of the path integration field is activated each time the animal passing by the origin.

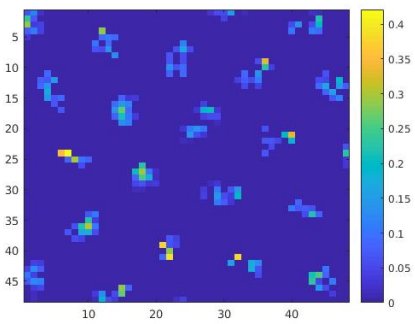


(a) Grid cells using neurons in the direction of 105 and 165 degrees.

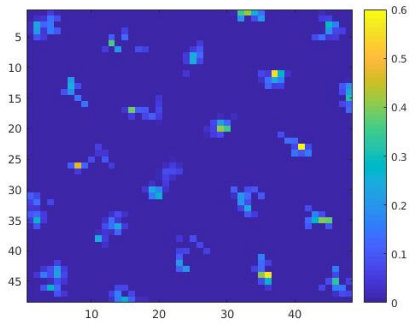


(b) Grid cells using neurons in the opposite direction of 105 and 165 degrees.

Figure 4.4: Two grid cells built from 2 pairs of neurons distant from 60 degrees on a path integration field. The origins of the animal in these two situations are in two different diagonal corners. Reset mechanism is activated each time the animal passing by the origin.

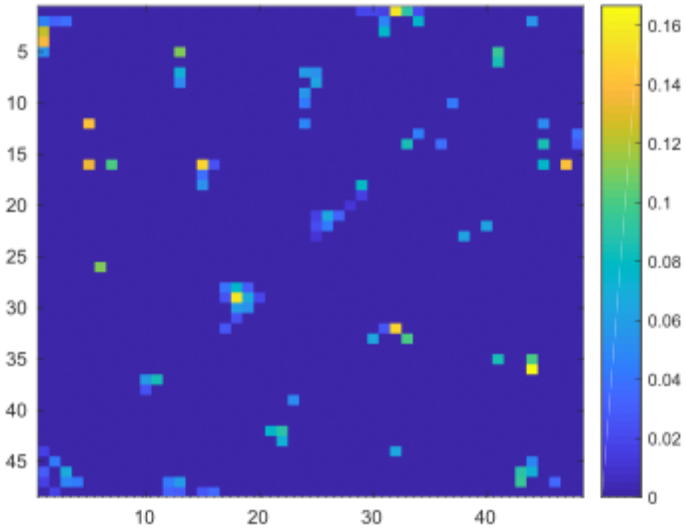


Figure 4.5: A grid cell built by the architecture illustrated in figure 4.3. The origin of the animal is in the middle of the environment. Reset mechanism is activated each time the animal passing by the origin.

The mathematical way of building the grid cells is based on 2 preconditions.

The first one is taking neurons of which the preferred directions are distant from 60 degrees. The second one is the compression of the neural information realized by the modulo operation between two layers of neurons. The two preconditions can be realized by the learning of neurons which will be further discussed in the following section.

### Grid cells generated by a classical conditioning learning mechanism

First of all, we tested if we can use a classical conditioning learning rule based on least mean square (LMS) to learn the grid pattern from a preexisting grid cell (fig.4.7) built by our computational model. The unconditioned input $US_i(t)$ is the teaching signal coming from Hipp while the conditioned stimulus $CS_i(t)$ comes from neurons on the modulo layer:

$$S_i^{GC}(t) = f(\sum W_{ij}(t) \cdot CS_i(t)) \ , \ f(x) = \begin{cases} 0 & \text{if } x < 0 \\ x & \text{if } 0 \leq x < 1 \\ 1 & \text{if } x > 1 \end{cases} \tag{4.1}$$

$S_i^{GC}(t)$ is the activity of the learned grid cells. The modification of the synaptic weights between the conditioned stimulus from the PI field and the grid cell can be presented as:

$$dW_{ij}(t) = \lambda \cdot (US_i(t) - S_i^{GC}(t)) \cdot CS_j(t) \tag{4.2}$$

Where $\lambda$ represents the learning rate. The unconditioned input is activated 5 percent of the time during the whole learning process and it will be forced to activate whenever the input grid cell is active. The illustration of the model is shown in figure (fig.4.6)

When the number of neurons in the discretization layer equals that of the modulo layer (i.e. a compression ratio of 1), the learned grid cell has the same hexagonal firing pattern (fig.4.8a) as the teaching signal.

To test if our classical conditioning learning mechanism is still capable to learn the GC using the compressed information. We decrease the number of neurons in the modulo layer in order to introduce a compression ratio of 6 to the information of the discretization layer. The firing field of a grid cell built by the same unconditioned stimulus is shown in figure 4.8b. The scale or the spacing of the grid pattern decreases when the conditioned stimulus is compressed. Notably, the scale of the modulo projection and the scale of the hexagonal teaching signal are independent. The conditioned input derives from path integration neural field while the hexagonal signal derives from Hipp. The classical conditioning learning mechanism based on the LMS algorithm can provide the generalization property for the learned grid cells. For instance, the grid cell learned by the hexagonal signal can be active outside the

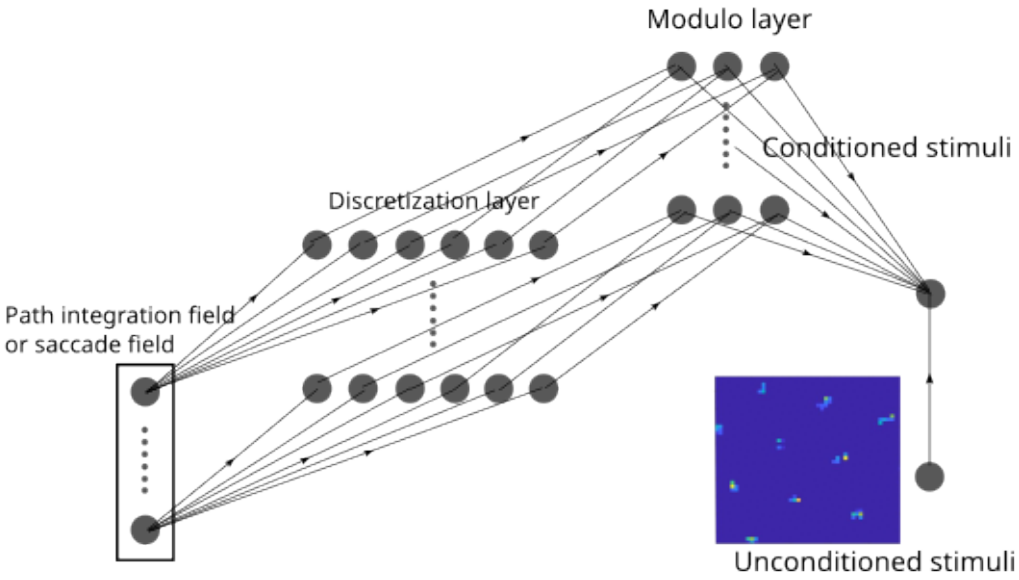


Figure 4.6: A model of grid cell using classical conditioning learning rule based on LMS to learn the grid pattern from a preexisting grid cell

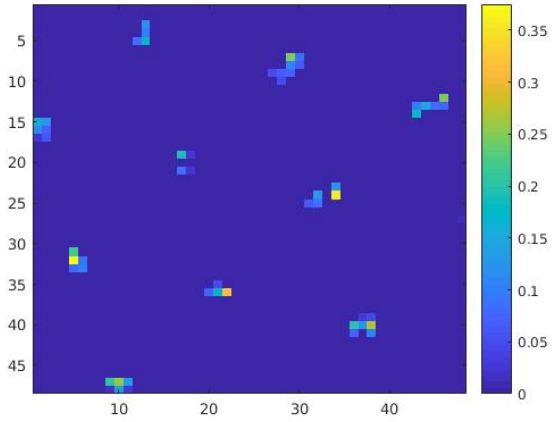


Figure 4.7: Firing field of a preexisting grid cell built by our computational model as a teaching signal.

firing field of the teaching signal.

### Discretization of the cortical information

The preceding results have proved the potential of our model in generating grid cells based on a classical conditioning learning mechanism with LMS. The grid cell taking input from a regular hexagonal signal can be generalized in a novel environment. Nevertheless, the discretization mechanism was mathematically realized

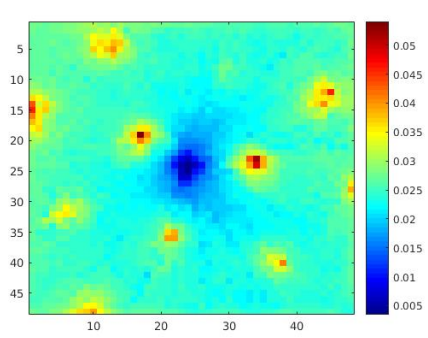


(a) Learning threshold of LMS equals 0.9, iterations equal 50000, number of neurons in the discretization layer equals 90, compression ratio equals 1

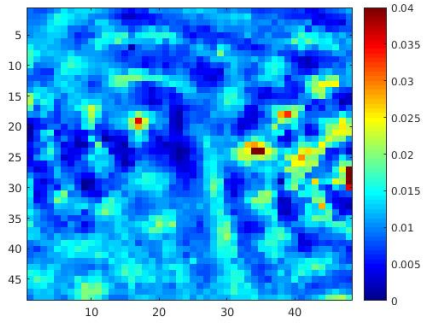


(b) Number of neurons in the discretization layer equals 90. The conditioned stimulus is compressed from the discretization layer with a compression ratio equal to 6

Figure 4.8: Grid cells learned by a classical conditioning learning rule based on LMS taking unconditioned stimulus from the preexisting grid cell built by our computational model.

without considering the biological plausibility. We turn to the Kohonen map for the discretization of the VIF and try to implement the compression after that. For the self-organizing algorithm of Kohonen, instead of using the distance between the vector of the input activity and the vector of weight pointing to each neuron on the Kohonen map, we use the scalar product to determine which pattern of weights is the most similar with the vector of input activity. Using scalar product can neglect 0 values of input activity and provide a more explicit representation of the difference between the vector of the input activity and the vector of weight. Nevertheless, that induces another problem in our model. The field to be discretized represents the path integration of an animal. The Cosine similarity will be almost constant if the animal keeps moving in one direction in which case the bell curve in the VIF will maintain almost the same shape even with different amplitudes leading to little change to the cos similarity. Thereby, we implement the input normalization by using two path integration fields $P_i$ and $Q_i$ as the input for the Kohonen map. $Q_i(t) = max(P_i) - P_i$. An explicit representation of the spatial context in RSC is obtained when the animal moves in one direction, The maximum of $P_i$ updates during the process of the PI. One Kohonen map representing a blob or a cortical column corresponds to one neuron on the path integration field (fig.4.9). Blobs or cortical columns in our model could be similar to sections of the visual cortex where groups of neurons that are sensitive to color assemble in cylindrical shapes. These two PI fields $P_i$ and $Q_i$ constitute an input field $I_j$ to the Kohonen map.

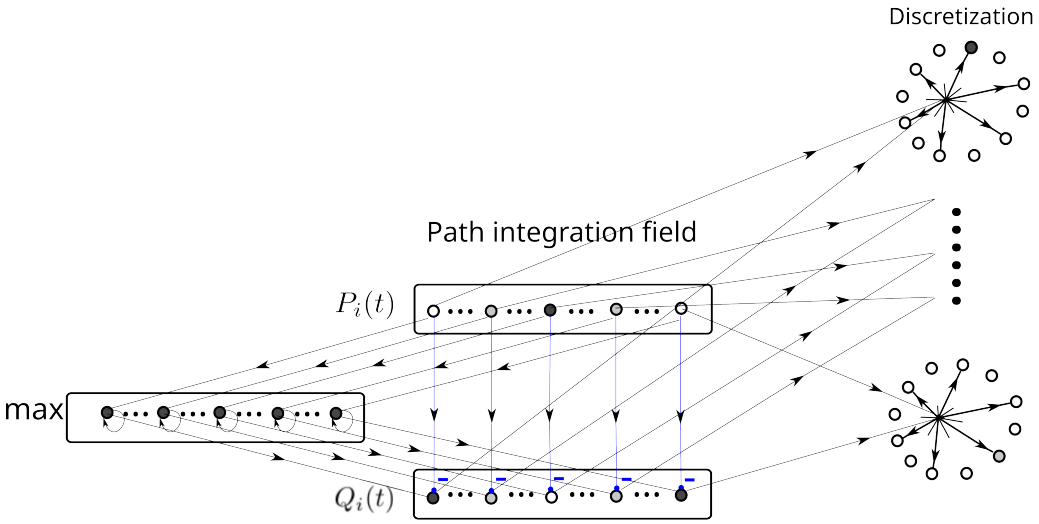


Figure 4.9: Two PI neural fields used as the input to the discretization field. The activity of neurons of the neural field Q is the maximum of the activity of neurons of the neural field P subtracting the activity of neurons of the neural field P.

The index of the winner neuron $k^w$ is defined by :

$$k^w(t) = arg\ max\left(\frac{\sum I_j(t) \cdot W_{jk}(t)}{\sqrt{\sum I_j(t)^2 \cdot \sum W_{jk}(t)^2}}\right), k \in [1, .., M] \tag{4.3}$$

M is the number of neurons on the 1D Kohonen map. The synaptic weights between neurons on the input field $I_j$ and neurons on the Kohonen map are updated by:

$$W_{jk}(t + dt) = \lambda \cdot (I_j(t) - W_{jk}(t)) \cdot S_k(t) \tag{4.4}$$

$\lambda$ is the learning rate of self-organization. The activity of neurons on the Kohonen map is subject to a DoG function $h_{kk^w}(t)$ similar to the Mexican hat.

$$S_k(t) = h_{kk^w}(t, d_k) \cdot S_{k^w}(t),\ k \in [1, k_{max}] \tag{4.5}$$

$S_k(t)$ is the activity of the kth neuron on the input PI field with $k_{max}$ the number of input neurons projecting to the self-organizing map. $d_k$ represents the distance between the winner neuron $k^w$ and neurons $k$ on the Kohonen map.

We have the following results (fig.4.10) from our model replacing the discretization group with a set of cortical column-structured Kohonen maps.

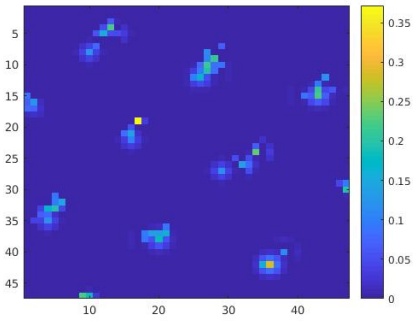


(a) Firing field of a preexisting grid cell built by our computational model replacing the discretization group with a set of cortical column-structured Kohonen maps.

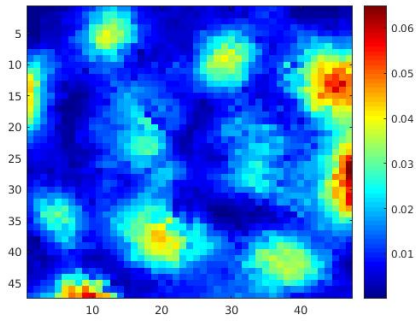


(b) Grid cells learned by a classical conditioning learning rule based on LMS taking unconditioned stimulus from the preexisting grid cell.

Figure 4.10: Build GC using a blob-structured Kohonen map to learn the discretization in each direction

### Compression of the cortical information

The modulo operation can be learned from a local learning rule maximizing the independence of the output neurons in EC. This learning process is entitled as the anti-Hebbian learning rule where the weight between two neurons increases if the two neurons activate simultaneously, and reduces if they activate separately. The excitatory synaptic connection between the neuron on the discretized field in the PPC or RSC and the neuron in EC is bindingly formed or maintained if the synaptic connection between these two neurons is the most excitatory or the least inhibitory. The lateral effect of neurons is simulated by the excitatory neuron of the discretization layer convolved with a Gaussian distribution as shown in (fig.4.11).

The synaptic connections between neighboring neurons of the excitatory neuron on the modulo field and the excitatory neuron on the discretized field are inhibited according to the lateral distance between the neighboring neurons and the excitatory neuron on the modulo field.

$$S_j = \begin{cases} E_i \cdot W_{ij} & \text{if } \max_i E_i \cdot W_{ij} \geq |\min_i E_i \cdot W_{ij}| \\ 0 & \text{otherwise} \end{cases} \tag{4.6}$$

The synaptic weight is updated in one shot subject to the following rule:

$$W_{ik} = \begin{cases} E_i & \text{if } E_i = 1 \\ -E_i & \text{otherwise} \end{cases} \quad \text{with } k = \arg\max_j S_j \tag{4.7}$$

Simple processing of the learning of the neuronal firing periodicity is illustrated

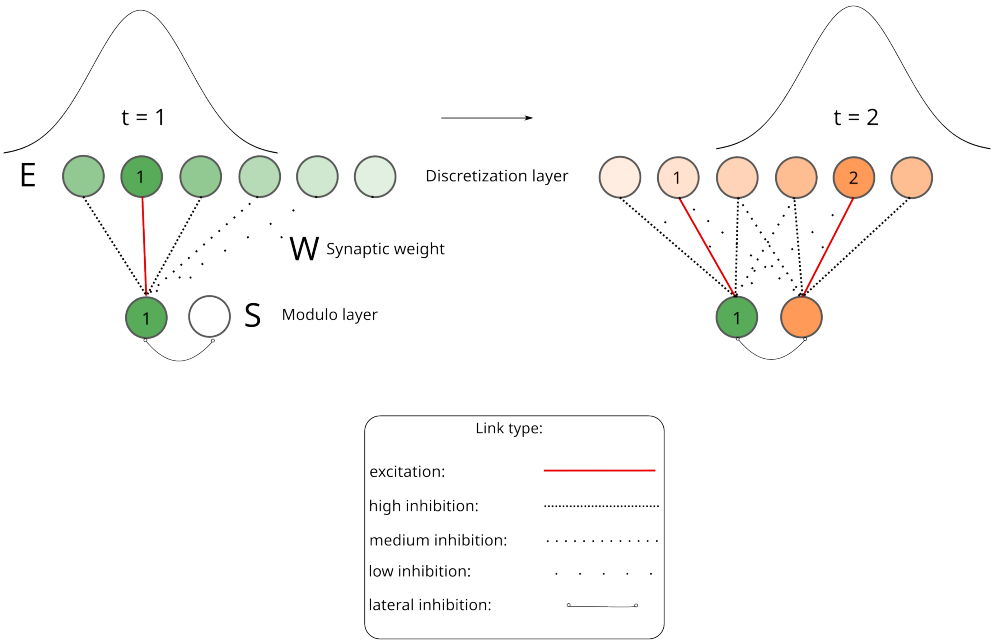


Figure 4.11: Illustration of the Hebbian/anti-Hebbian learning mechanism.

in figure 4.12.

The number of neurons indicates the order of their excitation. One single neuron is active on the upper layer each time. The neuron on the lower layer with the strongest synaptic connection with the exciting neuron on the upper layer will be bindingly active. The excitatory synaptic (red solid line) connection between them is thereby formed and will not be destroyed by lateral competition. The synaptic connection of the excitatory neuron on the upper layer and neighboring neurons of the active neuron on the lower layer will be inhibited. The strength of the inhibitory synaptic connection (black dashed lines) depends on the lateral distance between the active neuron and its neighboring neurons on the lower layer. There exists competition between the inhibitory connections in order to maximize the sparsity of the activation of neighbouring neurons on the lower layer. i.e. The inhibitory synaptic connection will only be updated by stronger lateral inhibition before the excitatory synaptic connection is formed.

A group of the limited number of neurons on the modulo field connected to the discretized field thereby realize the compression of the information from PPC or RSC to EC. We have the following results (fig.4.13) from our model with the compression mechanism based on the anti-Hebbian learning rule. 15 neurons are recruited for the modulo layer while the number of neurons in the discretization field equals to 90. Therefore, the compression ratio is equal to 6 (90/15).

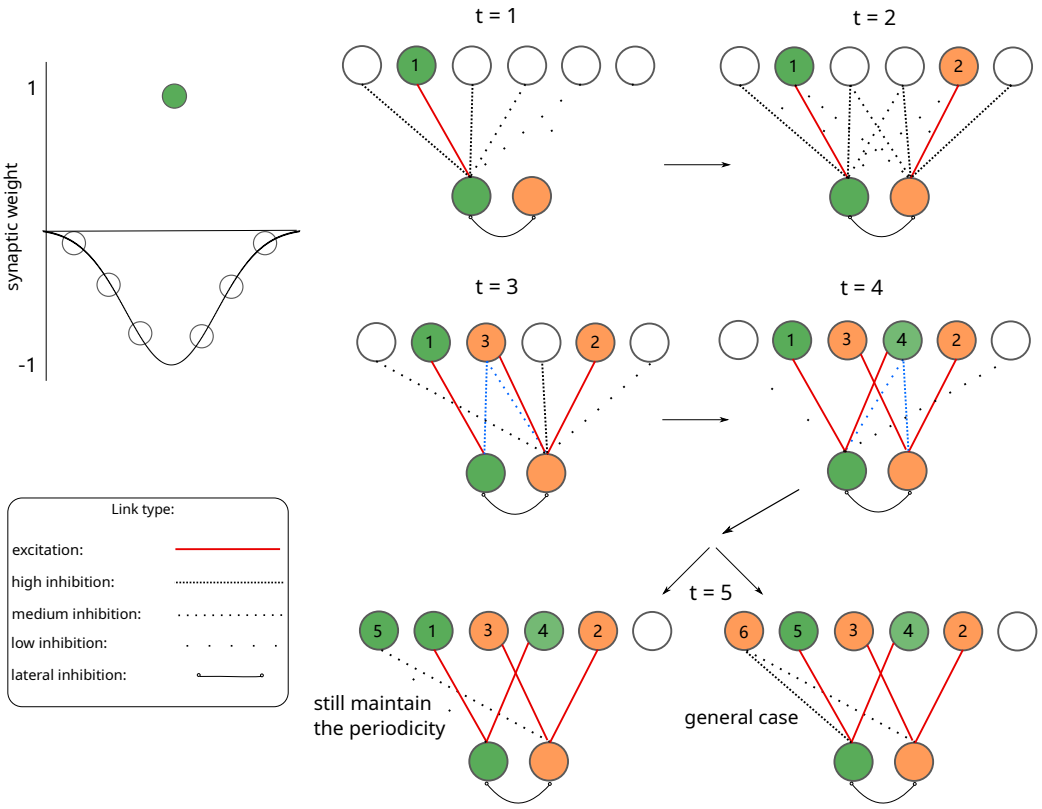


Figure 4.12: Illustration of the update of activities and synaptic connections of neurons subject to the anti-Hebbian learning rule. Left, the curve represents the strength of the synaptic weight as a function of the distance between the winning neuron and its neighbouring neurons in the cortical column. Right, the upper layer of neurons in the PPC is the input to the lower layer of neurons in EC.

The advantage of our modulo learning mechanism compared to the preceding used ring structure (fig. 4.2) is that the learning mechanism does not depend on the prerequisite wiring between neurons of the discretization layer and the modulo layer and has the possibility to deal with the issue of imprecision from the input layer.

### 4.2.1 Septal signal generated from cortical signature

We have proven in the previous sections that the grid cell activity could be learned by an LMS classical conditioning mechanism taking a regular hexagonal signal as the unconditioned input. However, how this hexagonal signal generates remains to be discovered. The PC activity from Hipp could be the teaching signal to the medial entorhinal cortex (Bonnevie et al., 2013) during early development. At this stage, place cells could emerge subject to a WTA learning rule based on the detection

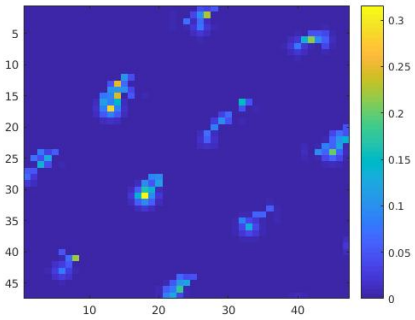


(a) Firing field of a preexisting grid cell built by our computational model with the compression mechanism based on the anti-Hebbian learning rule.

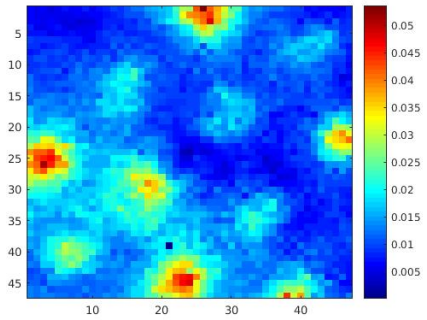


(b) Grid cells learned by a classical conditioning learning rule based on LMS taking unconditioned stimulus from the preexisting grid cell.

Figure 4.13: Build GC using a 2D anti-Hebb group to learn the modulo operation

of novelty taking input of non-grid activity of immature grid cells from EC. The immature grid cells during the early development could still emerge non-grid activity having random conditional synaptic connections with the cortical columns in PPC or RSC even without the unconditioned stimuli from Hipp which could be adapted during the development. If the recruitment of place cells is controlled by a winner take all mechanism then we obtain neurons coding for different places. The firing area of each neuron should have the same size depending on a constant vigilance parameter of the winner take all mechanism and form a hexagonal paving of the environment (as orange circles in figure 4.14). We suppose some septal neurons connected to a set of place cells will show a grid pattern of activation that will modulate the learning of neurons in EC as it is the case for the acetylcholine modulation related to the loop between CA and the septum (Hasselmo et al., 1995).

This reciprocal mechanism between PC and GC is consistent with the biological recordings where biologists found PC emerges before the maturation of the GC (Langston et al., 2010; Wills et al., 2010). We may question that if we've already had the grid cells pattern by merging the place cells firing field then why bother using EC to learn to build grid cells? It is known that one of the most important roles of Hipp is the detection of novelty, but the amount of neurons in Hipp is very limited. So we suppose EC can play the role of compressing and generalizing the information coming from cortices and Hipp. This hypothesis leads to our global model of the interaction between cortices and Hipp. For the sake of simplification in the following simulations, we build the hexagonal signal from the activity of immature grid cells and then use the hexagonal signal as the input to the learning mechanism of the grid cell with a regular hexagonal pattern. We thereby prevent the dynamic issue where the learning of grid cells could affect the learning of the hexagonal signal. A dynamic

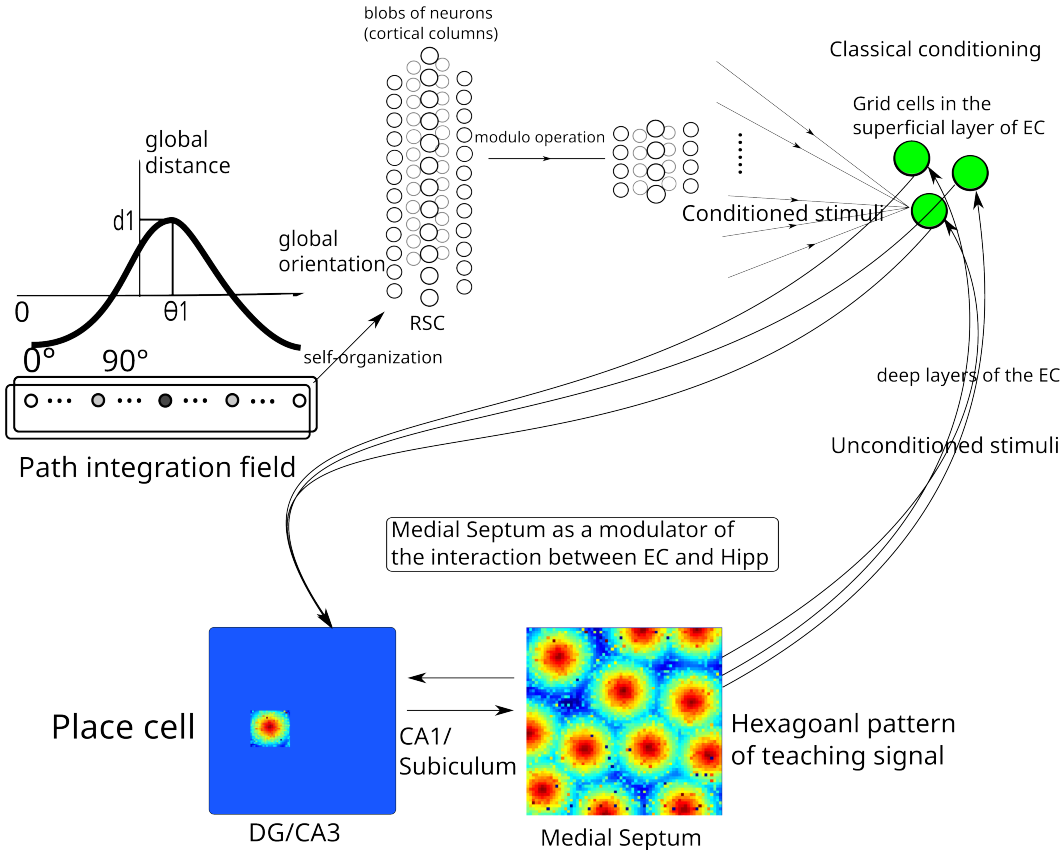


Figure 4.14: Model of the grid cell based on the reciprocal connection between the hippocampus and the entorhinal cortex.

and reciprocal learning mechanism between EC and Hipp is worth being studied in the future.

We build direct grid activities using a low-probability random connection from the discretization field. The activities of the product of different pairs of neurons taken from 20000 neurons are shown in figure 4.15.

Some of the activities show hexagonal grid patterns while most of them show a periodic non-hexagonal pattern. This simple simulation implicates the potential of neurons on the discretization field in forming the grid activity as long as the specific pair of neurons is correctly selected.

We suspect if our learning mechanism learns to find the appropriate pairs of neurons from the modulo layer, then the conjunction cell taking input from the pair of neurons should show grid pattern activity even if the animal explores outside the familiar area where the learning process took place. The hexagonal teaching signal generated by one-shot learning is shown in figure 4.16, a.

The activity of the grid cell learned from the hexagonal teaching signal (fig. 4.16,

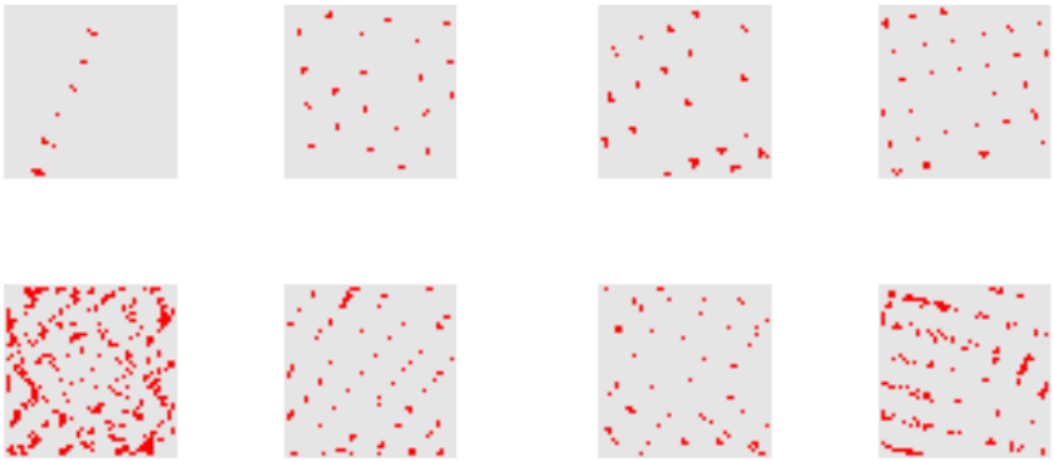

Figure 4.15: activities of the product of random pairs of neurons taken from 20000 neurons

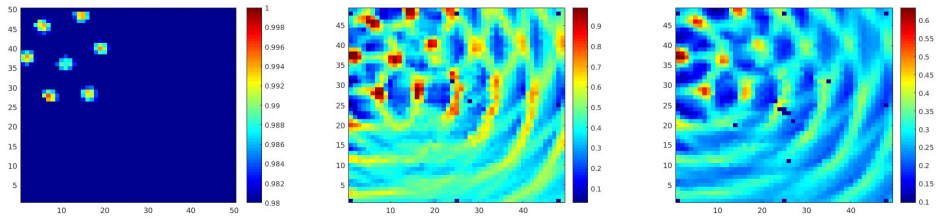

(a) (b) (c)

Figure 4.16: Grid cells learned from the hexagonal signal by one-shot learning. a) Hexagonal signal by one-shot learning. b) Grid cells learned from the hexagonal signal. Probability to activate the learning: 1. Learning rate of the classical conditioning mechanism: 0.01 c) Grid cells learned from the hexagonal signal. Probability to activate the learning: 0.5. Learning rate of the classical conditioning mechanism: 0.01

b, c) is more salient inside the learning area and fades away along with the distance from the learning position. The hexagonal signal built from the one-shot learning rule is not regular enough to modulate the grid cells in order to form a hexagonal grid pattern. As expected, different place cells possess firing fields with the same size owing to the constant vigilance value of one-shot learning. However, the position of different firing fields is not close to each other so the firing pattern of neurons is not compact enough to be hexagonal because the animal moves freely rather than diverges outward around the centre of the enclosure. In the last simulation, the vigilance had to be set to a value ensuring only 7 places were recognized in order to have a compact firing pattern. An adaptation mechanism should be added to the one-shot learning rule to solve the issue of irregular patterns. The firing fields of

winning neurons should be forced to adaptively moves close to each other. Due to time constraints, we turned to use the Kohonen map as discussed in chapter 3 to adaptively build the hexagonal signal. Notably, the topology of the SOM has not been found in the hippocampus. In a more realistic way, the hexagonal signal should be obtained by the dentate gyrus recruitment of neurons modulated by the septal signal. Multi-resolution of the grid pattern implies the possibility of several parts of the septum working in parallel with different thresholds of learning. We suppose if we succeed to build the hexagonal signal from the signature of immature grid cells by a SOM, then we will be able to implement an adaptive learning rule without any topological constraints to generate the hexagonal signal from the same input.

The recruitment of place cells is realized by implementing the self-organizing learning rule with a simplified Mexican hat-like distribution. i.e., the winning neuron on the self-organizing map has inhibitory connections to its neighbouring neurons subject to the simplified Mexican-hat-like distribution in order to maximize the distance between firing fields of different place cells. Each recognized place area should have the same size and be surrounded by other place areas. The place area which is near the learned area will not activate the same cell. We suppose neurons activated by the peak activity of a set of place cells will show a grid pattern of activation that modulates the learning of GC in EC. This process could be modulated by the medial septum as the acetylcholine modulation related to the loop between CA and the medial septum (Hasselmo et al., 1995).

We first tried with a one-dimensional Kohonen map with a few neurons. The size of the Mexican hat is modulated during the learning in order to maximize the firing field of each neuron on the Kohonen map.

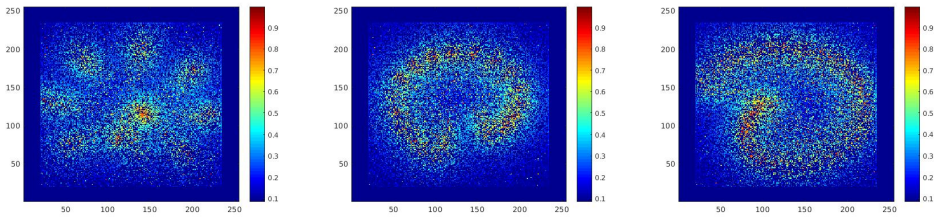

(a) (b) (c)

Figure 4.17: Septal signals built by one-dimensional Kohonen map with respectively a) 10, b) 20, and c) 50 neurons on the Kohonen map.

The one-directional Kohonen map failed to build a compact septal signal. A certain topology is required to map the two-dimensional environment. We then moved to the two-dimensional Kohonen map.

The number of neurons on the map should be large enough to increase the possibility of finally learning a hexagonal pattern, or the paving will be square. However,

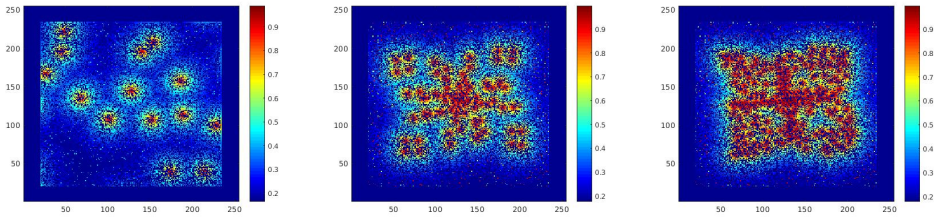

(a) (b) (c)

Figure 4.18: septal signals built by two-dimensional Kohonen map. a) Arrangement of neurons on the map: 5x5, b) Arrangement of neurons on the map: 10x10, c) Arrangement of neurons on the map: 20x20

if the number of neurons is too large, then the paving could be too crowded. The negative neighbourhood needs to be adjusted in order to ignore some of the neurons on the map. We then introduce one stage where we manipulate the neighbour kernel in the learning process. In the first stage of learning, a large positive neighbour kernel is used. Different shapes of the neighbour kernel are implemented in the second stage of the learning (fig. 4.19.a and 4.20.a). A negative neighbour kernel is used during the third stage. The size of the neighbour kernel is doubled to manipulate the spacing of the grid pattern after the third stage (fig. 4.20.c).

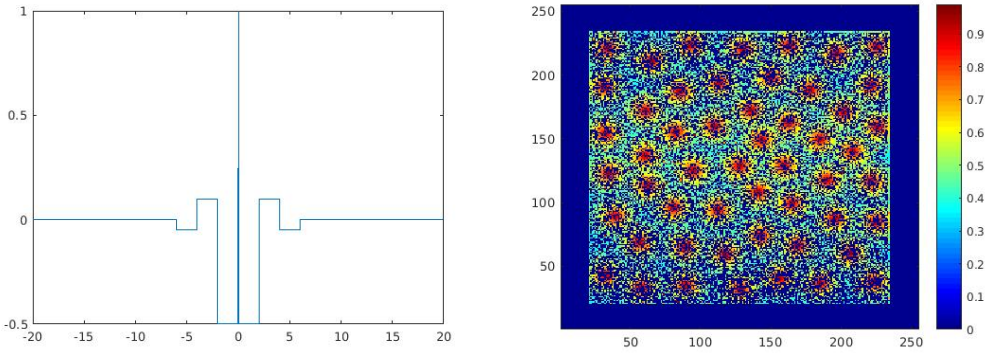

(a) neighbour kernel in the second stage

(b) activity of the septal signal

Figure 4.19: Activity of the septal signal learned by a self-organizing map when introducing a neighbour kernel in the second stage.

In the next chapter, we will assess the property of one grid cell built by the self-organizing mechanism presented in this chapter.

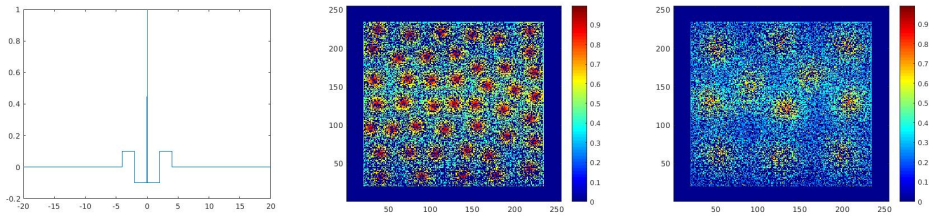

(a) (b) (c)

Figure 4.20: Activity of the septal signal learned by a self-organizing map when introducing a neighbour kernel in the second stage. a) Neighbor kernel in the second stage, b) Activity of the septal signal, c) Activity of the septal signal with the doubled size of the neighbour kernel.

## Discussion

The reciprocal connection between the entorhinal cortex and Hipp in our model could untangle the dilemma of the causal relationship between place cells and grid cells. Preliminary results showed the potential of our model in generating grid cells under a self-organizing learning mechanism.

The modulo compression mechanism can be built from a simple Hebbian/anti-Hebbian learning mechanism and the existence of positive lateral interactions over the bump of RSC activities. This feature could be generalized to any kind of other cortical information.

The hexagonal paving was not obtained as an emergent property of RSC projection from RSC to EC even if some interesting code can be built from the sole feedforward connections. To stabilize hexagonal grid patterns, we need to suppose the grid information is sufficient to form place cells. The self-organization of place cells then results in the building of a grid according to the threshold used to detect novel places. Different thresholds imply various maps of place cells and grid cells with different orientations and scales or spacing.

In our model, the interaction in the formation of place and grid cells agrees with some biological observations showing that place cells become stable before grid cells do and that grid cells remain stable when passing through an unknown environment as opposed to place cells.

The firing field of gird cells with the same grid orientation could pave the whole explored environment by slightly shifting in the grid phase. A population of grid cells with the same orientation but slightly different phases could be generated in our model (fig. 4.21) by introducing an aspect of replay of experience. Biological recordings revealed that one-directional 'place cells' with geographically neighbouring firing fields in one cortical column could fire in sequence during a Theta Cycle even without requiring the movement of the animal (Lisman and Jensen, 2013). These

one-directional place cells could be homogeneous to the ones found in RSC in (Mao et al., 2017) which has been successfully explained and reproduced by our model of the spatial representation in RSC (Ju and Gaussier, 2020). The neighbouring positions in one direction of the animal are thereby represented by these neighbouring 1D place cells as the unconditioned input to grid cells with the same hexagonal conditional signal leading to the learning of an ensemble of grid cells with phase shifts and the same orientation and space. Notably, place cell spiking patterns that occur during active states have been shown to reoccur in theta during subsequent REM sleep. REM sleep-associated theta may have a role in memory consolidation. Accordingly, the retrieval of experience such as going through the neighbouring area of the current position of animals could also be explained by the spacial memory reply during the sharp wave-ripples (Colgin, 2016).

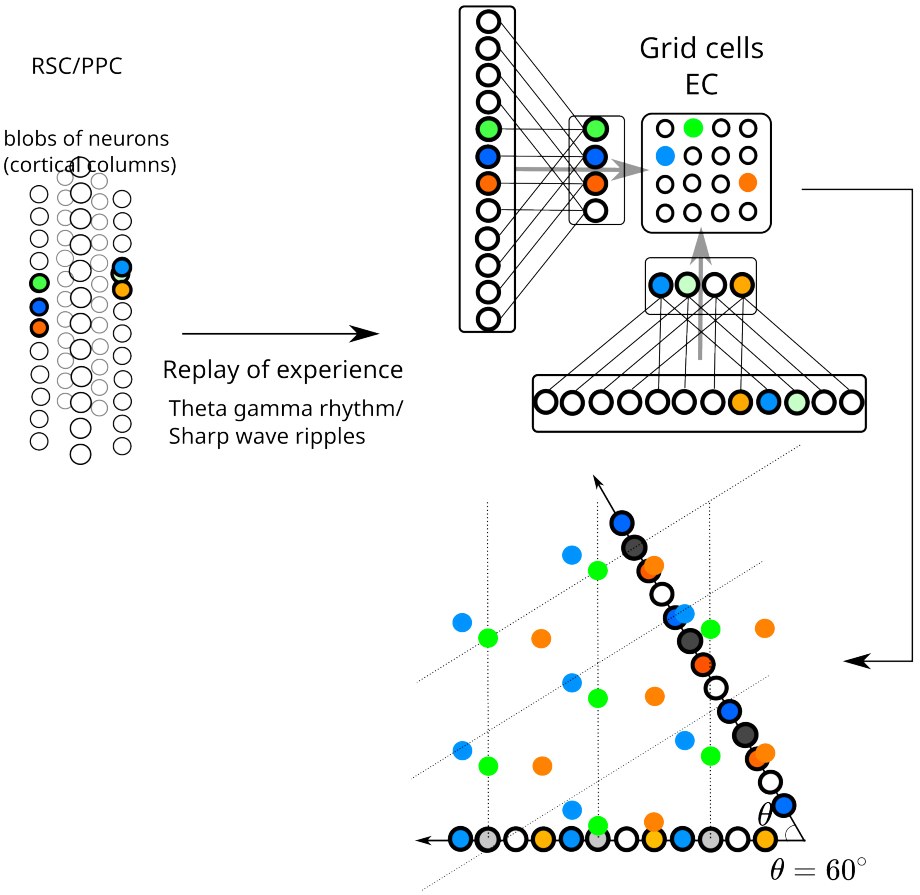


Figure 4.21: Illustration of the generation of grid cells. The input of the model is a path integration neural field. The activity of each neuron on the PI neural field is discretized before being performed the modulo operation. The Green points on top represent a grid cell built by performing a product operation between two discretized neurons distant from 60° on the PI neural field. Green points on the bottom indicate the active field of the grid cell in the environment. Blue and orange neurons are the neighbouring place cells on the cortical columns generated owing to the theta rhythm or the sharp wave ripples.

## Perspective

The self-organized generation of the grid cell relying on the reciprocal connection between Hipp and EC is worth further studying. Due to time limits, only preliminary results have been shown to prove the feasibility of this concept. The adaptive one-shot learning rule of the septal hexagonal signal and the dynamic and reciprocal learning mechanism between EC and Hipp should be addressed in the future.

In the next chapter, we will demonstrate how the visual stimuli (Saccade) could replace the self-motion proprioception (path integration) as the input to our model to generate visual grid cells while the model structure is unmodified. We will focus

on the role of the visual grid cell in visual recognition. The generalization capability of visual recognition is tested during movement on country roads and highways in simulation. The recognition mechanism based on visual grid cells could be combined with a self-motion-based system to provide efficient and stable spatial representation for robots during navigation tasks.

# Chapter 5

# A computational model of visual grid cells applied to image recognition

## 5.1 Abstract

The important contribution of grid cells in navigation has been widely accepted during the last two decades. Recent experiments revealed the emergence of the visual grid cells which are modulated by saccades or even the attention of animals during visual exploration. We propose here a general model explaining visual grid cells along with their involvement in visual recognition tasks irrelevant to navigation. We suggest that the entorhinal cortex builds a compressed code of the cortical activity in order to detect novel multi-model situations (i.e. situations involving new conjunction of patterns that may be not novel by themselves) or novel transitions between known multi-model states. The navigation features such as spatial grid cells and place cells could be the epiphenomenon of this general processing mechanism.

## 5.2 Introduction

The grid pattern activity in the entorhinal cortex has been widely reported among various species including rodents (Hafting et al., 2005), bats (Yartsev et al., 2011), primates (Killian et al., 2012), and humans (Jacobs et al., 2013; Nau et al., 2018). Considering the diverse findings of spatial, visual, or even mental grid cells, we have no reason not to think about the hypothesis that the grid cells could participate in the visual recognition of a complex visual scene besides navigation. This hypothesis attracts more attention from researchers following the discoveries of visual grid cells in primates and humans.

In 2012, Buffalo's team examined spatial representations in EC of head-fixed monkeys performing a free-viewing visual memory task (Killian et al., 2012). They found that EC neurons encode space during visual exploration, even without locomotion. The firing field of these EC neurons had spatial periodicity similar to a hexagonal pattern. Along with recordings of visual grid cells in primate entorhinal cortex modulated by saccade during visual exploration without locomotion, the same team found the emergence of hexagonal firing pattern in EC of monkeys in response to the spatial attention independent of any physical movements (Wilming et al., 2018). In addition to experiments on monkeys, research has been conducted on humans doing visual exploration tasks (Julian et al., 2018) where the human entorhinal cortex represents visual space using a boundary-anchored grid which is analogous to recordings in rodents performing navigation tasks.

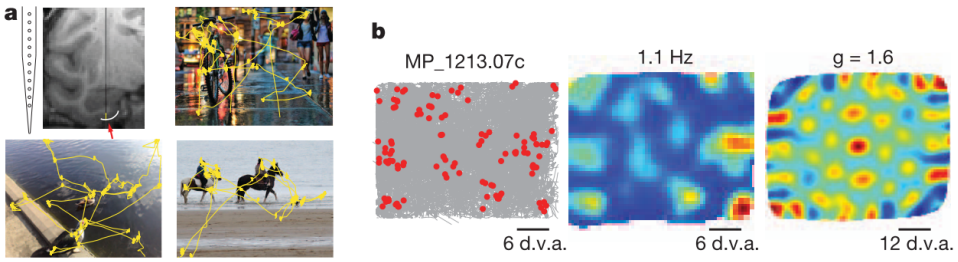


Figure 5.1: a, Recordings were carried out using a linear electrode array placed in the entorhinal cortex (red arrow). Three examples 10-s scan paths are shown in yellow. b, An example of an entorhinal grid cell. Left, plots of eye position (grey) and spikes (red) reveal non-uniform spatial density of spiking. For clarity, only spikes corresponding to locations of firing rate above half of the mean rate were plotted. The monkey's name and unit number are indicated at the top. Middle, spatial firing-rate maps show multiple distinct firing fields. Maps are colour coded from low (blue) to high (red) firing rates. The maximum firing rate of the map is indicated at the top. Right, the spatial periodicity of the firing fields shown against spatial autocorrelations. The colour scale limits are 61 (blue to red), with green being 0 correlation. d.v.a., degrees of visual angle; g, gridness score. (Killian et al., 2012)

Recent research provided evidence that neurons in EC could also display hexagonal firing patterns even without locomotion or any physical movement. We hereby aim to create a general model which is compatible with the generation of grid cells involved in the navigation (Gaussier et al., 2007) but also accounts for visual grid cells during the visual exploration.

It is known that EC receives multi-sensory information from various associative cortical and subcortical areas such as the parietal cortex (Colby, Goldberg, et al., 1999) and thalamic nuclei (Schlag-Rey and Schlag, 1984) of primates or the postrhinal cortex (Burwell and Amaral, 1998) and superior colliculus (Wang et al., 2015) of rodents. It also receives information of the path integration from the retrosple-

nial cortex (Ju and Gaussier, 2020), and the information of objects (Deshmukh and Knierim, 2011) from the inferior temporal cortex. We suppose this information is merged and compressed because of the connection pattern from afferent cortical areas to EC with the medial (MEC) and lateral (LEC) part conveying the spatial and object information respectively (fig.5.2).

We will suppose here that the recognition mechanism implies the merging of the 'where' and 'what' information in the perirhinal cortex (Mishkin et al., 1983). We made a comparison between the original model (Gaussier and Zrehen, 1995; Banquet et al., 2005) which takes relative azimuth to the landmark as the 'where' information (fig.5.3) and the current model using directly the firing field of grid cells to build a cognitive map combining the information of Area of interest (AoI) on images or views. The performance of the generalization of recognition and the robustness of our model is examined by modulating the compression effect of EC which is the main gateway to the hippocampus (Hipp).

With the successful implementation of our recognition model into the navigation and vision process (Gaussier et al., 1997; Giovannangeli et al., 2006; Jauffret et al., 2015), we hypothesise that our model provides a general method dealing with the global recognition process.

## 5.3 Computational model

### Model of the visual grid cell

We illustrate the model for the generation of visual grid cells in figure 5.4. The input to our model is the activity of neurons of the saccade field when the animal scans images (sequential exploration of an image). An efficient saccade selection was implemented by a dual foveal-peripheral visual processing model considering biological constraints (Daucé et al., 2020). The saccade selection is simplified in our model since the visuomotor process is not the focus of our work. Nevertheless, the computational model of visual attention based on the salient map proposed in (Itti and Koch, 2001) can be useful to further enrich our model. In our model, the sequential visual exploration of the animal is simulated by tracing the areas of interest in the image. To do so, a difference of Gaussian (DoG) filter is applied on the gradient image $[G]$. Local maxima are calculated to control attention.

The Gaussian filter is expressed as follows:

$$F_\sigma\left(x_f, y_f\right) = \frac{1}{2\pi\sigma^2} e^{-\frac{x_f^2+y_f^2}{\sigma^2}}$$

DoG is the difference between two $F$ with different $\sigma$: $DOG\left(x_f, y_f\right) = F_{\sigma_1}\left(x_f, y_f\right) - F_{\sigma_2}\left(x_f, y_f\right)$. The filtered map $[M]$ is the convolution between the DoG and the gra-

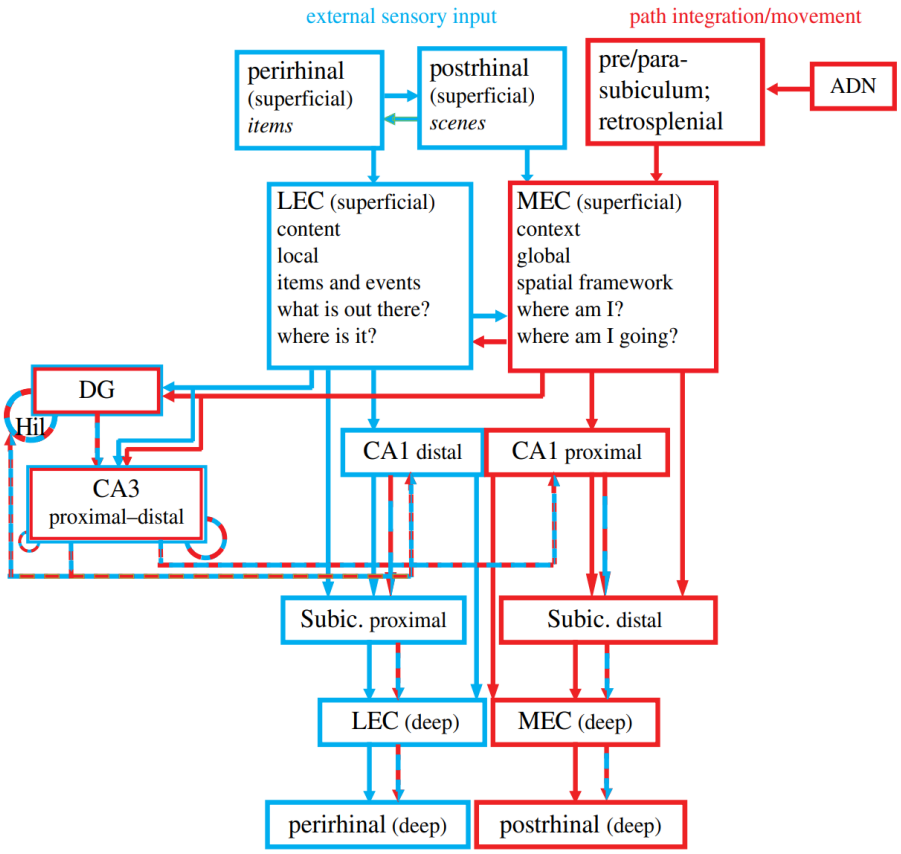


Figure 5.2: Parallel processing streams into the hippocampus. The structure of the diagram emphasizes the dual processing streams that pass through the LEC and MEC. Prior diagrams of these processing streams stressed their origins in the perirhinal-LEC and postrhinal-MEC connections [5–8]. Here, we add the critical connectivity between the MEC and limbic regions involved in movement, location and head direction processing (presubiculum, parasubiculum, retrosplenial cortex and anterior dorsal thalamus). The LEC and MEC connect to distinct regions of CA1 and subiculum, segregated along the transverse axis of the hippocampus (proximal–distal relative to the DG). CA1 and subiculum send return projections to the deep layers of the entorhinal cortex (EC), completing a processing loop. There is crosstalk along these pathways, both prior to their entry into the hippocampus and especially in the convergent projections to the DG and CA3. In this illustration, the DG and CA3 are represented as a 'side loop' of processing, in which the MEC and LEC streams are merged onto the same CA3 pyramidal cells and DG granule cells and the combined representations are then merged in CA1 with the separate input streams from the direct EC– CA1 projections. Specific mnemonic properties of the DG and CA3 regions are thought to be supported by the recurrent feedback loops represented by the dashed circles. ADN, anterior dorsal nucleus of the thalamus; DG, dentate gyrus; Subic., subiculum (Knierim et al., 2014).

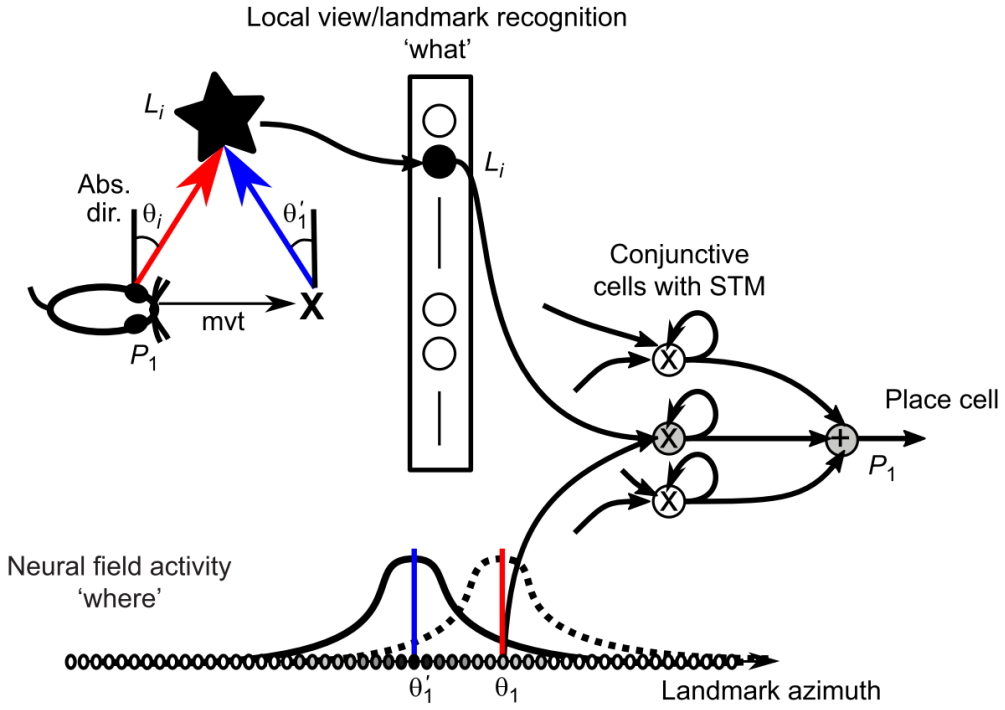


Figure 5.3: Visual place cell from the merging of 'what' and 'where' information. Landmark angular variation induces a decrease in landmark recognition. Li, neuron associated with the recognition of landmark i; P1, classical neuron performing the visual place recognition from the conjunctive (product) units; $\theta_i$, azimuth of landmark i (here, the black star) according to an absolute referential; $\theta'_i$, landmark azimuth after a movement shown by the vector mvt; STM, short-term memory. (Gaussier et al., 2019)

dient image:

$$\begin{aligned} M(x,y) &= [DoG] * [G] \\ &= \sum_{-\frac{i_{max}}{2}}^{\frac{i_{max}}{2}} \sum_{-\frac{j_{max}}{2}}^{\frac{i_{max}}{2}} DoG(i,j) \cdot (x+i, y+j) \end{aligned}$$

where $i_{max}$ and $j_{max}$ indicate the size of the DoG filter with x and y the coordinates of the filtered map. To obtain the points of interest relatively paving the whole image, the image is separated into different areas with the size of $(i_{max}, j_{max})$. Then a competition mechanism is applied on different areas in order to successively select salient spots on the map with the locally highest score of $[M]$. We suppose saccades attracted by focus points are coded in absolute polar coordinates in the parietal cortex (Sereno et al., 2001). The polar angle and the amplitude of the saccade are

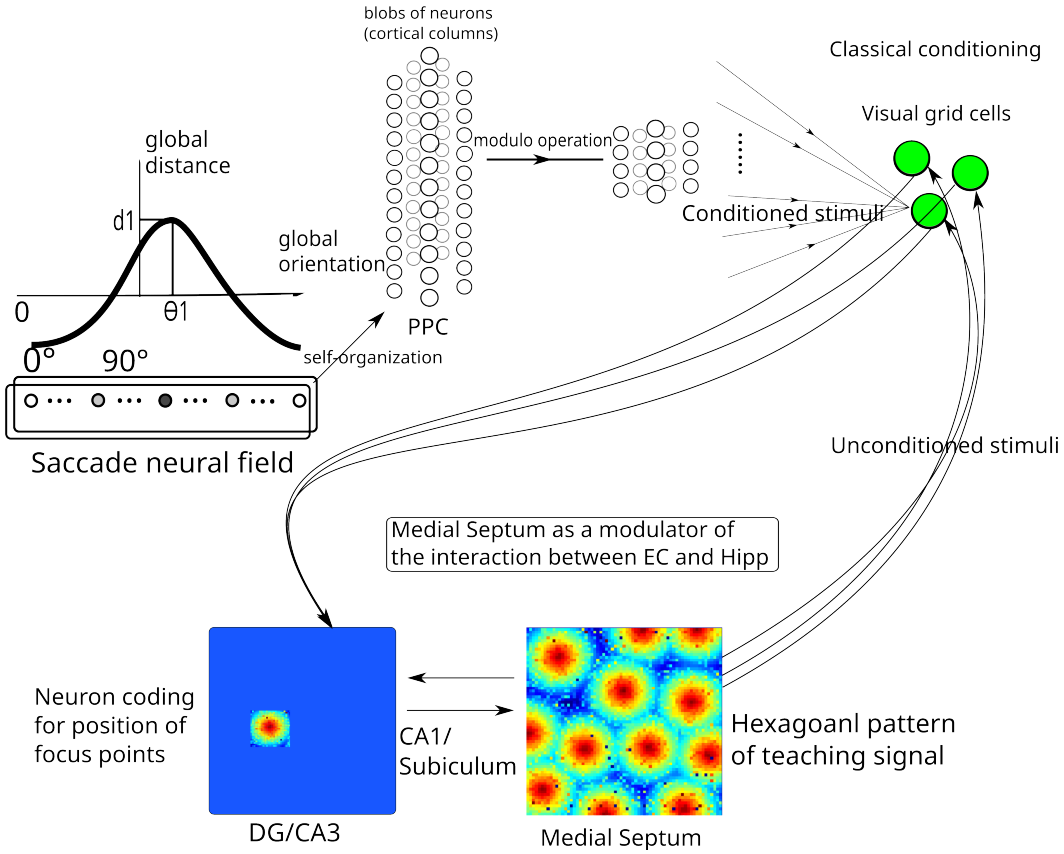


Figure 5.4: Biological model for the learning of one grid cell. The input of the model is the activity of neurons of the saccade field derived from the absolute polar coordinates of the gaze center during the saccade. We predict a kind of neuron in Hipp coding for the position of focus points on an image which is similar to place cells during navigation. Dark red points indicate the conditional input signal for the learning of a generalized pattern to build VGCs.

represented as a bump of activation on a ring of neurons. We suppose that a group of neurons is equally distributed to represent 360 degrees in order to simulate a vector integration field of the saccade. Each neuron has a preferred direction depending on the amount (N) of total neurons. The interval between each preferred direction is $360/N$. One neuron is excited when its preferred direction is accordant with the saccade direction while the intensity of the excitation depends on the saccade distance. The lateral neurons on the saccade field are active decreasingly subject to the Gaussian distribution along the distance from the excited neuron. The activity of the neuron whose preferential firing direction is $\theta$ on the saccade field: $S(\theta) = e^{-\frac{(\theta-\theta_i)^2}{2\sigma^2}}$ where $\sigma$ determines the width of the firing range of neurons on the saccade field with $\theta_i$ denoting the absolute orientation of the saccade. To simplify the calculation, we take $S(\theta) = cos(\theta - \theta_i)$. The saccade cells share some common properties with the

Head direction cells (Killian et al., 2015).

To realize the discretization of the activity of the bump of the saccade vector, we project the activity of each neuron of the saccade field onto a set of one-dimensional Kohonen maps. Each 1D self-organizing map can be considered as one cortical column (used to discretize the distance information in a given direction) (fig.5.4). A population of around one hundred mini-columns forms a hyper-column which discretizes the whole saccade field covering all the directions of saccades. This structure of hyper-column has been implemented in our model of RSC (Ju and Gaussier, 2020) to reproduce the biological results of (Mao et al., 2017) and explains the diverse spatial coding accessing to different levels of information efferent from this structure. The activity of each neuron on one mini-column represents one specific distance in the same direction. Within an orientation column, neurons throughout the vertical thickness of the cortex respond to stimuli oriented at the same angle (Hubel et al., 1977) with neighboring columns responding to a slightly different orientation. The cortical columns in RSC and PPC could be homogeneous considering their anatomic proximity and the similar nature between the neural field of path integration and the one of the saccade.

We presume the visual grid cell activity recorded in MEC can be a compressed code of the cortical activities in the PPC. The connection between the visual grid cells and neurons in the PPC can be modulated by the teaching signal from Hipp. The compression and learning mechanism is homologous to the one in chapter 4 implemented among Hipp, RSC, and dorsal MEC to generate grid cells when the animal moves in an open environment (Gaussier et al., 2007). We predict that a kind of neuron whose activity is modulated by the position of the eye, fovea, focus or attentional spotlight could be found in CA similar to the activity of place cells during the navigation of rodents. In our model, neurons recognizing the focus position could be built by a self-organizing map having a global connection to neurons of the saccade field (fig.5.4). This mechanism is identical to the one explained in chapter 2. The self-organizing generation of the visual grid cell could be homologous to that of the grid cells during navigation explained in the last chapter.

If 'what' information can be merged with 'where' information, we could obtain cells homologous to the spatial view cells (Rolls et al., 1997) found in the primate hippocampus responding when the monkey looked at a part of the environment. These hippocampal neurons depend on where the monkey is looking not on the place where the monkey is.

In the preceding results, grid cells during navigation can be learned if the conditioned input follows a regular grid pattern. We tried to generate the visual grid cells without modifying the structure of the model. The saccade instead of the path integration will be the primary input to our model. The saccade is more irregular and unpredictable compared to the self-motion in an enclosure. The generation of

the grid cell in our model will be more challenging considering the property of the saccade input. The simulation is performed based on the same biological basis as the visual grid cell studied in monkeys (Killian et al., 2012). In each training session, 2000 images are serially presented to the animal. An image is removed after the animal has at least 40 gaze locations on the image. The model used during the learning of visual grid cells is homologous to the one of grid cells during the simulation of navigation discussed in the last chapter. The activity of one grid cell learned from the septal teaching signal is shown in figure 5.5. The gridness score of this neuron is 0.59 which makes the neuron eligible to be considered as a grid cell. The gridness is calculated by the minimum between the rotational correlations at 60 and 120 degrees minus the maximum among the rotational correlations at 30, 90, and 150 degrees.

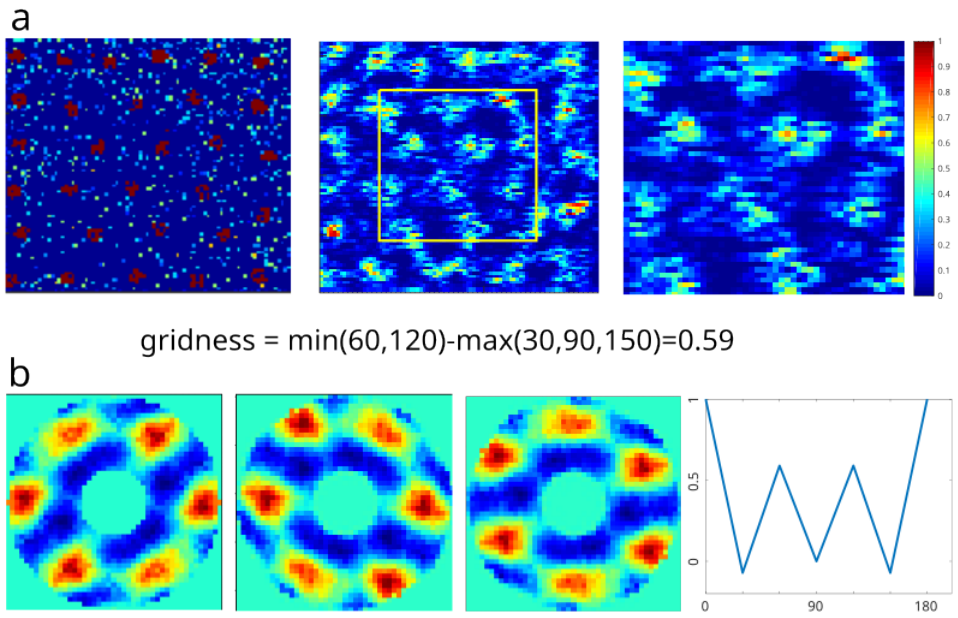


Figure 5.5: Hexagonal teaching signal and the activity of one grid cell learned from it. a.left, hexagonal teaching signal built from the self-organization of visual place cells activity in the hippocampus. a.middle, firing rate map of one grid cell. Yellow square circumscribes the middle part of the map which avoids the interference of the border effect of the environment. a.right, confined part by yellow square in a.left. b.first, autocorrelation of the firing rate map. The inner annulus masks the central peak of the autocorrelation in order to have an explicit autocorrelogram. Six peaks around the central peak are encircled by an outer annulus. b.second and b.third are the rotational correlations at 120 and 150 degrees. b.fourth, correlation coefficients from rotations of 30, 60, 90, 120, and 150 degrees. The gridness is calculated by the minimum of the set of rotational correlations at 60 and 120 degrees (b.left has the lower rotational correlation) minus the maximum of the set of rotational correlations at 30, 90, and 150 degrees (b.middle has the highest rotational correlation).

## 5.4 Model of the recognition mechanism relying on 'where' and 'what' information

In our current model, the information of location is provided by the visual grid cells from EC instead of the relative azimuth to the AoI. The information of AoI or objects could be conveyed from the temporal cortical area. The AoI is determined by the local-view exploration around focus points which are the start and end spots of each saccade. The focus points are obtained by detecting the transition of areas on views using gradient information. A circular focusing area is selected centered on each focus point as shown in figure 5.6.left. We suppose the fovea corresponds to the center of the focusing area. The Cartesian coordinates x and y in figure 5.6.right will then be transformed into our log-polar map in figure 5.6.left with $L = log\sqrt{x^2 + y^2}$ and $\theta = atan2\,(y, x)$.

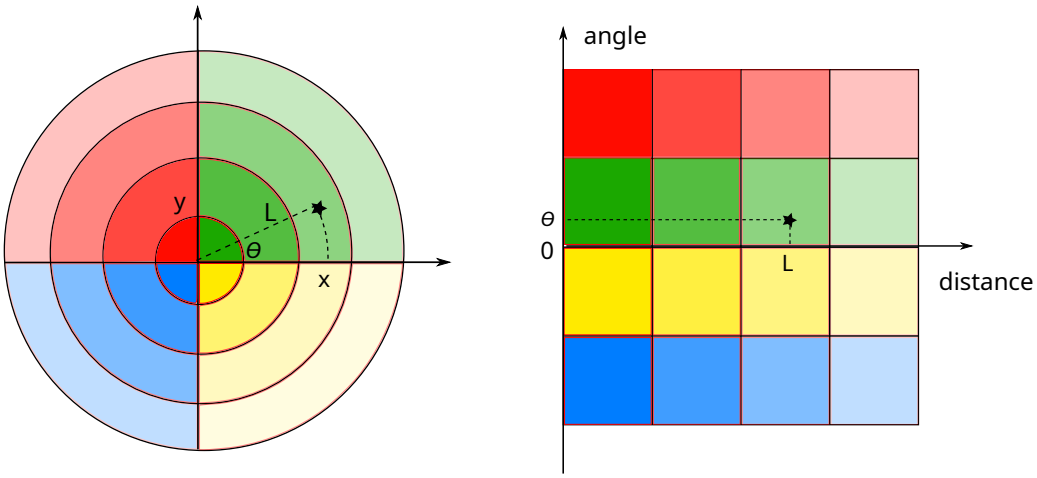


Figure 5.6: Illustration of the log-polar mapping. Left, a retinal image projection from a selected circular focusing area centered on each focus point with the fovea corresponding to the center of the focusing area. Right, the Cortical representation log-polar transformed from the retinal image projection. These two representations correspond colorwise.

This transformation emulates the retinal image projection based on studies about optic nerves and visual stimulus representation in the cerebellar cortex (Schwartz, 1977; Schwartz, 1980). The information near the center of the focusing area has the greatest weight. The weight of visual information decreases along the distance from the center of the focusing area (the darkest color on the map) and reaches the minimum at the outer ring of the visual field (the lightest color on the map). This process allows eyes to concentrate on the visual variation near the focus center

without losing the general perspective of the whole focusing area and could provide a conformal cortical representation of a visual stimulus. The focusing area transformed onto a log-polar map will then be the input to a winner take all competition layer where a new AoI cell is recruited and form the synaptic connection with input neurons when the local view input pattern obtained by log-polar mapping of optic flow is categorized as a new one. The competition of the input pattern is subject to a learning rule (eq.5.3 and 5.4) where one AoI neuron is recruited once the recognition level of the local view falls under a certain vigilance level. Increasing the vigilance value induces more neurons to be recruited. Each AoI Neuron receives input from all the neurons on the polar local-view field. The activity of the AoI neuron depends on the summation of the difference between the activity of the input neurons and the weights of synapses from input neurons to the AoI neuron. A constellation map combining AoI and their locations can be used as the input to the recognition cells in the Hipp to identify an image or an instant view. This merging mechanism is based on units calculating the product of 'what' and 'where' information.

$$\begin{gathered} S_k^{PR}(t) = S_k^{PR}(t-1) \cdot (1 - Rs(t)) + S_{i,k}^{EC-PR}(t) \cdot S_{j,k}^{IT-PR}(t) \\ k = (i-1) \cdot j_{max} + j \end{gathered} \tag{5.1}$$

with $i \in [1, i_{max}]$ and $j \in [1, j_{max}]$. $i_{max}$ is the number of grid cells conveying the spatial information of the AoI while $j_{max}$ represents the number of AoI neurons. $S$ represents the normalized activity of neurons fluctuating between 0 and 1. In equation 5.1, we suppose the activity of constellation neurons$S_k^{PR}$ in the perirhinal cortex is the product of the activity of grid cells$S_{i,k}^{EC-PR}$ in the entorhinal cortex and the activity of AoI neurons$S_{j,k}^{IT-PR}$ coming from the inferotemporal cortex. At each time step, one AoI neuron having the highest activity dominates the spatial information afferent to the constellation map: $j = arg\left(max_{q \in [1, j_{max}]} S_{q,k}^{IT-PR}(t)\right)$. $S_k^{PR}(t)$ is thereby the product of the activity of the winner of the AoI neurons and the activity of the simultaneously activated grid cells at time t. Neurons on the constellation map successively memorize the sequential combination of the winner of the AoI neurons and the simultaneously activated grid cells during the saccade exploration of one image (fig.5.7).

$Rs(t)$ is the activity of a strong inhibitory neuron connected to the constellation neurons. It plays the role of a reset mechanism of the constellation map:

$$Rs(t) = \begin{cases} 1 & \text{if } t = t_{new\ image} \\ 0 & \text{otherwise} \end{cases} \tag{5.2}$$

The inhibitory neuron is only activated only when a new image is shown to the agent and thereby resets the constellation map for the representation of a new image.

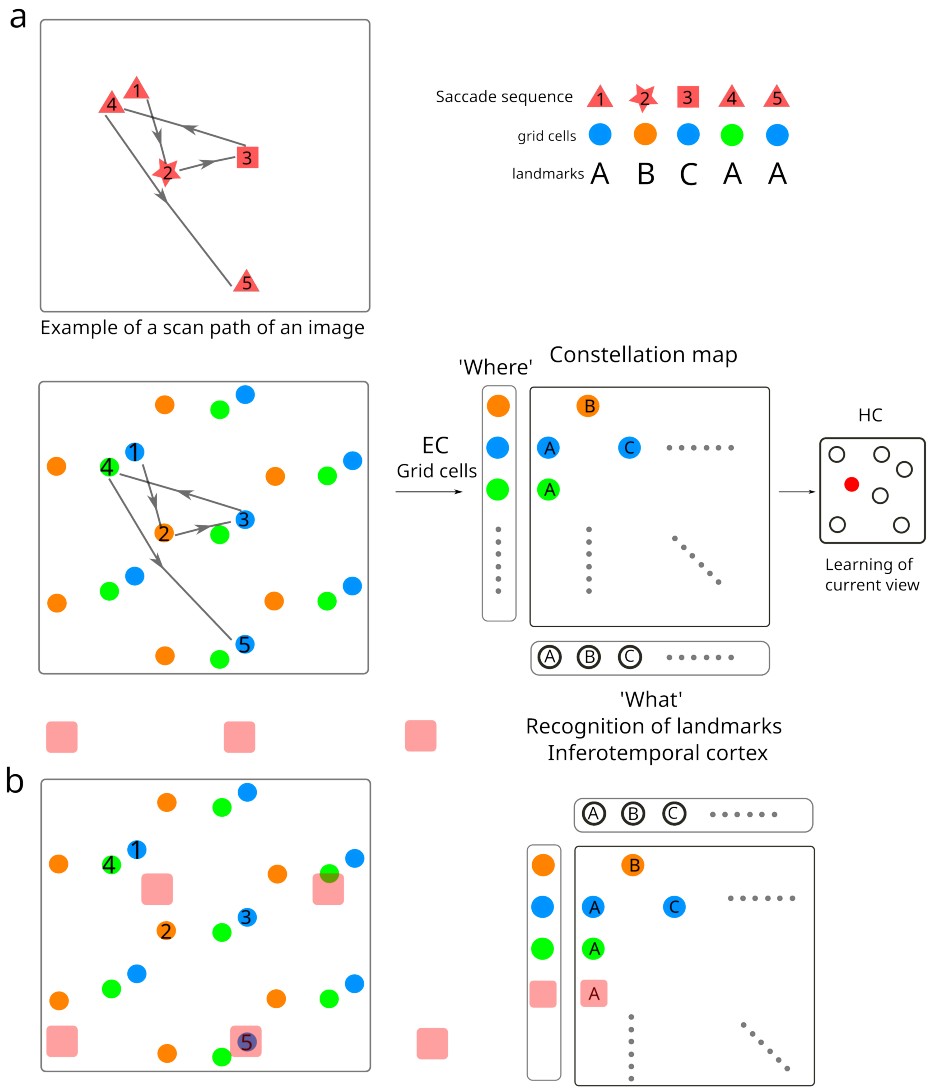


Figure 5.7: Images recognition using the combination of 'where' and 'what' information on the image. a, Sequence of the focus points: 1,2,3,4,5; We assume that the area of interest (AOI) around focus points 1, 4 and 5 are similar and thereby activate the same landmark cell A. Focus point 2 and 3 corresponds to landmark cell B and C respectively. The coding in the constellation map represents the 'where' and 'what' information of the image and is irrelevant to the temporal order of the focus points. Notably, no topology contiguity is required by any of the structures shown in the scheme. Neurons are conceptually arranged in order to simplify the illustration. b, Pink squares indicate the firing fields of a grid cell whose spacing and size are 1.5 times greater than those in fig.a.

Each Neuron on the recognition layer receives input from all the neurons on the constellation map. The activity of the recognition neuron$S_{l+1}^{HC}$ depends on the summation of the difference between the activity of the input neurons$S_k^{PR}$ and the weights of synapses from input neurons to the recognition neuron$W_{k,l+1}^{PR-HC}$. The activity of the recognition neuron or the recognition level approaches maximum if the summation of the difference tends to zero. The competition of the recognition neurons is subject to the local Winner-take-all learning rule. A new recognition neuron is recruited once the highest recognition level of recruited neurons on the recognition layer is under a certain vigilance level. A higher vigilance level leads to more recognition neurons being recruited.

$$\begin{gathered} S_{l+1}^{HC} = f\left(1 - \sum_{k=1}^{k_{max}} W_{k,l+1}^{PR-HC} \cdot S_k^{PR}\right);\ \forall l \in [0,l]\,,\ S_l^{HC} < Vig \\ with\ l \in [0, l_{max}]\ \ and\ S_0^{HC} = 0 \\ f(x) = \begin{cases} x & \text{if } x > 0 \\ 0 & \text{otherwise} \end{cases} \end{gathered} \tag{5.3}$$

We suppose the synaptic weights between neurons on the constellation map and the recognition neurons are subject to the one-shot learning rule:

$$W_{k,l}^{PR-HC} = S_k^{PR} \cdot S_l^{HC} \tag{5.4}$$

The synaptic connection between neurons on the constellation map and the winning neuron on the recognition layer restores the input pattern and thereby combines the winning recognition neuron with the concurrent firing pattern of neurons on the constellation map in the perirhinal cortex.

The competitive recognition process is realized by sigma-pi units (Rumelhart and Zipser, 1985) with the part of sigma (summation) and pi (product) as shown in equation 5.1 and 5.3 respectively.

This constellation map coupling 'what' and 'where' information originates from the work of Philippe Gaussier (Gaussier, 1992; Gaussier et al., 2002) where the recognition map could be memorized via 'what' and 'where' pathways (Mishkin et al., 1983) into the perirhinal cortex and the parahippocampus of primates (Aggleton and Brown, 1999) or postrhinal cortex of rodents. The 'where' information is conveyed via the pathway from the parietal cortex with the information of AoI or objects coming from the inferotemporal cortex. The performance and the feasibility of this recognition process based on the constellation map of 'where' and 'what' information has been widely tested in autonomous robots and vehicles (Hoang, 2021; Colomer et al., 2021). In our current model, we predict the constellation map could take place in EC of which the lateral part conveys information about items and events ('what')

and the medial part codes for the spatial framework ('where').

"What" and "Where" information collaborate together to provide a stable and efficient representation of the visual world. Instead of recruiting numerous neurons for the learning of the position of various AoI on different images, the combination of their positions on each image could be represented by a sequence of the product of the activation of grid cells and the appearance of the corresponding AoI (fig.5.7). Unlike the original model where the azimuth information of AoI is required, our current model recruits grid cells to indicate the location of AoI considering the direct connection between the perirhinal cortical and parahippocampal areas which possess the memory capacities (Aggleton and Brown, 1999) and EC where grid cells are found. Grid cells with an offset of the spatial phase sharing the same grid spacing and orientation pave the whole environment and thereby provide an efficient representation of the 'where' information. In figure 5.7.a, the firing field of three neurons is shown for a simple illustration knowing that the whole environment can be completely paved by grid cells having spatial offsets which are not drawn in the scheme. Recruiting one population of grid cells having the same grid spacing and orientation to provide the spatial information of AoI is the method we refer to as the monoscale GC mechanism. Notably, the representation realized by one set of grid cells having the same spacing and orientation is not exclusive. If one AoI cell is activated in different locations where the firing field of one grid cell is superposed, e.g., focus points 1 and 5 which are categorized as the same AoI in the different locations on the image are represented by the same product 'blue A' in the perirhinal cortex. In this case, recognition confusion gets severe with the increase of occurrences that the same AoI appears in the position that is covered by the firing field of one single grid cell. We further propose a second mechanism combining the 'where' information from two grid cells with different spatial scales knowing that the spacing and the size of the firing field of grid cells increase along the dorso-ventral axis of dorsal MEC (Hafting et al., 2005). In figure 5.7.b, focus point 5 is explicitly represented by the combination of the activity of AoI cells and the spatial information consisting of the activation of 2 grid cells with different spatial scales. This mechanism is capable of creating a relatively exclusive representation of the vision and therefore causes less confusion in the recognition. Combining more than one population of grid cells to form an explicit spatial code should increase robustness. It will be referred to as the multi-scale grid cell mechanism. Notably, only a few grid cells are shown while the whole environment can be completely paved by a set of grid cells having spatial offset with the same orientation. The firing field along with the firing rate of one grid cell is shown in figure 5.8. The x and y axis represent the coordinates on the image shown to the animal during the simulation. The color of the curve and the z-axis indicate the firing rate of the grid cell with darker color representing a higher firing rate. To simplify the simulation without losing biological plausibility, the distribution of

the firing rate on each firing field of the grid cell is assumed to be subject to the normal distribution. The distribution of the firing rate allows the measurement of the positional difference of AoI between the learned view and the current view and therefore improves the capability of the generalization of recognition.

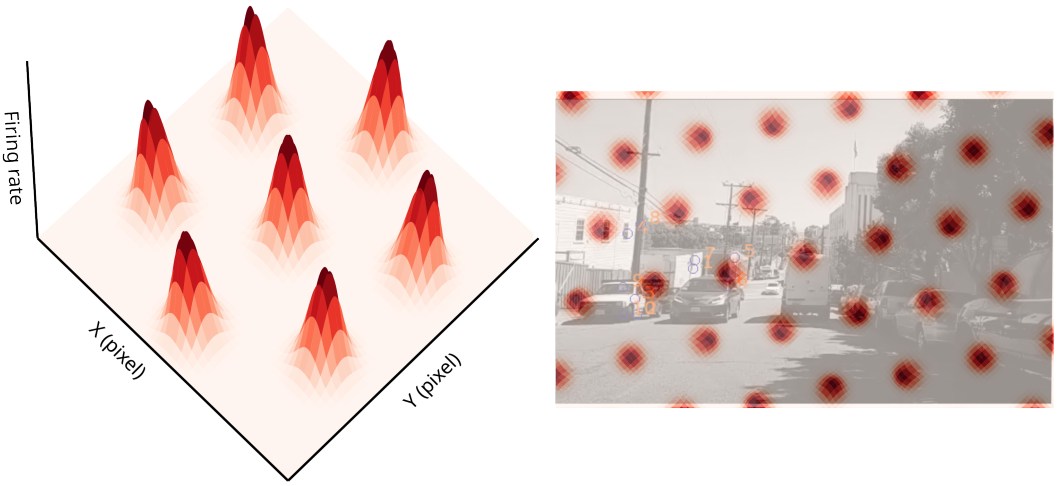


Figure 5.8: Distribution of the firing field of the grid cell used for the recognition tasks. Left, the firing field of one grid cell with the x and y axis representing the coordinates on the image shown to the animal during the simulation. The color of the curve and z-axis indicates the firing rate of the grid cell with darker color representing a higher firing rate. The distribution of the firing rate on each firing field of the grid cell is assumed to be subject to the normal distribution. The distribution of the firing rate allows the measurement of the positional difference of AoI between the learned view and the current view and therefore improves the capability of the generalization of recognition. Right, the firing field of the grid cell superposed with an image used for the testing session.

For the recognition task in the next session, the use of the monoscale GC mechanism is sufficient to perform the recognition tasks where a large set of different visual stimuli exist in the environment.

## 5.5 Results of simulations of the image recognition

The simulation is performed based on the same biological basis as the visual grid cell studied in monkeys (Killian et al., 2012). In each training session, 2000 images are serially presented to the animal. An image is removed after the animal has explored at least 40 gaze locations on the image. In our model, the gaze locations of animals are simulated by searching for the local maxima of an off-center filter applied on the gradient image in order to obtain potential focus points (fig. 5.9).

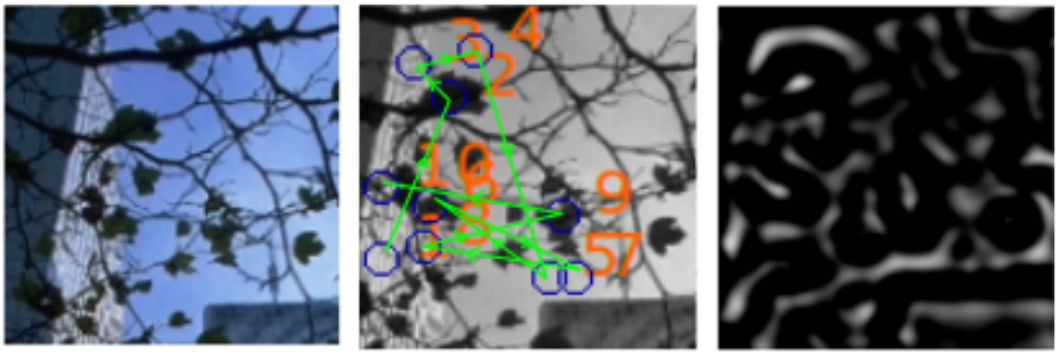


Figure 5.9: One image used for the training session. Left, original image. Middle, gray-scale image with blue circles indicating the focus points, and the number in orange representing the order of focus points. Right, gradient extraction image.

### Non spatial task: object or image recognition

We presume the mature grid cells (as shown in chapter 4, fig 4.21) have been generated by our proposed reciprocal mechanism between PC and VGC after the early development and thereby participate in the recognition process. Nevertheless, more biological evidence remains to be further revealed to support our hypothesis of the reciprocal connection.

To assess the recognition performance, we present 200 images during the training session. An image is removed when the animal has explored 10 locations on the image. 9 grid cells with different spatial offsets paving the whole image are combined with 2000 Area of interest (AoI) cells to build the 'where'-'what' coding. A population of no more than 200 neurons will be recruited for the recognition of images. Notably, depending on the learning vigilance, one AoI cell could activate different focus points if they have a similar local view and one recognition cell could also respond to multiple similar input patterns from the constellation map. After the training session, 7 images are randomly selected from the data set of 200 images (fig.5.10). The activity of 200 cells in response to these 7 images is shown in figure 5.11.top. The results indicated that 7 neurons activate selectively in response to the corresponding image. These winning neurons almost recognize their corresponding images instantly after the first gaze on the image owing to the explicit coding in the constellation map. However, explicit coding is not efficient on the level of the number of neurons used. A compress mechanism which is homogeneous to the one implemented in the generation of grid cells based on the anti-Hebbian learning rule is thereby implemented in the AoI cells. We hypothesize that the visual and object information (Wilson et al., 2013) could both be compressed respectively in the MEC and LEC depending on the homogeneous modulo mechanism. The activity of the same neurons in figure 5.11.top with a supplementary compress mechanism are

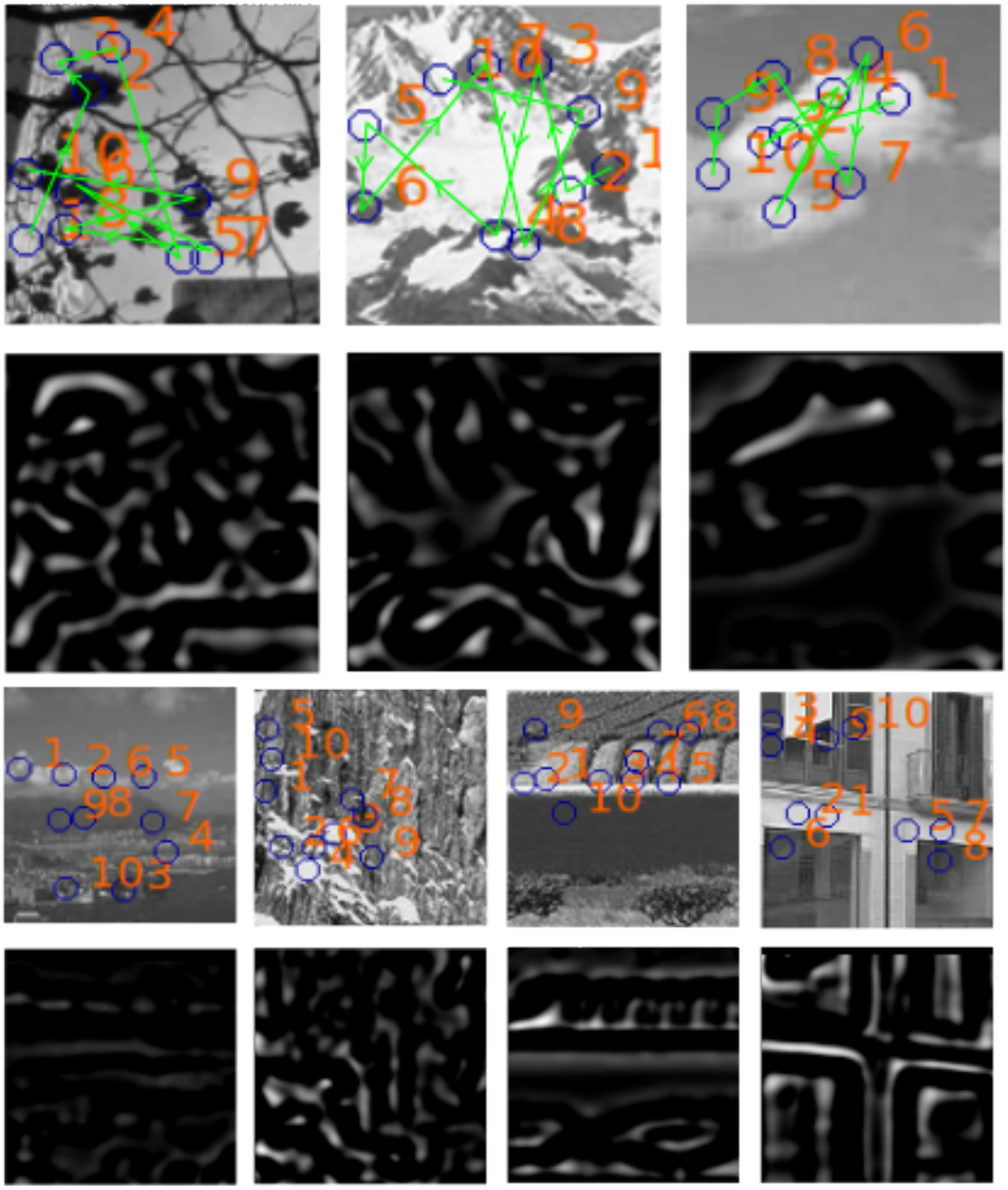

Figure 5.10: For the test session, 7 images are randomly selected from the data set of 200 images. On each image, the top part is the gray-scale image with the gradient extraction image on the bottom. The blue circle on gray-scale images indicates the focus points, and the number in orange represents the order of focus points. Sequential order has no effect on recognition. 10 AoI are obtained for each image during training and testing session

shown in figure 5.11.middle. 2000 AoI cells are compressed into 20 cells. With such a large compression of the AoI information from the image, the confusion is high at the

beginning of the image exploration. However, after the exploration of several images, neurons manage to recognize their corresponding images. The exploration of no more than 4 areas is sufficient for good recognition. To further decrease the confusion level during the recognition, we implement the combined VGC mechanism illustrated in figure 5.7.b to introduce an explicit 'where' information (fig.5.11.bottom).

A larger data set is further used to assess the generalization of our recognition mechanism of which the statistical analysis is conducted.

### Generalization of the recognition to neighbor views

The generalization of the recognition is tested by showing the agent a sequence of images successively recorded from the view of the driver in a car slowly travelling on the country road. Each image is removed when the animal has 10 gaze locations on the image. The video of 300 seconds is averagely sampled into 4000 images as the data set. 400 images averagely selected at the same interval from the data set are used for the training session. The generalization of the recognition is tested with the whole data set. 9 grid cells with spatial offset paving the whole image are combined with 4000 AoI cells to build the recognition coding. The views during the travel for 4 seconds sampled into 7 images as in figure 5.12 are learned respectively by 7 neurons. 10 gazes are made on each image taking 10 time steps. The testing session is ten times longer than the training session with 9 images reinserting between every two images of the training session. The activities of 7 neurons in response to 70 successive views are shown in figure 5.13. The performance of generalized recognition is tested by taking 'where' information from two different mechanisms. On top of the figure is the result obtained by using 'where' information from 9 neurons representing the azimuth of AoI while on the bottom, a population of 9 grid cells paving the whole view is used to provide the spatial information of AoI in views. We could find that each neuron managed to learn a generalized recognition of not only the view during the training session but also the adjacent views with slight differences. The statistical analysis of the performance of generalization using these two mechanisms is discussed in the following section.

A compression modulation which is homogeneous to the one of the saccade information to generate VGC in EC is later implemented to the AoI cells. The results are shown in figure 5.14 with top, the activity of 7 neurons taking 'where' information from 9 neurons representing azimuth of AoI and bottom, the activity of the same 7 neurons using the activity of one population of 9 grid cells as 'where' information. i.e., 9 grid cells with spatial offset paving the whole image are combined with 40 AoI cells to build the recognition coding. In both cases, the AoI information is compressed by a factor of 1/100s. 100 times fewer AoI cells are recruited for the recognition compared to the setup of the last simulation. We observed that many

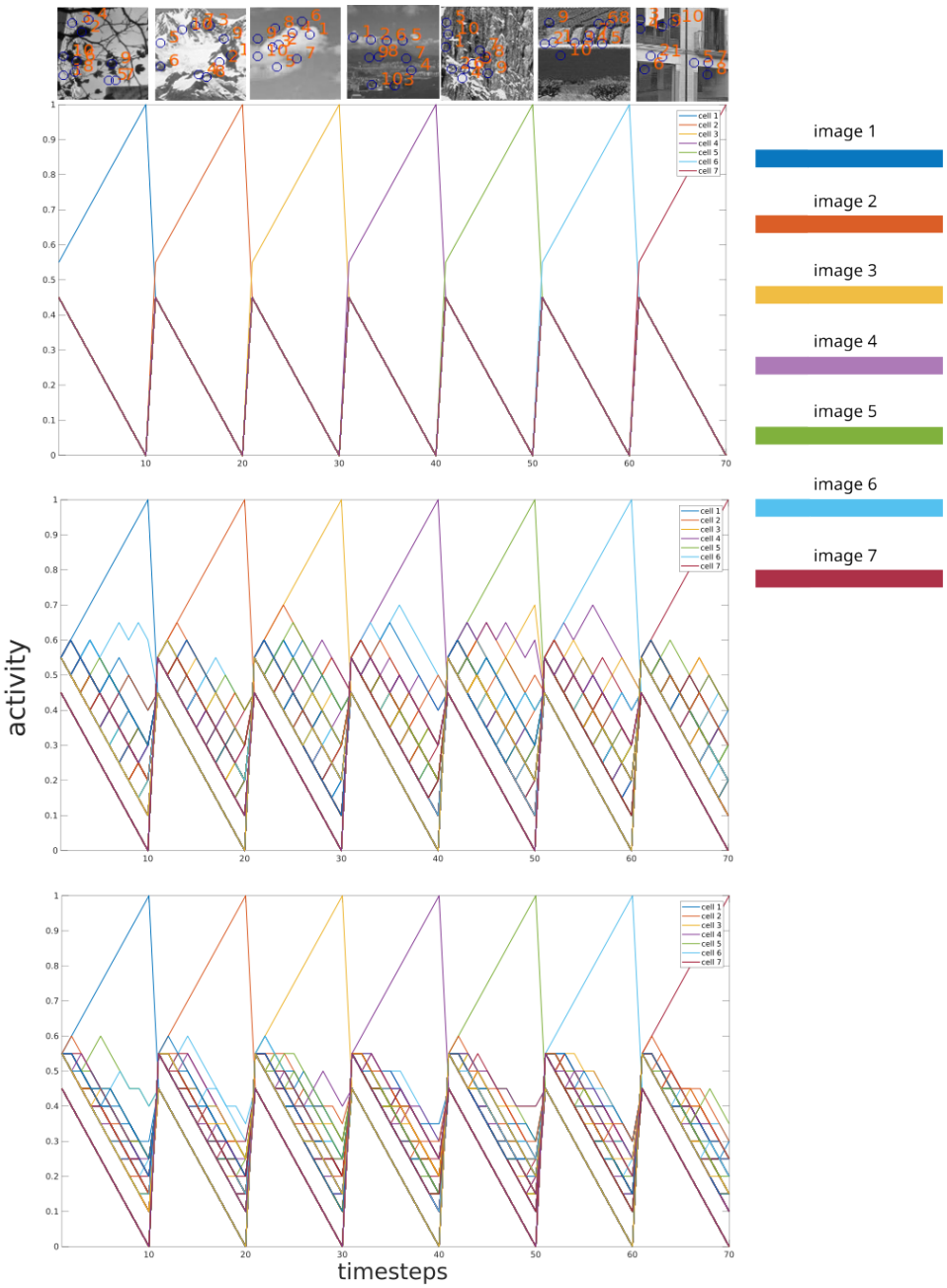


Figure 5.11: top, the activity of 7 cells represents respectively 7 images presented sequentially. middle, the activity of the same neurons in (a) with a supplementary compress mechanism implemented to the AoI cells. 2000 AoI cells are compressed into 20 cells. bottom, results with a multi-scale VGC mechanism are added as illustrated in figure 5.7.b

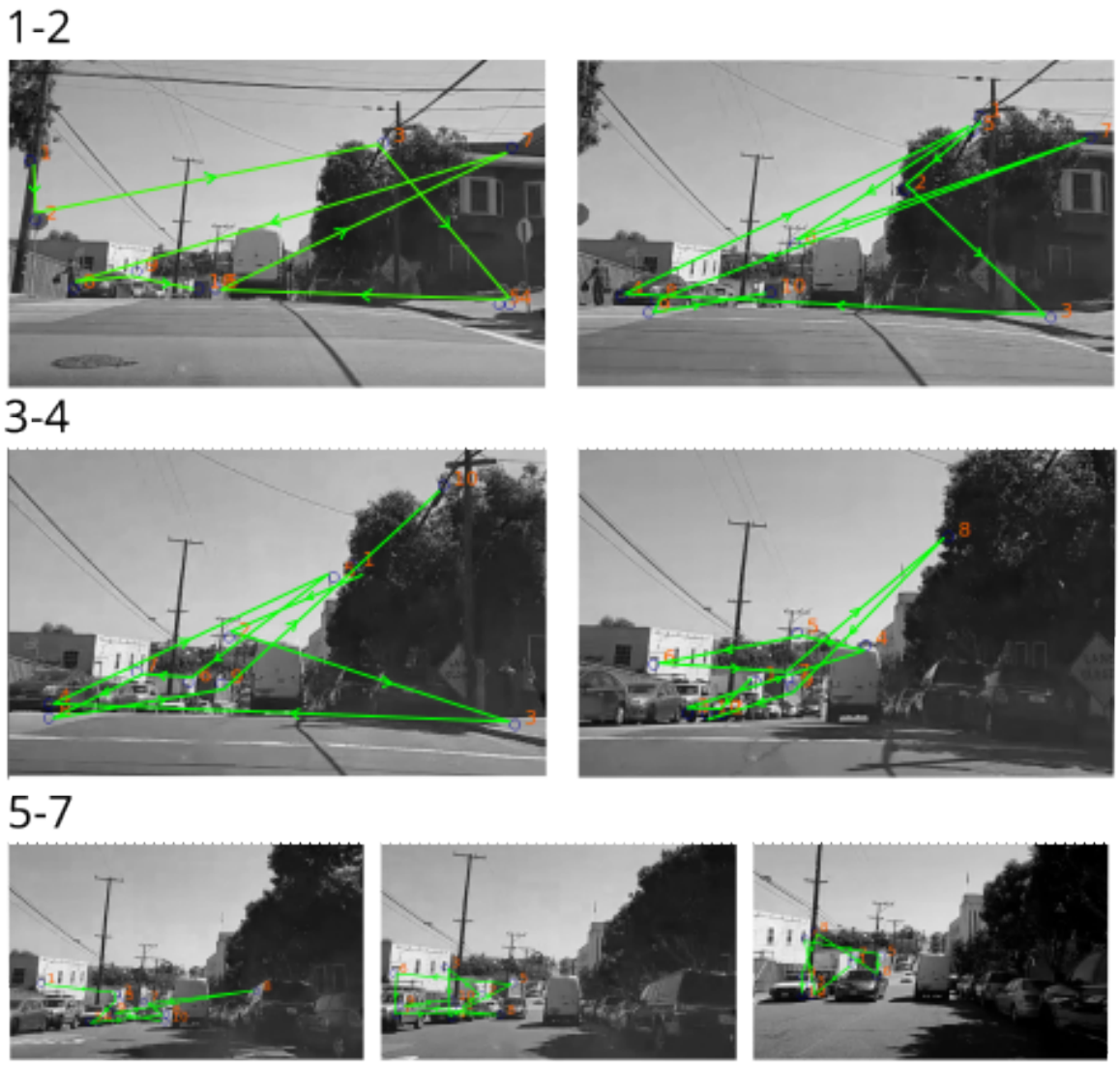


Figure 5.12: Example of Seven successive views from the data-set of 4000 images on the road which are respectively learned by 7 neurons during the training session. The blue circle on gray-scale images indicates the focus points, and the number in orange represents the order of focus points. Sequential order has no effect on recognition. 10 AoI points are obtained for each image during the training and testing sessions.

other neurons start to respond to their non-preferential views due to the increasing ambiguity of the adjacent views caused by the compression of AoI information. Nevertheless, the winning neurons maintain their maximum activity in response to their learned view and its adjacent views which are reinserted during the testing session. The generalized recognition is not destroyed by the compression operation. However, with the increasing activity of neurons in response to their non-preferential views, the robustness of the recognition declines. In other words, the probability of


Figure 5.13: top, The activities of 7 neurons in response to 70 successive views taking 'where' information from 9 neurons representing azimuth of AoI. bottom, activities of 7 neurons using the activity of one population of 9 grid cells as 'where' information.

neurons winning at their non-preferential views increases and therefore interrupts the recognition during the task of successive views. To deal with the recession of performance due to the compression of information, we implement a multi-scale grid cell mechanism combining the 'where' information from two grid cells with different spatial scales as shown in figure 5.7.b. This mechanism is capable of creating a more exclusive representation of the vision compared to the monoscale grid cell mechanism and therefore produces less confusion in the recognition with a negligibly increasing energy cost. The activity of the same seven neurons during the task of the successive view as in the previous simulations is shown in figure 5.15. The conflict between

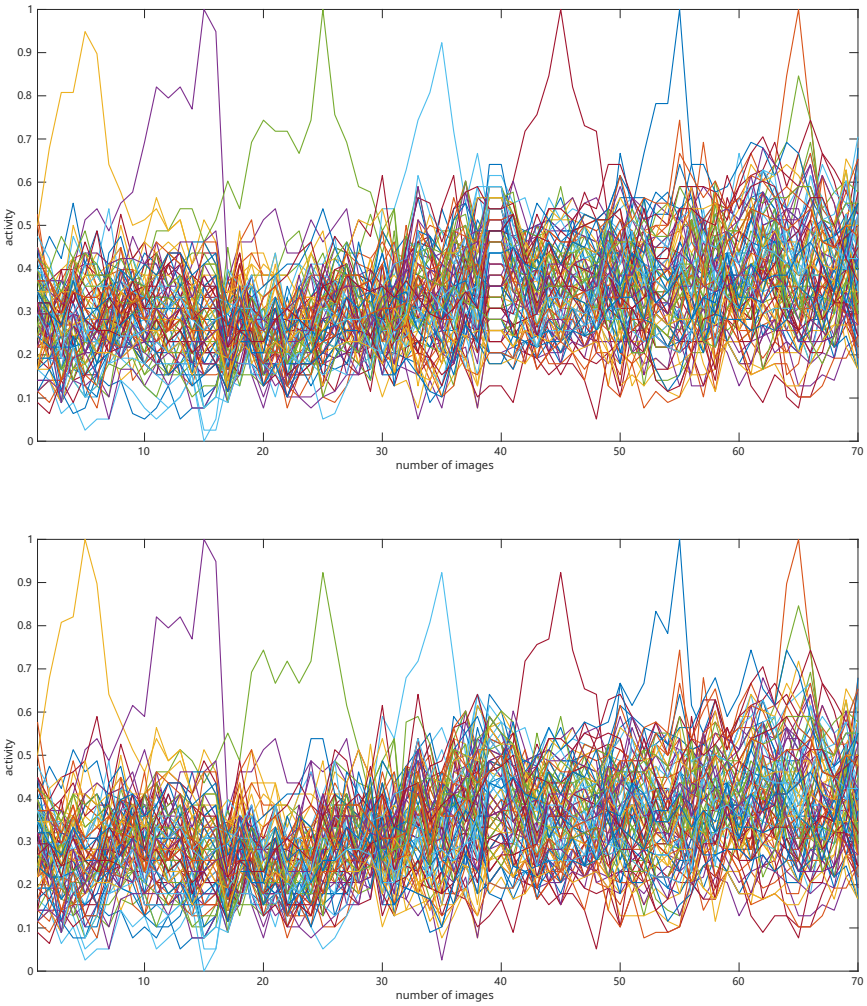


Figure 5.14: The activities of 7 neurons in response to 70 successive views taking AoI information compressed by a factor of 100. top, The activities of 7 neurons taking 'where' information from 9 neurons representing the azimuth of AoI. bottom, activities of 7 neurons using the activity of one population of 9 grid cells as 'where' information.

different neurons during the recognition task has been intuitively reduced.

To assess the generalization and its robustness of our model performing the recognition tasks, two metrics are introduced. 7 neurons win respectively to their preferential sequence of views during the sample time step. The generalization score (GS) of the i-th ($i \in [1, 7]$) winning neuron is calculated by its winning times of views ($N_i^{win}$) during its preferential sequence of views divided by the number of reinserted views ($N_{view} = 10$).

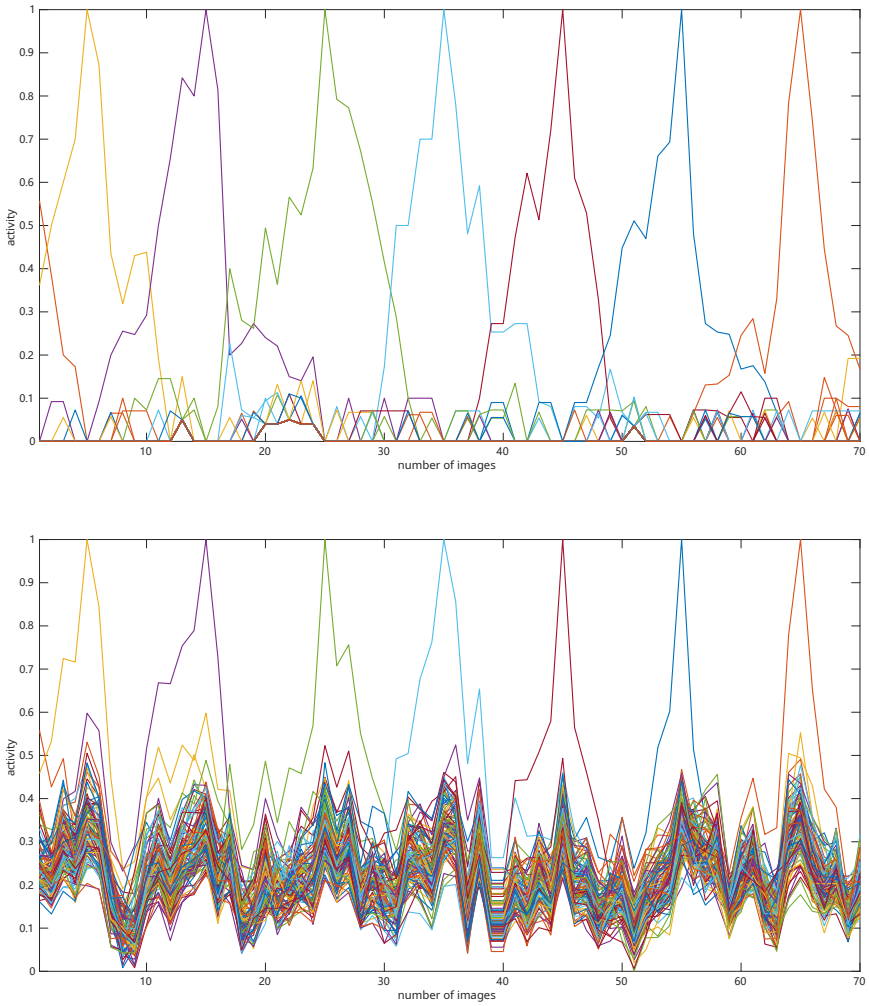


Figure 5.15: The activities of 7 neurons in response to 70 successive views taking 'where' information from a population of multi-scale grid cells. top, without the compression of the AoI information. bottom, information of AoI is compressed by a factor of 1/100.

$$G = f\left(\frac{N_i^{win}}{N_{view}}\right), \quad f(x) = \begin{cases} 1 & \text{if } x > 1 \\ 0 & \text{otherwise} \end{cases} \tag{5.5}$$

The mean score of seven neurons responding to their preferential sequence of views represents the recognition score of the model.

The robustness level is defined by the average sum of the difference($\overline{R_i}$ in fig.5.16) between the activity of the i-th winning neuron $S_i^{max}$ and the activity of the i-th second highest neuron $S_i^{sh}$ during the winner's preferential sequence of views

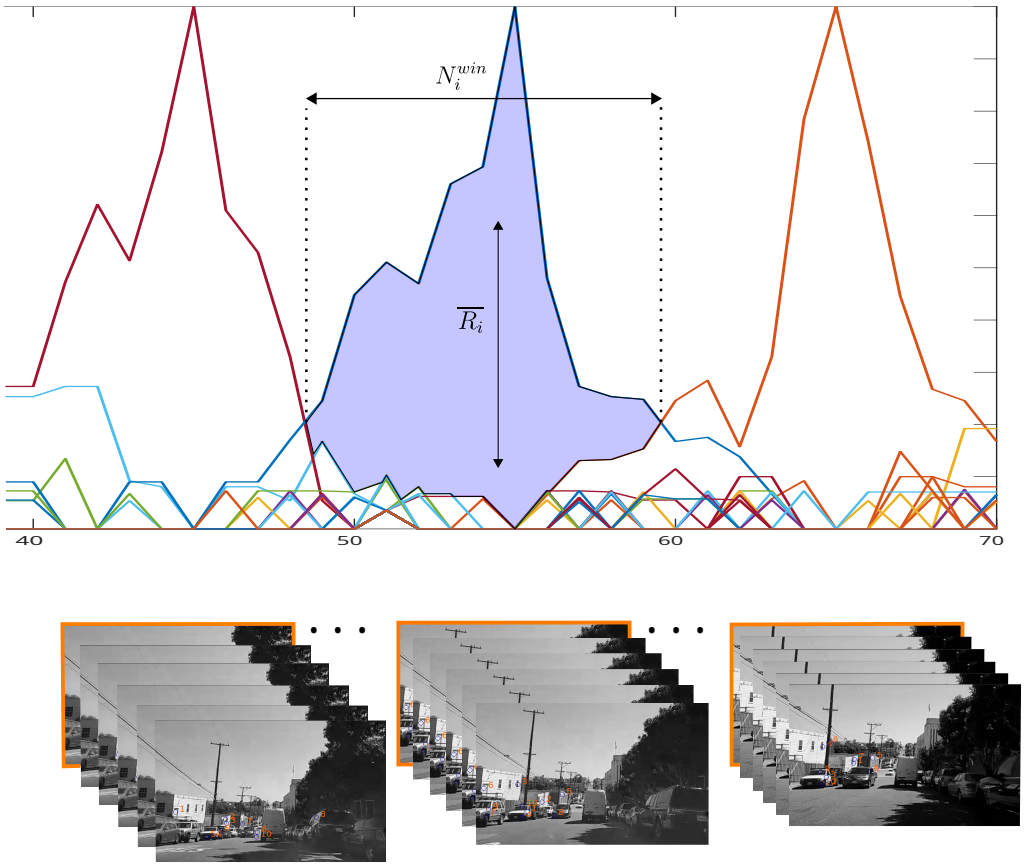


Figure 5.16: Illustration of the generalization score (GS) and the robustness level of 3 sampled neurons during the process of the testing session. top, curves of activity of the last three neurons in the previous simulations. $N_i^{win}$ is the winning times of views of i-th neuron which is in direct proportion to the GS. $\overline{R_i}$ indicates its robustness of the generalization of the recognition. bottom, views enclosed by orange rectangles are those learned by the corresponding neurons during the training session, and views without the orange rectangles are those reinserted during the testing session. Between each pair of training views, 10 successive views are inserted for the recognition task.

$(t \in [1, N_{view}])$.

$$\overline{R_i} = \frac{\sum_{t=1}^{t=N_{view}} \left(S_i^{max}(t) - S_i^{sh}(t)\right)}{N_{view}} \tag{5.6}$$

The winner's preferential sequence of views is composed of 10 successive views ($N_{view} = 10$) reinserted between views of the training session. Notably, the robust-

ness level alone is meaningless without considering the GS.

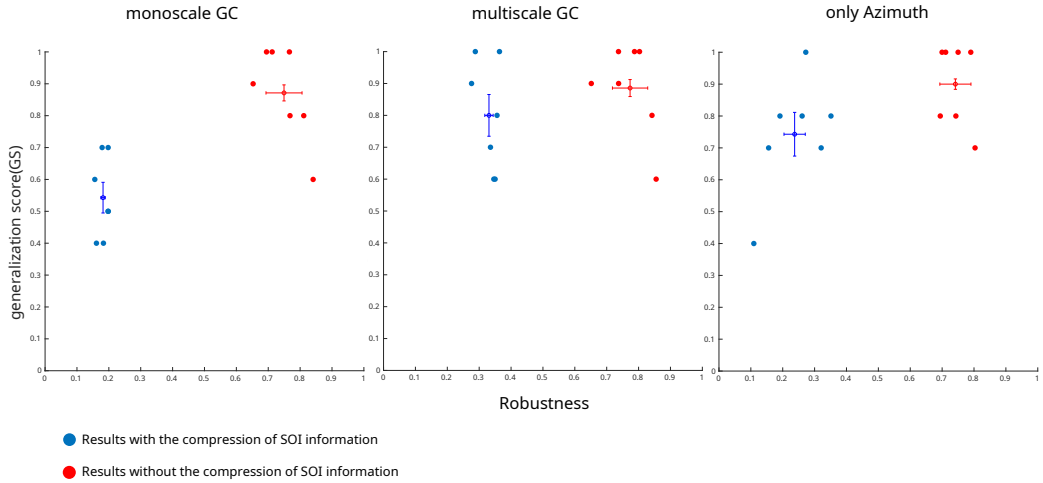


Figure 5.17: Scatter figure showing the GS and Robustness of the recognition of 7 neurons under different setups for visual localization. Blue circles indicate results without the compression of AoI information while red circles are those with the compression. X and Y axis represent respectively the normalized GS and the robustness level which are both scaled from 0 to 1 with a higher value indicating better performance. From the left figure to the right, the spatial information of the AoI is performed by three different mechanisms which are respectively monoscale grid cells, multi-scale grid cells, and azimuth to the AoI provided by the foveated vision.

In figure 5.17, we showed the GS and the robustness level of models using three different mechanisms retrieving the location of the AoI with or without the compression of the AoI cells. Curves from the left to the right correspond respectively to the mechanism of single-scaled GC, multi-scale GC, and Azimuth. In each figure, blue dots represent results with the compression of AoI information while the red ones are those without the implementation of the compression. Y-axis shows the GS of the recognition with the x-axis indicating the robustness of the generalization. The dot with the SEM bar represents the mean value of each group.

To better visualize the comparison of the performance of the model using different mechanisms to retrieve the location of AoI before and after the compression of AoI cells, the results of three recognition setups are compared: the classical one without compression (fig. 5.18.a) and those undergoing the compression of AoI cells (fig. 5.18.b). Blue bars represent the GS of the recognition with red ones indicating the robustness of the generalization.

We observed that all three setups undergo a declining performance after the implementation of the compression of AoI cells. Nevertheless, except for the model with the single-scared GC whose GS and the robustness level are all sensitive to the compression mechanism, the model of the multi-scale GC and the azimuth showed

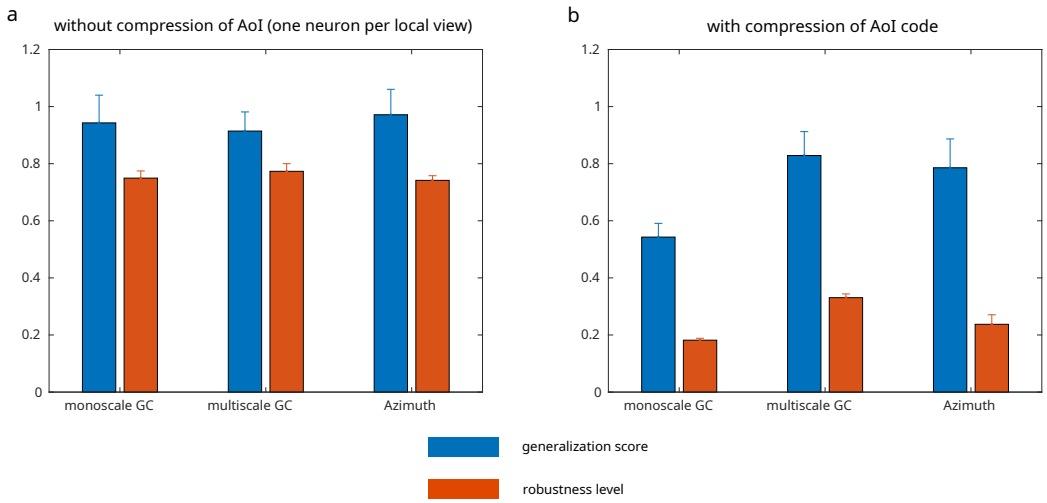


Figure 5.18: The comparison of mean values of the GS and Robustness of the recognition of 7 neurons under different setups. The blue bar represents the GS while the red stands for the robustness level. a, results without the compression of AoI information. b, results with the compression of AoI information.

high consistency of the generalization of the recognition after the implementation of the compression of the AoI cells. The recognition mechanism in our model is robust to the misrecognition of a few AoI or the noise inside the activity of grid cells owing to the combination of the two types of visual information (what and where) creating an explicit and generalized recognition coding in the constellation map.

| Description | Module | Symbol & Value |
|---|---|---|
| Variance of the Gaussian filter | DoG | $\sigma_1 = 2, \sigma_2 = 5$(pixels) |
| Size of the filter | | $i_{max}, j_{max} = 10$ |
| $Nb_{nr}$ representing 360° | Saccade field | $N = 30$ |
| $Nb_{nr}$ on the Kohonen map | Discretization | $M = 15$ |
| $Nb_{nr}$ on the modulo field | Anti-Hebbian learning | $j_1 = 3$ |
| | | $j_2 = 5$ |
| $Nb_{nr}$ conveying spatial information | Azimuth | $N_{azi} = 9$ |
| $Nb_{nr}$ on the polar local-view field | Retinal projection | 400 |
| Learning rate of LMS conditioning learning | Generation of GC | $\lambda = 0.01$ |
| Nb of monoscale grid cells | | $N_{mono} = j_1^2 = 9$ |
| Nb of multi-scale grid cells | | $N_{multi} = N_{mono} + j_2^2 = 34$ |
| Vigilance value during learning process | AoI | $Vig = 0.95$ |
| Vigilance value after learning process | | $Vig = 0$ |
| $Nb_{nr}$ recruited for the learning of local views | | $= N_{AoI} = 2000$ |
| $Nb_{nr}$ on the constellation map | Constellation map | $M_{mono} = N_{mono} \cdot N_{AoI}$ |
| | | $M_{multi} = N_{multi} \cdot N_{AoI}$ |
| | | $M_{azimuth} = N_{azi} \cdot N_{AoI}$ |
| Vigilance value during learning process | Recognition | $Vig = 1$ |
| Vigilance value after learning process | | $Vig = 0$ |
| $Nb_{nr}$ recruited for the recognition | | 400 |
| Modulo factor applied to the AoI | Compression ratio | 100 |

Table 5.1: Parameters of the model. $Nb_{nr}$ stands for the number of neurons.
DoG: difference of Gaussian. GC: grid cells. AoI: area of interest.

## 5.6 Conclusion

We explained how a homogeneous model as the one of the path integration proposed precedingly could be applied to the visual exploration by saccade and account for the generation of the visual grid cells. We emphasized that the place cell and grid cell could form reciprocal connectivity with the medial septum playing the role of a modulator to eventually stabilize an efficient representation of the space or view after the early development of the brain.

We proposed a recognition mechanism combining the firing field of grid cells and the activity of the corresponding AoI cells of the images. The learning rule is based on novelty detection. A new neuron will be recruited if the input pattern is relatively new to all the learned neurons. This new neuron thereby represents the input pattern by forming certain synaptic connections with the input neurons subject to the Hebbian learning rule. The recruitment of the AoI neurons for the detection of the novel focus points relies on the same learning rule.

We assessed the compression effect of the modulo mechanism during image recognition. The performance of the recognition was maintained intact even with a very high compression ratio. The constellation map combining compressed 'where' and 'what' information provides an efficient and quasi-explicit coding of the visual representation.

In addition, the misrecognition of a few focus points due to the unstable learning process or the noise in the firing field of grid cells can not destroy the recognition of images owing to the redundant localized AoI.

The generalization capability of visual recognition is tested during movement on country roads and highways in simulation. The recognition mechanism based on visual grid cells could be combined with a self-motion-based system to provide efficient and stable spatial representation for robots during navigation tasks.

The visual and spatial grid cells are two different sets of similar neurons in our model. They have a similar property while receiving different kinds of input. The recognition level increases and decreases continuously as the agent approaches and moves away from one certain view as shown in figure 5.15 during the recognition task. This recognition variance based on visual information can be helpful to indicate the distance between the agent and the view during navigation tasks.

# Chapter 6

# Discussion

The retrosplenial cortex (RSC) is densely innervated with the hippocampus (Hipp) and shares reciprocal connections with the entorhinal cortex. Biological recordings have shown that RSC is directly linked to rodent spatial behaviours. Our work advocates the hypothesis that the path integration could pre-exist before EC 'grid cells' and hippocampal 'place cells' as proposed by (Gaussier et al., 2007). In our model, RSC is nothing more than a classical cortex performing a low pass filtering of its inputs related to HD cells and using blobs of neurons to 'recognize' or quantify those activities. We predict in our model that the path integration could be computed outside the hippocampal formation and is conveyed via RSC. Notably, place cell-like activity is found in RSC when a mouse moves on a one-way treadmill with its head fixed. We simulated the same experiment using our computational model of RSC. Neurons in RSC are simulated by a one-dimensional self-organizing map. Those neurons fire in sequences during movement on the treadmill in the same direction showing the same property as neurons recorded in biological experiments. Place cells and head direction cells are also generated during free movement by simply modifying the learning rate of the path integration field and the breadth of the connectivity between cortices in our model. Our simulation results explain why the place cell-like activity in RSC can be found during movement in the same direction while no such activity has been reported during free movement. Due to the local connectivity between cortices, the place cell-like activity can be only observed in RSC when the animal moves in one direction on the treadmill with its head fixed (Mao et al., 2017). A wide range of spatially involved neuronal activity such as place cells and head direction cells has been produced by our PI model assuming the brain area has full access to the upstream cortex or subcortex where the PI could originate. We have shown in our simulations that a global connection to the path integration neural field requires a large number of neurons and synaptic connections. The cost even increases if we consider the need for redundant neurons for robust coding in case of perturbation and malfunction of neurons. Therefore,

the global connectivity between cortices and Hipp is not plausible considering the limited number of neurons and synaptic connections of each neuron in Hipp, not to mention numerous afferent signals to Hipp including the proprioception of self-motion and the information of different types of perceptions. Considering the rich innervation between EC and Hipp, we propose that EC could play the role of a hub to compress the cortical information involved in navigation, vision and other recognition tasks and interact with Hipp to generate place cells. The entorhinal cortex could maintain the global feature of the cortical information with sparse connectivity to the afferent cortices owing to the modulo projection. The grid cell activity in EC could be an epiphenomenon of this general compression mechanism. This compression mechanism is realized by introducing a modulo operation between EC and its afferent cortices.

The path integration is proven to be instrumental for grid cell spatial firing of rats in a circular 1D environment (Jacob et al., 2019). An increased size/scale of the grid firing field between the arena and the track was observed, while it was unmodified in arenas of different sizes. One hypothesis has been proposed that the lack of visual cues during navigation could be responsible for the metrical properties of the grid cell map.

Our model of the generation of grid cells is compatible with this hypothesis. During the early development, the firing field spacing/grid scale is determined by the teaching signal from Hipp. The larger the size of the place cell firing field is, the larger will be the spacing or scale of the grid firing field. We predict that the size of the place cell firing field is relatively larger when there are fewer external cues and animals have to depend more on the path integration for navigation. After the early development, the grid firing field spacing can be simply modulated by the divisor of the modulo operation mechanism in our model. Increasing the divisor (recruiting more grid cells in our model) will enlarge the spacing or scale of the grid firing field. We predict that more grid cells will be recruited to compensate for the reduced accuracy of the self-localization solely depending on the self-motion proprioception when the availability of the external information is reduced.

We proposed a reciprocal mechanism between Hipp and EC explaining the hexagonal pattern of grid cells and the emergency of place cells and grid cells. The hexagonal pattern can be learned without the need for topological contiguity or artificial selection of neurons that many other models require. In some other models, the generation of place cells highly depends on the stable grid cells. However, places cells could exist before grid cells during the development of the brain and affect the generation of the latter. In our model, we don't have to deal with the causality dilemma of the egg or the chicken. We hold the view that these two cells could form reciprocal connectivity with the medial septum playing the role of a modulator in order to eventually stabilize an efficient representation of the space after the early

development of the brain.

We propose an image recognition mechanism combining 'where' information from the visual grid cells and 'what' information from the activity of the neurons coding for areas of interest in the images. Our model explains the existence of the visual grid cells found in primates during visual exploration and predicts the contribution of the visual grid cell in recognition. We suppose that the formation of a constellation map could take place in EC taking compressed 'where' input from MEC and compressed 'what' input from LEC. Grid cells with periodic firing fields can be a trace of the compression mechanism we proposed in our model.

We assessed the compression effect of the modulo mechanism during image recognition. The performance of the recognition was maintained intact even with a very high compression ratio. The constellation map combining compressed 'where' and 'what' information provides an efficient and quasi-explicit coding of the visual representation. The generalization capability of visual recognition is tested during movement on country roads and highways in simulation. The recognition mechanism based on visual grid cells could be combined with a self-motion-based system to provide efficient and stable spatial representation for robots during navigation tasks.

An illustration of pathways between cortices and the hippocampus accounting for the spatial representation and image recognition is shown in figure 6.1. Color bars indicate the contribution of different chapters.

Our model can also realize both allocentric and egocentric tasks by using distant or local cues as the landmark to recalibrate HD cells and/or PI as long as the visual information is added. RSC in our model could play a role as a hub where the visual and proprioceptive information can be merged. The interaction of the allocentric and egocentric information should allow the animal to switch between different reference frames for complex spatial navigation tasks. Simulation results and interpretations are in an ongoing paper.

Our model could be further extended to recalibrate and generate the bi-directional cells observed in (Jacob et al., 2017) by merging visual and proprioceptive information. RSC is known to manipulate visual information and to translate between egocentric (self-centered) and allocentric (world-centered) spatial information (Alexander and Nitz, 2015). Visual information can be very important for the recalibration of HD cells in RSC. The bi-directional HD cells found in RSC might be explained by the local connectivity between RSC and the afferent areas. For instance, if one RSC neuron receives input from only two neurons of the afferent neural field, this RSC neuron will probably present a bi-directional HD cell activity.

The results of the reciprocal learning mechanism between grid cells and place cells are still preliminary. Some difficulty remains unsolved. The self-organized hexagonal signal could be stabilized with the help of border cells or other information as a recalibration mechanism. The adaptive one-shot learning rule of the septal hexagonal

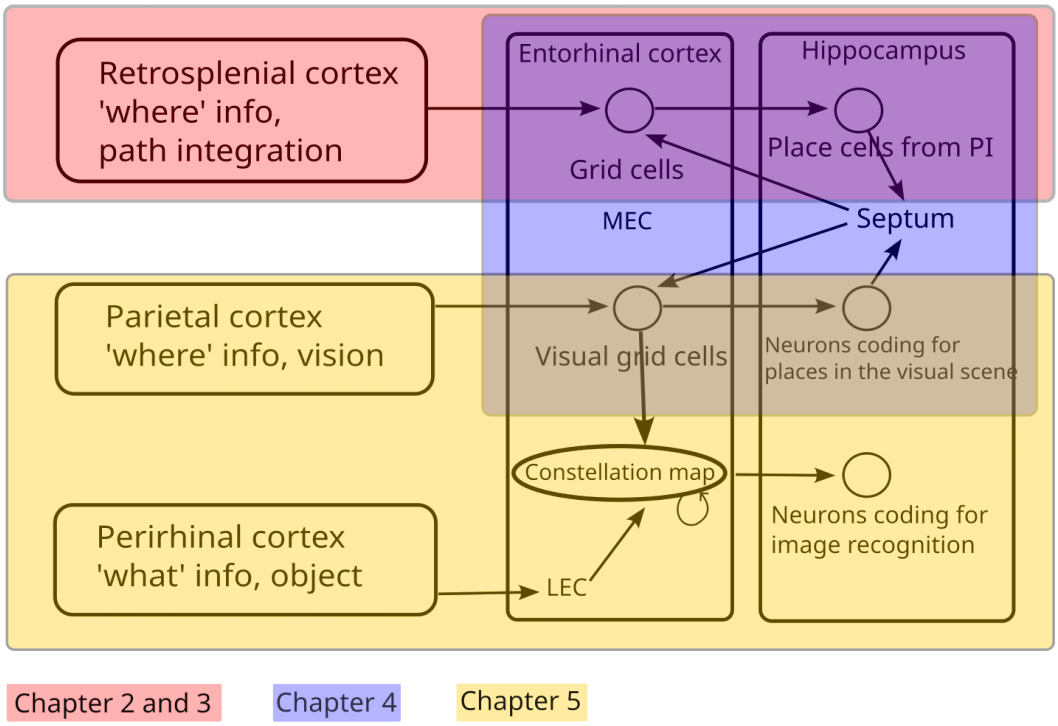


Figure 6.1: Illustration of pathways between cortices and the hippocampus accounting for the spatial representation and image recognition. Color bars indicate the contribution of different chapters.

signal and the dynamic and reciprocal learning mechanism between EC and Hipp need to be further studied. The synchronization of place cells and grid cells might be achieved by taking into consideration of the theta and gamma rhythm. We predict that a mechanism of the replay of experience realised by theta and gamma rhythm (Lisman and Jensen, 2013) or sharp wave ripples (Jadhav et al., 2012; Eschenko et al., 2008) could account for the generation of grid cells with a spatial offset of which the firing field tiles the whole environment.

Disrupted Place Cell Remapping and Impaired Grid Cells are found in amyloid precursor protein knockin mice with impaired spatial memory (Jun et al., 2020). Recent research found that the impairment of the Gcs in the EC of aged people could be a forewarning of Alzheimer's disease. Compromised grid-cell-like representations along with path integration (PI) deficits have been found in the human entorhinal cortex (EC) in old age. This recording suggests that impaired grid cell function or PI deficits might predict an age-related decline in cognitive functions (Stangl et al., 2018). The dysfunction of the Hipp may impair the acetylcholine modulation so as to cause the impairment of the Gcs, the deficits of PI can also have the same effect on GCs. Our model explaining the generation of place cells and grid cells could be further studied and has the potential to help the understanding of the

circuit mechanism underlying the spatial disorder related to Alzheimer's disease and therefore helps with the prediction and intervention of Alzheimer's disease.

Our model of the interaction between RSC, EC, and Hipp has the potential to be a paradigm explaining not only the place and visual recognition but also the formation of episodic memories.

# Bibliography


Aggleton, John P and Malcolm W Brown (1999). "Episodic memory, amnesia, and the hippocampal–anterior thalamic axis". In: *Behavioral and brain sciences* 22.3, pp. 425–444.

Alexander, Andrew S and Douglas A Nitz (2015). "Retrosplenial cortex maps the conjunction of internal and external spaces". In: *Nature neuroscience* 18.8, p. 1143.

Alonso, Angel and Christer Köhler (1984). "A study of the reciprocal connections between the septum and the entorhinal area using anterograde and retrograde axonal transport methods in the rat brain". In: *Journal of Comparative Neurology* 225.3, pp. 327–343.

Amari, S. (1977a). "Dynamics of pattern formation in lateral-inhibition type neural fields". In: *Biological Cybernetics* 27, pp. 77–87.

Amari, Shun-Ichi (1980). "Topographic organization of nerve fields". In: *Bulletin of Mathematical Biology* 42.3, pp. 339–364.

Amari, Shun-ichi (1977b). "Dynamics of pattern formation in lateral-inhibition type neural fields". In: *Biological cybernetics* 27.2, pp. 77–87.

Andersen, Per, Richard Morris, David Amaral, Tim Bliss, and John O'Keefe (2006). *The hippocampus book*. Oxford university press.

Arleo, Angelo and Wulfram Gerstner (2000). "Spatial cognition and neuro-mimetic navigation: a model of hippocampal place cell activity". In: *Biological cybernetics* 83.3, pp. 287–299.

Banquet, Jean P, Philippe Gaussier, Jean Claude Dreher, Cédric Joulain, Arnaud Revel, and Wilfried Günther (1997). "Space-time, order, and hierarchy in fronto-hippocampal system: A neural basis of personality". In: *Advances in Psychology*. Vol. 124. Elsevier, pp. 123–189.

Banquet, Jean-Paul, Ph Gaussier, Mathias Quoy, Arnaud Revel, and Yves Burnod (2005). "A hierarchy of associations in hippocampo-cortical systems: cognitive maps and navigation strategies". In: *Neural Computation* 17.6, pp. 1339–1384.

Beurle, R. L. (1956). "Properties of a mass of cells capable of regenerating pulses". In: *Philosophical Transactions of the Royal Society B* 240(669), pp. 55–94.

Bicanski, Andrej and Neil Burgess (2016). "Environmental anchoring of head direction in a computational model of retrosplenial cortex". In: *Journal of Neuroscience* 36.46, pp. 11601–11618.

— (2018). "A neural-level model of spatial memory and imagery". In: *Elife* 7, e33752.

Bjerknes, Tale L, Nenitha C Dagslott, Edvard I Moser, and May-Britt Moser (2018). "Path integration in place cells of developing rats". In: *Proceedings of the National Academy of Sciences* 115.7, E1637–E1646.

Blayo, Francois (1992). "Kohonen self-organizing maps: Is the normalization necessary?" In: *Complex Systems* 6.6, pp. 105–123.

Bonnevie, Tora, Benjamin Dunn, Marianne Fyhn, Torkel Hafting, Dori Derdikman, John L Kubie, Yasser Roudi, Edvard I Moser, and May-Britt Moser (2013). "Grid cells require excitatory drive from the hippocampus". In: *Nature neuroscience* 16.3, pp. 309–317.

Brandon, Mark P, Julie Koenig, Jill K Leutgeb, and Stefan Leutgeb (2014). "New and distinct hippocampal place codes are generated in a new environment during septal inactivation". In: *Neuron* 82.4, pp. 789–796.

Bunsey, M and H Eichenbaum (1996). "Conservation of hippocampal memory function in rats and humans". In: *Nature* 379.6562, pp. 255–257.

Burak, Yoram and Ila R Fiete (2009). "Accurate path integration in continuous attractor network models of grid cells". In: *PLoS computational biology* 5.2, e1000291.

Burgess, Neil (2008). "Grid cells and theta as oscillatory interference: theory and predictions". In: *Hippocampus* 18.12, pp. 1157–1174.

Burgess, Neil, Caswell Barry, and John O'keefe (2007). "An oscillatory interference model of grid cell firing". In: *Hippocampus* 17.9, pp. 801–812.

Burnod, Yves, Pierre Baraduc, Alexandra Battaglia-Mayer, Emmanuel Guigon, Etienne Koechlin, Stefano Ferraina, Francesco Lacquaniti, and Roberto Caminiti (1999). "Parieto-frontal coding of reaching: an integrated framework". In: *Experimental brain research* 129.3, pp. 325–346.

Burwell, Rebecca D and David G Amaral (1998). "Perirhinal and postrhinal cortices of the rat: interconnectivity and connections with the entorhinal cortex". In: *Journal of Comparative Neurology* 391.3, pp. 293–321.

Bush, Daniel, Caswell Barry, and Neil Burgess (2014). "What do grid cells contribute to place cell firing?" In: *Trends in neurosciences* 37.3, pp. 136–145.

Buzsáki, György and Edvard I Moser (2013). "Memory, navigation and theta rhythm in the hippocampal-entorhinal system". In: *Nature neuroscience* 16.2, pp. 130–138.

Byrne, Patrick, Suzanna Becker, and Neil Burgess (2007). "Remembering the past and imagining the future: a neural model of spatial memory and imagery." In: *Psychological review* 114.2, p. 340.

Chen, Guifen, John A King, Neil Burgess, and John O'Keefe (2013). "How vision and movement combine in the hippocampal place code". In: *Proceedings of the National Academy of Sciences* 110.1, pp. 378–383.

Colby, Carol L, Michael E Goldberg, et al. (1999). "Space and attention in parietal cortex". In: *Annual review of neuroscience* 22.1, pp. 319–349.

Colgin, Laura Lee (2016). "Rhythms of the hippocampal network". In: *Nature Reviews Neuroscience* 17.4, pp. 239–249.

Collett, TS, J Baron, and K Sellen (1996). "On the encoding of movement vectors by honeybees. Are distance and direction represented independently?" In: *Journal of Comparative Physiology A* 179.3, pp. 395–406.

Colomer, Sylvain, Nicolas Cuperlier, Guillaume Bresson, Philippe Gaussier, and Olivier Romain (2021). "LPMP: A Bio-Inspired Model for Visual Localization in Challenging Environments." In: *Frontiers in Robotics and AI* 8, pp. 703811–703811.

Cooper, Brenton G, Theodore F Manka, and Sheri JY Mizumori (2001). "Finding your way in the dark: the retrosplenial cortex contributes to spatial memory and navigation without visual cues." In: *Behavioral neuroscience* 115.5, p. 1012.

Cooper, Brenton G and Sheri JY Mizumori (1999). "Retrosplenial cortex inactivation selectively impairs navigation in darkness". In: *Neuroreport* 10.3, pp. 625–630.

Crawford, Morris LJ, Ronald S Harwerth, Earl L Smith, Stephen Mills, and Bryan Ewing (2001). "Experimental glaucoma in primates: changes in cytochrome oxidase blobs in V1 cortex". In: *Investigative ophthalmology & visual science* 42.2, pp. 358–364.

Cullen, Kathleen E and Jeffrey S Taube (2017). "Our sense of direction: progress, controversies and challenges". In: *Nature neuroscience* 20.11, pp. 1465–1473.

Cuperlier, Nicolas, Mathias Quoy, Christophe Giovannangeli, Philippe Gaussier, and Philippe Laroque (2006). "Transition cells for navigation and planning in an unknown environment". In: *International Conference on Simulation of Adaptive Behavior*. Springer, pp. 286–297.

Czajkowski, Rafał, Balaji Jayaprakash, Brian Wiltgen, Thomas Rogerson, Mikael C Guzman-Karlsson, Alison L Barth, Joshua T Trachtenberg, and Alcino J Silva (2014). "Encoding and storage of spatial information in the retrosplenial cortex". In: *Proceedings of the National Academy of Sciences* 111.23, pp. 8661–8666.

Czajkowski, Rafał, Jørgen Sugar, Sheng-Jia Zhang, Jonathan J Couey, Jing Ye, and Menno P Witter (2013). "Superficially projecting principal neurons in layer V of medial entorhinal cortex in the rat receive excitatory retrosplenial input". In: *Journal of Neuroscience* 33.40, pp. 15779–15792.

Daucé, Emmanuel, Pierre Albiges, and Laurent U Perrinet (2020). "A dual foveal-peripheral visual processing model implements efficient saccade selection". In: *Journal of Vision* 20.8, pp. 22–22.

Deshmukh, Sachin S and James J Knierim (2011). "Representation of non-spatial and spatial information in the lateral entorhinal cortex". In: *Frontiers in behavioral neuroscience* 5, p. 69.

Detorakis, Georgios Is and Nicolas P Rougier (2012). "A neural field model of the somatosensory cortex: formation, maintenance and reorganization of ordered topographic maps". In: *PloS one* 7.7, e40257.

Dominey, Peter, Michael Arbib, and Jean-Paul Joseph (1995). "A model of corticostriatal plasticity for learning oculomotor associations and sequences". In: *Journal of cognitive neuroscience* 7.3, pp. 311–336.

Eichenbaum, Howard, Tim Otto, and Neal J Cohen (1994). "Two functional components of the hippocampal memory system". In: *Behavioral and Brain Sciences* 17.3, pp. 449–472.

Elduayen, Coralie and Etienne Save (2014). "The retrosplenial cortex is necessary for path integration in the dark". In: *Behavioural Brain Research* 272, pp. 303–307.

Elman, Jeffrey L (1993). "Learning and development in neural networks: The importance of starting small". In: *Cognition* 48.1, pp. 71–99.

Eschenko, Oxana, Wiam Ramadan, Matthias Mölle, Jan Born, and Susan J Sara (2008). "Sustained increase in hippocampal sharp-wave ripple activity during slow-wave sleep after learning". In: *Learning & memory* 15.4, pp. 222–228.

Etienne, Ariane S and Kathryn J Jeffery (2004). "Path integration in mammals". In: *Hippocampus* 14.2, pp. 180–192.

Fuhs, Mark C and David S Touretzky (2006). "A spin glass model of path integration in rat medial entorhinal cortex". In: *Journal of Neuroscience* 26.16, pp. 4266–4276.

Gardner, Richard J, Erik Hermansen, Marius Pachitariu, Yoram Burak, Nils A Baas, Benjamin A Dunn, May-Britt Moser, and Edvard I Moser (2022). "Toroidal topology of population activity in grid cells". In: *Nature* 602.7895, pp. 123–128.

Gaussier, Ph, JP Banquet, F Sargolini, C Giovannangeli, E Save, and Bruno Poucet (2007). "A model of grid cells involving extra hippocampal path integration, and the hippocampal loop". In: *Journal of integrative neuroscience* 6.03, pp. 447–476.

Gaussier, Philippe (1992). "Simulation d'un système visuel comprenant plusieurs aires corticales: Application à l'analyse de scènes". PhD thesis. Paris 11.

Gaussier, Philippe, Jean Paul Banquet, Nicolas Cuperlier, Mathias Quoy, Lise Aubin, Pierre-Yves Jacob, Francesca Sargolini, Etienne Save, Jeffrey L Krichmar, and Bruno Poucet (2019). "Merging information in the entorhinal cortex: what can we learn from robotics experiments and modeling?" In: *Journal of Experimental Biology* 222.Suppl_1, jeb186932.

Gaussier, Philippe, Cédric Joulain, Stéphane Zrehen, Jean-Paul Banquet, and Arnaud Revel (1997). "Visual navigation in an open environment without map". In: *Proceedings of the 1997 IEEE/RSJ International Conference on Intelligent Robot*

*and Systems. Innovative Robotics for Real-World Applications. IROS'97*. Vol. 2. IEEE, pp. 545–550.

Gaussier, Philippe, Ju Mingda, and Jeffrey L Krichmar (2020). "a joint paper submitted to scientific reports, A parsimonious computational model explaining path integration in cortex," in: *Scientific Reports*.

Gaussier, Philippe, Sorin Moga, Mathias Quoy, and Jean-Paul Banquet (1998). "From perception-action loops to imitation processes: A bottom-up approach of learning by imitation". In: *Applied Artificial Intelligence* 12.7-8, pp. 701–727.

Gaussier, Philippe, Arnaud Revel, Jean-Paul Banquet, and Vincent Babeau (2002). "From view cells and place cells to cognitive map learning: processing stages of the hippocampal system". In: *Biological cybernetics* 86.1, pp. 15–28.

Gaussier, Philippe and Stéphane Zrehen (1995). "Perac: A neural architecture to control artificial animals". In: *Robotics and Autonomous Systems* 16.2-4, pp. 291–320.

Giovannangeli, C, Ph Gaussier, and JP Banquet (2006). "Robustness of visual place cells in dynamic indoor and outdoor environment". In: *International Journal of Advanced Robotic Systems* 3.2, p. 19.

Gray, Henry (1878). *Anatomy of the human body*. Vol. 8. Lea & Febiger.

Grossberg, Stephen (1969). "On the serial learning of lists". In: *Mathematical Biosciences* 4.1, pp. 201–253.

— (1978). "Behavioral contrast in short term memory: Serial binary memory models or parallel continuous memory models?" In: *Journal of Mathematical Psychology* 17.3, pp. 199–219.

— (1982). "How does a brain build a cognitive code?" In: *Studies of mind and brain*. Springer, pp. 1–52.

— (2017). "Towards solving the hard problem of consciousness: The varieties of brain resonances and the conscious experiences that they support". In: *Neural Networks* 87, pp. 38–95.

Grossberg, Stephen and Praveen K Pilly (2012). "How entorhinal grid cells may learn multiple spatial scales from a dorsoventral gradient of cell response rates in a self-organizing map". In.

Hafting, Torkel, Marianne Fyhn, Sturla Molden, May-Britt Moser, and Edvard I Moser (2005). "Microstructure of a spatial map in the entorhinal cortex". In: *Nature* 436.7052, pp. 801–806.

Hasselmo, Michael E (2008). "Grid cell mechanisms and function: contributions of entorhinal persistent spiking and phase resetting". In: *Hippocampus* 18.12, pp. 1213–1229.

Hasselmo, Michael E, Eric Schnell, and Edi Barkai (1995). "Dynamics of learning and recall at excitatory recurrent synapses and cholinergic modulation in rat hippocampal region CA3". In: *Journal of Neuroscience* 15.7, pp. 5249–5262.

Hoang, Kevin (2021). “Exploration et reconnaissance active de scènes visuelles: Impact de l’usage d’une caméra événementielle”. PhD thesis. CY Cergy Paris Université.

Hoh, Timothy E, Bryan Kolb, Ayelet Eppel, CH Vanderwolf, and Donald P Cain (2003). “Role of the neocortex in the water maze task in the rat: a detailed behavioral and Golgi-Cox analysis”. In: *Behavioural brain research* 138.1, pp. 81–94.

Høydal, Morten A, Ulrik Wisløff, Ole J Kemi, and Øyvind Ellingsen (2007). “Running speed and maximal oxygen uptake in rats and mice: practical implications for exercise training”. In: *European Journal of Cardiovascular Prevention & Rehabilitation* 14.6, pp. 753–760.

Hubel, David H and Torsten N Wiesel (1968). “Receptive fields and functional architecture of monkey striate cortex”. In: *The Journal of physiology* 195.1, pp. 215–243.

Hubel, David H, Torsten N Wiesel, and Michael P Stryker (1977). “Orientation columns in macaque monkey visual cortex demonstrated by the 2-deoxyglucose autoradiographic technique”. In: *Nature* 269.5626, pp. 328–330.

Itti, Laurent and Christof Koch (2001). “Computational modelling of visual attention”. In: *Nature reviews neuroscience* 2.3, pp. 194–203.

Jacob, Pierre-Yves, Fabrizio Capitano, Bruno Poucet, Etienne Save, and Francesca Sargolini (2019). “Path integration maintains spatial periodicity of grid cell firing in a 1D circular track”. In: *Nature Communications* 10.1, pp. 1–13.

Jacob, Pierre-Yves, Giulio Casali, Laure Spieser, Hector Page, Dorothy Overington, and Kate Jeffery (2017). “An independent, landmark-dominated head-direction signal in dysgranular retrosplenial cortex”. In: *Nature neuroscience* 20.2, p. 173.

Jacobs, Joshua, Christoph T Weidemann, Jonathan F Miller, Alec Solway, John F Burke, Xue-Xin Wei, Nanthia Suthana, Michael R Sperling, Ashwini D Sharan, Itzhak Fried, et al. (2013). “Direct recordings of grid-like neuronal activity in human spatial navigation”. In: *Nature neuroscience* 16.9, pp. 1188–1190.

Jadhav, Shantanu P, Caleb Kemere, P Walter German, and Loren M Frank (2012). “Awake hippocampal sharp-wave ripples support spatial memory”. In: *Science* 336.6087, pp. 1454–1458.

Jauffret, Adrien, Nicolas Cuperlier, and Philippe Gaussier (2015). “From grid cells and visual place cells to multimodal place cell: a new robotic architecture”. In: *Frontiers in neurorobotics* 9, p. 1.

Jauffret, Adrien, Caroline Grand, Nicolas Cuperlier, Philippe Gaussier, and Philippe Tarroux (2013). “How can a robot evaluate its own behavior? a neural model for self-assessment”. In: *The 2013 International Joint Conference on Neural Networks (IJCNN)*. IEEE, pp. 1–8.

Ju, Mingda and Philippe Gaussier (2020). “A model of path integration and representation of spatial context in the retrosplenial cortex”. In: *Biological cybernetics* 114.2, pp. 303–313.

Julian, Joshua B, Alexandra T Keinath, Giulia Frazzetta, and Russell A Epstein (2018). “Human entorhinal cortex represents visual space using a boundary-anchored grid”. In: *Nature neuroscience* 21.2, pp. 191–194.

Jun, Heechul, Allen Bramian, Shogo Soma, Takashi Saito, Takaomi C Saido, and Kei M Igarashi (2020). “Disrupted place cell remapping and impaired grid cells in a knockin model of Alzheimer’s disease”. In: *Neuron* 107.6, pp. 1095–1112.

Jung, Min W, Sidney I Wiener, and Bruce L McNaughton (1994). “Comparison of spatial firing characteristics of units in dorsal and ventral hippocampus of the rat”. In: *Journal of Neuroscience* 14.12, pp. 7347–7356.

Killian, Nathaniel J, Michael J Jutras, and Elizabeth A Buffalo (2012). “A map of visual space in the primate entorhinal cortex”. In: *Nature* 491.7426, pp. 761–764.

Killian, Nathaniel J, Steve M Potter, and Elizabeth A Buffalo (2015). “Saccade direction encoding in the primate entorhinal cortex during visual exploration”. In: *Proceedings of the National Academy of Sciences* 112.51, pp. 15743–15748.

Kjelstrup, Kirsten Brun, Trygve Solstad, Vegard Heimly Brun, Torkel Hafting, Stefan Leutgeb, Menno P Witter, Edvard I Moser, and May-Britt Moser (2008). “Finite scale of spatial representation in the hippocampus”. In: *Science* 321.5885, pp. 140–143.

Knierim, James J, Joshua P Neunuebel, and Sachin S Deshmukh (2014). “Functional correlates of the lateral and medial entorhinal cortex: objects, path integration and local–global reference frames”. In: *Philosophical Transactions of the Royal Society B: Biological Sciences* 369.1635, p. 20130369.

Kohonen, Teuvo (1982). “Self-organized formation of topologically correct feature maps”. In: *Biological cybernetics* 43.1, pp. 59–69.

— (1990). “The self-organizing map”. In: *Proceedings of the IEEE* 78.9, pp. 1464–1480.

Kropff, Emilio, James E Carmichael, May-Britt Moser, and Edvard I Moser (2015). “Speed cells in the medial entorhinal cortex”. In: *Nature* 523.7561, p. 419.

Langston, Rosamund F, James A Ainge, Jonathan J Couey, Cathrin B Canto, Tale L Bjerknes, Menno P Witter, Edvard I Moser, and May-Britt Moser (2010). “Development of the spatial representation system in the rat”. In: *Science* 328.5985, pp. 1576–1580.

Lisman, John E and Ole Jensen (2013). “The theta-gamma neural code”. In: *Neuron* 77.6, pp. 1002–1016.

Lozano, Yave Roberto, Hector Page, Pierre-Yves Jacob, Eleonora Lomi, James Street, and Kate Jeffery (2017). “Retrosplenial and postsubicular head direction cells

compared during visual landmark discrimination". In: *Brain and neuroscience advances* 1, p. 2398212817721859.

Manns, ID, L Mainville, and BE Jones (2001). "Evidence for glutamate, in addition to acetylcholine and GABA, neurotransmitter synthesis in basal forebrain neurons projecting to the entorhinal cortex". In: *Neuroscience* 107.2, pp. 249–263.

Mao, Dun, Steffen Kandler, Bruce L McNaughton, and Vincent Bonin (2017). "Sparse orthogonal population representation of spatial context in the retrosplenial cortex". In: *Nature communications* 8.1, p. 243.

Markou, Markos and Sameer Singh (2003). "Novelty detection: a review—part 2:: neural network based approaches". In: *Signal processing* 83.12, pp. 2499–2521.

Marston, HM, BJ Everitt, and TW Robbins (1993). "Comparative effects of excitotoxic lesions of the hippocampus and septum/diagonal band on conditional visual discrimination and spatial learning". In: *Neuropsychologia* 31.10, pp. 1099–1118.

McClelland, James L, Bruce L McNaughton, and Randall C O'Reilly (1995). "Why there are complementary learning systems in the hippocampus and neocortex: insights from the successes and failures of connectionist models of learning and memory." In: *Psychological review* 102.3, p. 419.

McNaughton, BL, LL Chen, and EJ Markus (1991). ""Dead reckoning," landmark learning, and the sense of direction: a neurophysiological and computational hypothesis". In: *Journal of Cognitive Neuroscience* 3.2, pp. 190–202.

McNaughton, Bruce L, Carol A Barnes, Jason L Gerrard, Katalin Gothard, Min W Jung, James J Knierim, H Kudrimoti, Y Qin, WE Skaggs, M Suster, et al. (1996). "Deciphering the hippocampal polyglot: the hippocampus as a path integration system." In: *Journal of Experimental Biology* 199.1, pp. 173–185.

McNaughton, Bruce L, Francesco P Battaglia, Ole Jensen, Edvard I Moser, and May-Britt Moser (2006). "Path integration and the neural basis of the'cognitive map"'. In: *Nature Reviews Neuroscience* 7.8, p. 663.

Mhatre, Himanshu, Anatoli Gorchetchnikov, and Stephen Grossberg (2012). "Grid cell hexagonal patterns formed by fast self-organized learning within entorhinal cortex". In: *Hippocampus* 22.2, pp. 320–334.

Milczarek, Michal M and Seralynne D Vann (2020). "The retrosplenial cortex and long-term spatial memory: from the cell to the network". In: *Current Opinion in Behavioral Sciences* 32, pp. 50–56.

Milford, Michael J, Gordon F Wyeth, and David Prasser (2004). "RatSLAM: a hippocampal model for simultaneous localization and mapping". In: *IEEE International Conference on Robotics and Automation, 2004. Proceedings. ICRA'04. 2004.* Vol. 1. IEEE, pp. 403–408.

Mishkin, Mortimer, Leslie G Ungerleider, and Kathleen A Macko (1983). "Object vision and spatial vision: two cortical pathways". In: *Trends in neurosciences* 6, pp. 414–417.

Mitchell, Anna S, Rafal Czajkowski, Ningyu Zhang, Kate Jeffery, and Andrew JD Nelson (2018). "Retrosplenial cortex and its role in spatial cognition". In: *Brain and neuroscience advances* 2, p. 2398212818757098.

Morris, Richard GM (1981). "Spatial localization does not require the presence of local cues". In: *Learning and motivation* 12.2, pp. 239–260.

Moser, May-Britt, David C Rowland, and Edvard I Moser (2015). "Place cells, grid cells, and memory". In: *Cold Spring Harbor perspectives in biology* 7.2, a021808.

Muessig, Laurenz, Jonas Hauser, Thomas Joseph Wills, and Francesca Cacucci (2015). "A developmental switch in place cell accuracy coincides with grid cell maturation". In: *Neuron* 86.5, pp. 1167–1173.

Nau, Matthias, Tobias Navarro Schröder, Jacob LS Bellmund, and Christian F Doeller (2018). "Hexadirectional coding of visual space in human entorhinal cortex". In: *Nature neuroscience* 21.2, pp. 188–190.

Nitz, Douglas A (2006). "Tracking route progression in the posterior parietal cortex". In: *Neuron* 49.5, pp. 747–756.

— (2012). "Spaces within spaces: rat parietal cortex neurons register position across three reference frames". In: *Nature neuroscience* 15.10, pp. 1365–1367.

O'Keefe, John (1976). "Place units in the hippocampus of the freely moving rat". In: *Experimental neurology* 51.1, pp. 78–109.

O'keefe, John and Neil Burgess (2005). "Dual phase and rate coding in hippocampal place cells: theoretical significance and relationship to entorhinal grid cells". In: *Hippocampus* 15.7, pp. 853–866.

O'Keefe, John and Jonathan Dostrovsky (1971). "The hippocampus as a spatial map: Preliminary evidence from unit activity in the freely-moving rat." In: *Brain research*.

O'keefe, John and Lynn Nadel (1979). "Précis of O'Keefe & Nadel's The hippocampus as a cognitive map". In: *Behavioral and Brain Sciences* 2.4, pp. 487–494.

O'Keefe, John and Michael L Recce (1993). "Phase relationship between hippocampal place units and the EEG theta rhythm". In: *Hippocampus* 3.3, pp. 317–330.

Pasquet, Matthieu O, Matthieu Tihy, Aurélie Gourgeon, Marco N Pompili, Bill P Godsil, Clément Léna, and Guillaume P Dugué (2016). "Wireless inertial measurement of head kinematics in freely-moving rats". In: *Scientific reports* 6, p. 35689.

Pilly, Praveen K and Stephen Grossberg (2012). "How do spatial learning and memory occur in the brain? Coordinated learning of entorhinal grid cells and hippocampal place cells". In: *Journal of cognitive neuroscience* 24.5, pp. 1031–1054.

Pisokas, Ioannis, Wolfgang Rössler, Barbara Webb, Jochen Zeil, and Ajay Narendra (2022). "Anesthesia disrupts distance, but not direction, of path integration memory". In: *Current Biology* 32.2, pp. 445–452.

Poucet, Bruno, Franck Chaillan, Bruno Truchet, Etienne Save, Francesca Sargolini, and Vincent Hok (2015). "Is there a pilot in the brain? Contribution of the self-positioning system to spatial navigation". In: *Frontiers in behavioral neuroscience* 9, p. 292.

Rall, Wilfrid (1960). "Membrane potential transients and membrane time constant of motoneurons". In: *Experimental neurology* 2.5, pp. 503–532.

Raudies, Florian, Mark P Brandon, G William Chapman, and Michael E Hasselmo (2015). "Head direction is coded more strongly than movement direction in a population of entorhinal neurons". In: *Brain research* 1621, pp. 355–367.

Redish, A David, Adam N Elga, and David S Touretzky (1996). "A coupled attractor model of the rodent head direction system". In: *Network: computation in neural systems* 7.4, p. 671.

Redish, A David and David S Touretzky (1997). "Cognitive maps beyond the hippocampus". In: *Hippocampus* 7.1, pp. 15–35.

Reep, RL, HC Chandler, V King, and JV Corwin (1994). "Rat posterior parietal cortex: topography of corticocortical and thalamic connections". In: *Experimental brain research* 100.1, pp. 67–84.

Rescorla, Robert A, Allan R Wagner, et al. (1972). "A theory of Pavlovian conditioning: Variations in the effectiveness of reinforcement and nonreinforcement". In: *Classical conditioning II: Current research and theory* 2, pp. 64–99.

Ritchey, Maureen, Laura A Libby, and Charan Ranganath (2015). "Cortico-hippocampal systems involved in memory and cognition: the PMAT framework". In: *Progress in brain research* 219, pp. 45–64.

Rolls, Edmund T, Robert G Robertson, and Pierre Georges-François (1997). "Spatial view cells in the primate hippocampus". In: *European Journal of Neuroscience* 9.8, pp. 1789–1794.

Rolls, Edmund T and Sylvia Wirth (2018). "Spatial representations in the primate hippocampus, and their functions in memory and navigation". In: *Progress in neurobiology* 171, pp. 90–113.

Rosenbaum, R Shayna, Asaf Gilboa, and Morris Moscovitch (2014). "Case studies continue to illuminate the cognitive neuroscience of memory". In: *Annals of the New York Academy of Sciences* 1316.1, pp. 105–133.

Rumelhart, David E and David Zipser (1985). "Feature discovery by competitive learning". In: *Cognitive science* 9.1, pp. 75–112.

Samsonovich, Alexei and Bruce L McNaughton (1997). "Path integration and cognitive mapping in a continuous attractor neural network model". In: *Journal of Neuroscience* 17.15, pp. 5900–5920.

Sargolini, Francesca (2005). "Conjunctive Representation of Position, Direction". In: *Proc. Natl. Acad. Sci. USA* 102, p. 12950.

Sargolini, Francesca, Marianne Fyhn, Torkel Hafting, Bruce L McNaughton, Menno P Witter, May-Britt Moser, and Edvard I Moser (2006). "Conjunctive representation of position, direction, and velocity in entorhinal cortex". In: *Science* 312.5774, pp. 758–762.

Save, Etienne, Arnaud Cressant, Catherine Thinus-Blanc, and Bruno Poucet (1998). "Spatial firing of hippocampal place cells in blind rats". In: *Journal of Neuroscience* 18.5, pp. 1818–1826.

Save, Etienne, Alex Guazzelli, and Bruno Poucet (2001). "Dissociation of the effects of bilateral lesions of the dorsal hippocampus and parietal cortex on path integration in the rat." In: *Behavioral neuroscience* 115.6, p. 1212.

Schlag-Rey, MADELEINE and JOHN Schlag (1984). "Visuomotor functions of central thalamus in monkey. I. Unit activity related to spontaneous eye movements". In: *Journal of neurophysiology* 51.6, pp. 1149–1174.

Schöner, G., M. Dose, and C. Engels (1995a). "Dynamics of behavior: theory and applications for autonomous robot architectures". In: *Robotics and Autonomous System* 16.2-4, pp. 213–245.

Schöner, Gregor, Michael Dose, and Christoph Engels (1995b). "Dynamics of behavior: Theory and applications for autonomous robot architectures". In: *Robotics and autonomous systems* 16.2-4, pp. 213–245.

Schwartz, Eric L (1977). "Spatial mapping in the primate sensory projection: analytic structure and relevance to perception". In: *Biological cybernetics* 25.4, pp. 181–194.

— (1980). "Computational anatomy and functional architecture of striate cortex: a spatial mapping approach to perceptual coding". In: *Vision research* 20.8, pp. 645–669.

Scoville, William Beecher and Brenda Milner (1957). "Loss of recent memory after bilateral hippocampal lesions". In: *Journal of neurology, neurosurgery, and psychiatry* 20.1, p. 11.

Sereno, MI, S Pitzalis, and A Martinez (2001). "Mapping of contralateral space in retinotopic coordinates by a parietal cortical area in humans". In: *Science* 294.5545, pp. 1350–1354.

Sharp, Patricia E, Amanda Tinkelman, and Jeiwon Cho (2001). "Angular velocity and head direction signals recorded from the dorsal tegmental nucleus of gudden in the rat: implications for path integration in the head direction cell circuit." In: *Behavioral neuroscience* 115.3, p. 571.

Sheynikhovich, Denis, Ricardo Chavarriaga, Thomas Strösslin, Angelo Arleo, and Wulfram Gerstner (2009). "Is there a geometric module for spatial orientation? Insights from a rodent navigation model." In: *Psychological review* 116.3, p. 540.

Skaggs, William, James Knierim, Hemant Kudrimoti, and Bruce McNaughton (1994). "A model of the neural basis of the rat's sense of direction". In: *Advances in neural information processing systems* 7.

Skaggs, William E, Bruce L McNaughton, Matthew A Wilson, and Carol A Barnes (1996). "Theta phase precession in hippocampal neuronal populations and the compression of temporal sequences". In: *Hippocampus* 6.2, pp. 149–172.

Stacho, Martin and Denise Manahan-Vaughan (2022). "Mechanistic flexibility of the retrosplenial cortex enables its contribution to spatial cognition". In: *Trends in Neurosciences*.

Stangl, Matthias, Johannes Achtzehn, Karin Huber, Caroline Dietrich, Claus Tempelmann, and Thomas Wolbers (2018). "Compromised grid-cell-like representations in old age as a key mechanism to explain age-related navigational deficits". In: *Current Biology* 28.7, pp. 1108–1115.

Steffenach, Hill-Aina, Menno Witter, May-Britt Moser, and Edvard I Moser (2005). "Spatial memory in the rat requires the dorsolateral band of the entorhinal cortex". In: *Neuron* 45.2, pp. 301–313.

Stone, Thomas, Barbara Webb, Andrea Adden, Nicolai Ben Weddig, Anna Honkanen, Rachel Templin, William Wcislo, Luca Scimeca, Eric Warrant, and Stanley Heinze (2017). "An anatomically constrained model for path integration in the bee brain". In: *Current Biology* 27.20, pp. 3069–3085.

Taube, Jeffrey S (1995). "Head direction cells recorded in the anterior thalamic nuclei of freely moving rats". In: *Journal of Neuroscience* 15.1, pp. 70–86.

— (1998). "Head direction cells and the neurophysiological basis for a sense of direction". In: *Progress in neurobiology* 55.3, pp. 225–256.

Taube, Jeffrey S, Robert U Muller, and James B Ranck (1990a). "Head-direction cells recorded from the postsubiculum in freely moving rats. I. Description and quantitative analysis". In: *Journal of Neuroscience* 10.2, pp. 420–435.

— (1990b). "Head-direction cells recorded from the postsubiculum in freely moving rats. II. Effects of environmental manipulations". In: *Journal of Neuroscience* 10.2, pp. 436–447.

Teyler, Timothy J and Jerry W Rudy (2007). "The hippocampal indexing theory and episodic memory: updating the index". In: *Hippocampus* 17.12, pp. 1158–1169.

Todd, Travis P and David J Bucci (2015). "Retrosplenial cortex and long-term memory: molecules to behavior". In: *Neural plasticity* 2015.

Van Cauter, Tiffany, Jeremy Camon, Alice Alvernhe, Coralie Elduayen, Francesca Sargolini, and Etienne Save (2013). "Distinct Roles of Medial and Lateral Entorhinal Cortex in Spatial Cognition". In: *Cerebral Cortex* 23, pp. 451–459.

Vann, Seralynne D, John P Aggleton, and Eleanor A Maguire (2009). "What does the retrosplenial cortex do?" In: *Nature reviews neuroscience* 10.11, pp. 792–802.

Wang, Lupeng, Mingna Liu, Mark A Segraves, and Jianhua Cang (2015). "Visual experience is required for the development of eye movement maps in the mouse superior colliculus". In: *Journal of Neuroscience* 35.35, pp. 12281–12286.

Wehner, R., B. Michel, and P. Antonsen (1996). "Visual navigation in insects: coupling of egocentric and geocentric information". In: *Journal of Experimental Biology* 199, pp. 129–140.

Widrow, Bernard and Marcian E Hoff (1960). *Adaptive switching circuits*. Tech. rep. Stanford Univ Ca Stanford Electronics Labs.

Wills, Tom J, Francesca Cacucci, Neil Burgess, and John O'Keefe (2010). "Development of the hippocampal cognitive map in preweanling rats". In: *science* 328.5985, pp. 1573–1576.

Wilming, Niklas, Peter König, Seth König, and Elizabeth A Buffalo (2018). "Entorhinal cortex receptive fields are modulated by spatial attention, even without movement". In: *Elife* 7, e31745.

Wilson, David IG, Rosamund F Langston, Magdalene I Schlesiger, Monica Wagner, Sakurako Watanabe, and James A Ainge (2013). "Lateral entorhinal cortex is critical for novel object-context recognition". In: *Hippocampus* 23.5, pp. 352–366.

Wilson, Matthew A and Bruce L McNaughton (1993). "Dynamics of the hippocampal ensemble code for space". In: *Science* 261.5124, pp. 1055–1058.

Wittmann, Thomas and Helmut Schwegler (1995). "Path integration - a network model". In: *Biological Cybernetics* 12.73, pp. 569–575.

Wyass, J Michael and Thomas Van Groen (1992). "Connections between the retrosplenial cortex and the hippocampal formation in the rat: a review". In: *Hippocampus* 2.1, pp. 1–11.

Yartsev, Michael M, Menno P Witter, and Nachum Ulanovsky (2011). "Grid cells without theta oscillations in the entorhinal cortex of bats". In: *Nature* 479.7371, pp. 103–107.

Zhang, Kechen (1996). "Representation of spatial orientation by the intrinsic dynamics of the head-direction cell ensemble: a theory". In: *Journal of Neuroscience* 16.6, pp. 2112–2126.

Zhang, Sijie and Denise Manahan-Vaughan (2015). "Spatial olfactory learning contributes to place field formation in the hippocampus". In: *Cerebral cortex* 25.2, pp. 423–432.